



# A Study of the Degradation of a SilicaGel Based-Thermal Energy Storage System.

## Master Thesis

*Study programme:*

N2301 Mechanical Engineering

*Study branch:*

Machines and Equipment Design

*Author:*

**Emmanuel Nyarko Ayisi**

*Thesis Supervisors:*

prof. Ing. Karel Fraňa, Ph.D.

Department of Power Engineering Equipment





## Master Thesis Assignment Form

# A Study of the Degradation of a SilicaGel Based-Thermal Energy Storage System.

*Name and surname:* **Emmanuel Nyarko Ayisi**  
*Identification number:* S18000391  
*Study programme:* N2301 Mechanical Engineering  
*Study branch:* Machines and Equipment Design  
*Assigning department:* Department of Power Engineering Equipment  
*Academic year:* **2019/2020**

### Rules for Elaboration:

The need to raise the efficiency of thermal systems has created the need to develop technologies of Thermal Energy Storage, TES. Such technologies would be able to absorb thermal energy when it is abundant and store it to be used when it is scarce.

1. Introduction of the heat storage.
2. Design of the working cycle of heat disposal and recovery and study the dynamics of the heat storage process with special attention being given to the effect of cycle repetition on the process efficiency.
3. Components description of the experimental model, 3D sketch.
4. Experimental measurement at the working cycle, prove of the temperature effects on the heat storage.
5. Introduction of the fundamental calculation of the heat process.

*Scope of Graphic Work:* 10  
*Scope of Report:* 60  
*Thesis Form:* printed/electronic  
*Thesis Language:* English



### **List of Specialised Literature:**

1. ID, Salvatore Vasta, Vincenza BRANCATO, Davide La ROSA, Valeria PALOMBA, Giovanni RESTUCCIA, Alessio SAPIENZA, Andrea FRAZZICA, C N R ITAE, Tecnologie AVANZATE, Energia NICOLA, Via SALITA a S LUCIA, Adsorption Heat Storage: State-of-the-Art and Future Perspectives, 2018
2. ZHOU, D., C. Y. ZHAO a Y. TIAN, Review on thermal energy storage with phase change materials (PCMs) in building applications, Applied Energy 2012, 92, 593-605
3. PIELICHOWSKA, Kinga a Krzysztof PIELICHOWSKI, Phase change materials for thermal energy storage, JOURNAL OF PROGRESS IN MATERIALS SCIENCE, 2014, 65, 67-123, ISSN 0079-6425

*Thesis Supervisors:* prof. Ing. Karel Fraňa, Ph.D.  
Department of Power Engineering Equipment

*Date of Thesis Assignment:* November 1, 2019

*Date of Thesis Submission:* April 30, 2021

prof. Dr. Ing. Petr Lenfeld  
Dean

L.S.

doc. Ing. Petra Dančová, Ph.D.  
Head of Department

## Declaration

I hereby certify, I, myself, have written my master thesis as an original and primary work using the literature listed below and consulting it with my thesis supervisor and my thesis counsellor.

I acknowledge that my bachelor master thesis is fully governed by Act No. 121/2000 Coll., the Copyright Act, in particular Article 60 – School Work.

I acknowledge that the Technical University of Liberec does not infringe my copyrights by using my master thesis for internal purposes of the Technical University of Liberec.

I am aware of my obligation to inform the Technical University of Liberec on having used or granted license to use the results of my master thesis; in such a case the Technical University of Liberec may require reimbursement of the costs incurred for creating the result up to their actual amount.

At the same time, I honestly declare that the text of the printed version of my master thesis is identical with the text of the electronic version uploaded into the IS/STAG.

I acknowledge that the Technical University of Liberec will make my master thesis public in accordance with paragraph 47b of Act No. 111/1998 Coll., on Higher Education Institutions and on Amendment to Other Acts (the Higher Education Act), as amended.

I am aware of the consequences which may under the Higher Education Act result from a breach of this declaration.

June 12, 2020

Emmanuel Nyarko Ayisi

## **ABSTRACT**

An energy storage system was designed to test the adsorption capacity and cycle repeatability of silica gel using a low-grade heat for the desorption phase. The design specification requirement was to maximize adsorption of the silica gel and test the number of cycles that can be achieved and the total energy obtained while a low-grade heat energy is used for the desorption phase. The D – A model was chosen for the determination of the maximum adsorption capacity and activation energy of the silica gel due to better performance in fitting. A mean specific power of 29.5 W/kg was obtained for cycle 1, with a 22.7 % loss in the specific power at the end of the 5 cycles. The mean specific energy density of (292 – 225) kJ/kg after 165 mins was obtained. It was also observed that, higher flowrate aid in higher adsorption and desorption rates while lower flowrates aid in lower desorption and adsorption rate.

**Keywords: Silica Gel, Adsorption, Energy Storage, Material Degradation, Experimental Device.**

## **ACKNOWLEDGEMENTS**

My deepest appreciation goes to God for the mercies and blessings He has bestowed upon me throughout my tertiary education and a successful completion of my graduate studies.

I particularly wish to show appreciation to my supervisor Professor Karel Frana to him I owe a lot of thanks for his unrelenting support, supervision and time during this project work.

Furthermore, I would want to thank Ing. Millos Muller PhD and Ing. Magda Vestfalova Phd for their support and guide from the beginning of the project right to the end.

My appreciation also goes to Ing. Novotni PhD and Ing. Jerje for their support through lab sections and for their encouragement.

Many colleagues have been generous with discussion, criticism, and constructive suggestions.

## Nomenclature

$b, b_0$	Adsorption equilibrium constant, adsorption affinity constant.
$D_s, D_{s0}$	Surface diffusivity, pre-exponential term $2.54 \cdot 10^4 \text{ m}^2/\text{s}$
$E_a$	Activation energy, $\text{kJmol}^{-1}$
$\Delta H$	Heat of adsorption, $\text{Jkg}^{-1}$
$K_m$	Overall mass transfer coefficient of adsorption
$p$	Pressure, Pa
$R$	Universal gas constant, $8.314 \text{ J/mol/K}$
$R_p$	Pore radius of adsorbent, nm
$T$	Temperature, K
$T_{out.avg}$	Average temperature out, $^{\circ}\text{C}$
$T_{lift}$	Average temperature lift, $^{\circ}\text{C}$
$X, X_0$	Water uptake, adsorbent capacity
$y$	Fractional surface coverage
$P$	Power, W

## Table of Contents

1	Introduction.....	12
2	Literature Review.....	13
2.1	Thermal Energy Storage .....	13
2.1.1	Quantification Of Thermal Energy Storage .....	14
2.1.2	Classification Of Tes System.....	17
2.2	Sensible.....	19
2.2.1	Materials For Sensible Heat Storage.....	20
2.2.2	Applications .....	21
2.3	Latent Heat Energy Storage .....	22
2.3.1	Classification Of Phase Changing Materials.....	24
2.3.2	Characterization Of Lhs Materials .....	25
2.3.3	Factors Influencing Lhs Systems .....	26
2.3.4	Basic Pcm Models.....	27
2.4	Sorption.....	27
2.4.1	Opened And Closed Sorption Systems .....	28
2.4.2	Classification Of Sorption.....	30
2.4.3	Sorption Materials.....	37
2.4.4	Silica Gel.....	44
2.4.5	Adsorption Working Pairs .....	53
2.5	Kinetics Of Sorption And Adsorption Models.....	59
2.5.1	Adsorption Isotherms.....	59
2.5.2	Langmuir Isotherm Model .....	59
2.5.3	Isosteric Heat Of Adsorption .....	60
2.5.4	Freundlich Isotherm .....	61
2.5.5	Dubinin Isotherms.....	62
2.5.6	Toth Isotherm.....	63
2.5.7	Brunauer – Emmet – Teller (Bet) Isotherm .....	63
2.5.8	Adsorption Rate .....	65
2.6	Energy Balance .....	66
3	Design Of Thermal Storage System.....	68
3.1	Functional Analysis.....	68
3.2	System Specification.....	71



3.2.1	Moist Air Calculation.....	71
3.2.2	Sorption Tube Design Calculation And 3d Printing .....	73
3.2.3	Selected Concept.....	75
4	Experimental Design.....	77
4.1	Experimental Setup.....	77
4.1.1	Material Properties Of Silica Gel.....	78
4.1.2	Adsorption Phase .....	79
4.1.3	Desorption Phase.....	80
4.1.4	Regeneration Of Silica Gel .....	80
4.2	Adsorption Isotherm And Parameters For Calculation .....	80
5	Results And Discussion .....	82
5.1	Adsorption And Desorption Test With Low Grade Heat.....	82
5.2	Adsorption Test For 5 Cycles Using Low Grade Heat .....	86
	<i>Adsorption</i> .....	86
	<i>Temperature</i> .....	89
5.3	Effect Of Flow Velocity On Adsorption And Desorption Phases .....	94
6	Conclusion .....	97
7	References.....	98

## LIST TABLES

Table 2.1	below illustrates the typical parameters of the system by Hauer, A. ....	16
Table 2.2	Properties of solid-liquid materials for sensible heat storage [19].....	21
Table 2.3.	Properties for selecting PCMs. ....	23
Table 2.4	Characteristics of some common adsorbents [88][92][91][93]. ....	53
Table 3.1	Specification after calculation.....	74
Table 4.1	showing properties of the silica gel at T = 23 (+2) °C obtained from Manufacturer. ....	78
Table 4.2.	Parameter obtained after fitting the experimental data. ....	81
Table 4.3.	Parameters used for the analysis of the system.....	81

## LIST OF FIGURES

Figure 2.1 Above show the types of thermal energy storage [16].	18
Figure 2.2.this figure shows the dependence of sensible heat on change in temperature and independence of latent heat on temperature change [17].	19
Figure 2.3. Classification of PCM and some examples [22].	24
Figure 2.4 diagram showing molecular sorption and solid sorption [117].	28
Figure 2.5 Depiction of a closed energy storage system [38].	29
Figure 2.6 Diagram of Sorptive and Chemical thermal energy storage methods [41].	30
Figure 2.7 a diagram showing monolayer and multilayer adsorption [43].	32
Figure 2.8 Diagram showing chemisorption and physisorption processes and their relation with distance away from the surface [44].	32
Figure 2.9 Relation of temperature effect on physical adsorption and chemisorption processes [45].	33
Figure 2.10 Illustration of the Lennard – Jones potential [48].	35
Figure 2.11 Zeolite A and b) faujasite, zeolite X and Y [75].	43
figure 2.12 shows the adsorption rates for silica gel and other adsorbents. it shows the amount of water vapor adsorbed at a given relative humidity [83].	46
Figure 2.13. Relation between adsorption capacity and temperature [83].	47
Figure 3.1. Functional architecture of proposed storage system	68
Figure 3.2. A schematic diagram illustrating the proposed design	70
Figure 3.3. This shows the Mollier diagram for stages moist air	71
Figure 3.4. 2D drawing of the system	75
Figure 3.5. 3D drawing of system.	76
Figure 4.1. Depicts the experimental set up where the heat gun (A), upstream duct (E), sorption tube (F), downstream duct (G), pump (C), atomizer (B), compressor (D), data acquisition device (H) and computer (I).	77
Figure 4.2a figure showing silica gel after adsorption.	79
Figure 4.3 A graph showing data fitting of experimental data of water adsorption by silica gel.	80
Figure 5.1 Illustration of the phase and the cumulative amount of moisture adsorbed per kg of silica gel.	82
Figure 5.2 Depicting the temperature out of the sorption tube and that of the bed.	83
Figure 5.3 Illustration of the desorption of silica gel with time.	84
Figure 5.4 Showing the temperature profile for the inlet and outlet temperatures during desorption.	85
Figure 5.5. Adsorption of moisture in the bed for all cycles.	86
Figure 5.6. Phase mass adsorbed	86
Figure 5.7. Cumulative mass adsorbed over 165 mins.	88
Figure 5.8. A graph showing temperature out and average temperature lift.	89
Figure 5.9. Output temperatures for all cycles	90
Figure 5.10. Average temperature lift to the number of cycles	90
Figure 5.11 Comparison of reaction power generated at a given time for all cycles	91
Figure 5.12 Change in Mean Specific Power Over Five Cycles	92
Figure 5.13. Cumulative Power of reactive heat generation	93

Figure 5.14. Total energy produced .....	93
Figure 5.15 A diagram showing amount of water adsorbed for different flowrates. ....	94
Figure 5.16. A diagram showing the amount of water desorbed using different flowrates. ....	95

## 1 INTRODUCTION

Currently, more than 80% of the world's energy demand is still produced from fossil fuels which in its final form as pollution and greenhouse gas emissions causes significant harm to the environment. According to recent studies by the International Renewable energy Agency and the U.S Energy Information Administration, the worlds energy demand will increase by 50% by 2050[1][2]. Based on certain trends such as population growth, increased urbanization, aging population and a shift in global economic power, it is obvious that the world will be resource and carbon constrained which will force the society to undergo major transformations. As a result, supply of resource is going to be under immense pressure. For this reason, it becomes imperative that renewable energy technologies are developed in order to turn the tide of climate change and attain sustainable development. These include ones that are efficient, cost effective and has zero CO<sub>2</sub> emissions.

A myriad of renewable energy technologies has been developed for decades now. However, energy efficiency and cost effectiveness has been holding these technologies aback, with renewable energy holding very small percentage in the total energy mix. There are several options to improve energy efficiency which includes the development of energy storage systems to reduce the mismatch between various forms of energy during conversion. Based on the energy technology used, quiet a significant amount of energy is lost through transfer into other forms and this is normally seen as losses. Energy storage systems therefore improves the performance and allows systems to work within an optimal range. The various forms of energy that can be stored are chemical energy, electrical energy (by batteries), thermal energy (Latent heat, sensible heat and thermochemical heat), and mechanical energy (compressed air, gravitational, flywheels). This research delves into thermal energy storage (specifically sorption materials), materials that can be used, a designed system that is capable of undergoing charging and discharging cycles and their various applications.

## **2 LITERATURE REVIEW**

### **2.1 Thermal energy storage**

Energy storage over the years has become a very important aspect of renewable energy technology. Thermal energy storage is a technology that stores energy in a storage material or medium through heating, cooling, vaporizing, solidifying or melting the system in order to retrieve the stored thermal energy at a later time. The stored energy can be transferred into other forms of energy or directly applied in various applications such as in building, industrial and so on. The most prominent advantage of the thermal energy system is its reliability and ability to increase the overall efficiency. Others include lower or no CO<sub>2</sub> emissions, thus, environmentally friendly, and reduction in running and investment cost. Thermal energy storage (TES) combined with solar power plants has become increasingly relevant in order to store solar heat for electricity for a full 24 h operation [3].

Solar ratio is how much solar radiation is needed for cooling or heating purposes. Storage density (the amount of energy per unit volume or mass) is important in the optimization of solar ratio, energy consumption and efficiency. For this reason, it is necessary to give a lot of research to phase-changing materials [4][5]. This is because these materials can increase the solar fraction for a given volume and increase the energy density of the material. However, on a large scale, very few solar thermal power plants have employed the thermal energy system. Moreover, the design of solar thermal systems for domestic applications is an on-going research [6]. Other methods such as numerical simulation and computational fluid dynamics are being used to analyze these thermal systems [7][8]. There are certain characteristics as shown in Table1, that are used to effectively describe and quantify the thermal storage systems, and they are as follows:

### 2.1.1 Quantification of thermal energy storage

Since the development of TES systems, latent heat and sensible heat system have made it to the stage of commercial availability, while sorption and chemical energy storage systems still remain in the prototype phase [9]. These systems are assessed on a common scale normally called performance indicators, which indicate whether or not a TES is suitable for commercialization. These indicators are grouped into technical, repeatability and economic.

#### 2.1.1.1 Technical performance indicators

This performance indicator takes into account the parameter for the TES system design, functioning and control. The technical indicator further classifies the parameters into energy, structure, development and dynamics [10].

**Energy performance indicators** considered in energy storage upraise the ability of the system to charge (store the energy) and discharge (supply the energy). Since this is a cycle process, it becomes important that the energy performance indicator is described by the thermal efficiency and the energy storage capacity of the system.

*Thermal efficiency* ( $\eta$ ) of the TES system is the useful energy obtained from the heat storage material ( $Q_{discharge}$ ) to the energy needed to charge the energy storage system ( $Q_{charge}$ ).

$$\eta = \frac{Q_{discharge}}{Q_{charge}} \quad (1)$$

*Energy storage capacity* (C) (**kJ**) is the amount of the energy that can be stored in the system and is dependent on the size, mass, storage process and the medium of the system. It constitutes the sensible heat of the storage material at the design temperature difference ( $\Delta T$ ), the heat of reaction for thermochemical storage and the latent heat storage of a PCM. The total storage capacity is the sum of the storage capacity of the storage medium and each component that reaches similar temperatures.

$$C = C_{mat} + C_{comp} [kJ] \quad (2)$$

**Structural performance indicators** embody all physical characteristics of the system, and mainly the storage material. This indicator is the mass and volume ratio of the storage material to that of the system.

*Storage material mass ratio* ( $m_{m-s}$ ) is the mass ( $m_m$ ) of the storage material to that of the system ( $m_s$ ).

$$m_{m-s} = \frac{m_m}{m_s} \quad (3)$$

*Storage material volume ratio* ( $V_{m-s}$ ) is the volume of the storage material ( $V_m$ ) to that of the system  $V_s$ . This is also known as the packing factor.

$$V_{m-s} = \frac{V_m}{V_s} \quad (4)$$

**Dynamic performance indicators** consider the parameters used in the operation of the TES system such as the charge and discharge time, the power and the response time.

*Charge ( $t_c$ ) and discharge ( $t_{dc}$ ) time (s, min)* is how much time is needed to charge and discharge the thermal system, and this is highly dependent on the technology used as well as the storage medium.

*Power*, in **KW** is the rate of discharge ( $P_{discharge}$ ) or charge ( $P_{charge}$ ) of the storage medium.

*Minimum cycle length* (MinCyc) is the shortest time for charge and discharge cycle of the system to take place without any storage process.

$$MinCyc = \frac{C}{P_{charge}} + \frac{C}{P_{discharge}} \quad [min, h, d] \quad (5)$$

**Development indicators** describe the phase or stage reached by the TES system. This give the further analysis to be done in order to reach commercialization, as well as other needed improvements.

### 2.1.1.2 Repeatability or Life Cycle Performance Indicators

Repeatability is how many cycles the storage medium can be charged and discharged before it begins to lose its properties. A minimum of 1000 charge and discharge cycles are desired for research purposes to estimate the how fast the TES system deteriorates in performance. Important indicators include but not limited to the **global warming potential (GWP)** and the **global energy requirement (GER)**.

The global warming potential estimates the carbon foot print given during the operation of the TES system and the global energy requirement gives the overall energy consumed by the TES system during its whole life cycle.

### 2.1.1.3 Economic Performance indicators

Cost depends on the repeatability, the investment and running cost of the energy storage system. This performance indicator is divided into the storage material cost ration, specific investment cost and the payback time. Table 2.1 below compares typical performance indicators for sensible, latent and thermochemical TES systems.

**TABLE 2.1 BELOW ILLUSTRATES THE TYPICAL PARAMETERS OF THE SYSTEM BY HAUER, A.**

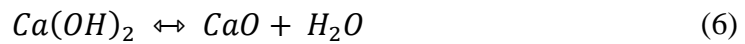
<b>TES System</b>	<b>Storage Period</b>	<b>Storage Capacity (KWh/t)</b>	<b>Power (MW)</b>	<b>Cost (€/kwh)</b>	<b>Efficiency (%)</b>
<b>Sensible (Hot water)</b>	Days/months	10 – 50	0.001 – 10	0.1 – 10	50 – 90
<b>PCM</b>	Hours/months	50 – 150	0.001 – 1	10 – 50	75 – 90
<b>Thermochemical reactions</b>	Hours/days	120 – 250	0.01 – 1	8 – 100	75 – 100



### 2.1.2 Classification of TES System

Thermal energy can be stored as thermochemical, latent or sensible by cooling, heating, vaporization or melting the thermal material as shown in figure 1 below. The energy is then utilized by reversing the storage process. Many TES systems are normally classified as latent heat thermal energy storage or sensible heat thermal energy storage. Sensible heat storage is realized when the storage material is exposed to heat resulting in an increase or decrease in the temperature of the material. Sensible heat storage systems depend on the specific heat capacity of the storage material. The stored thermal energy is a function of the difference in temperature between the storage material and the heat source. It can either exist as liquid or solid as shown in Figure 1. Sensible heat storage systems are relatively cheaper to implement, has simplicity in design and they have a wide temperature range of applications. Nevertheless, certain characteristic such as degradation of the stored thermal energy due to heat dissipation and low heat storage densities limits its implementation on a large scale. Table 1 further show their relatively low storage capacities in general. Phase changing materials (PCM) on the other hand, compared to sensible heat storage systems allows small volumes to accumulate large amount of energy [11]. Thus, they accumulate energy densities at a relatively small temperature range and sometimes nearly isothermal conditions. PCM materials is a material the releases or stores large amount of latent heat at certain temperatures. During the availability of solar radiation, the PCM material stores the energy by changing its phase to solid, liquid or gaseous called the charging phase, and delivers the heat energy in at certain reverse conditions called the discharging phase. Due to the aforementioned advantages of the PCM systems, it has been applied in certain low temperature applications such as refrigeration systems, solar cooling and heating systems [12][13], buildings heating and air-conditioning systems. Disadvantages related to PCM systems are slow charging and discharge power emanating from the slow kinetics of the phase transition, the volume variation due to phase change and the repeatability of the PCM with fear of losing its material properties. Moreover, due to its heat dissipation downsides, storage period is quiet a problem and this limits its long-term thermal energy storage applications. Finally, most PCM materials have low thermal conductivity leading to poor heat transfer between the heat source and the phase changing material during the charging phase [14].

Thermochemical storage of energy distributes or store heat by reversible exothermic or endothermic processes. During its desorption phase, heat from a source is applied to a material A, which leads to its disintegration into say two daughter products M + N and energy is stored. During the discharge phase, the two daughter products are mixed at a suitable temperature and pressure which causes the release of the stored energy. A lot of research has proceeded in this direction for decades. For example, Fujii et al, among others have studied energy storage by thermal decomposition of calcium hydroxide (Ca (OH)<sub>2</sub>) [15].



The forward reaction will proceed at temperatures above 450 °C. The reverse exothermic reaction delivers the stored energy with ease. This method of thermal energy storage provides the highest energy density, therefore has the highest storage capacity. However, its major pit falls are instability, very slow reaction kinetics and high level of degradation over time. Heat transfer resistance of the TES material could also pose as a draw back. This technology has physical reactions as part where a refrigerant reacts with a liquid or a solid sorbent. Physical reactions involving a liquid sorbent are termed absorption systems and ones involving solid sorbent are called adsorption systems.

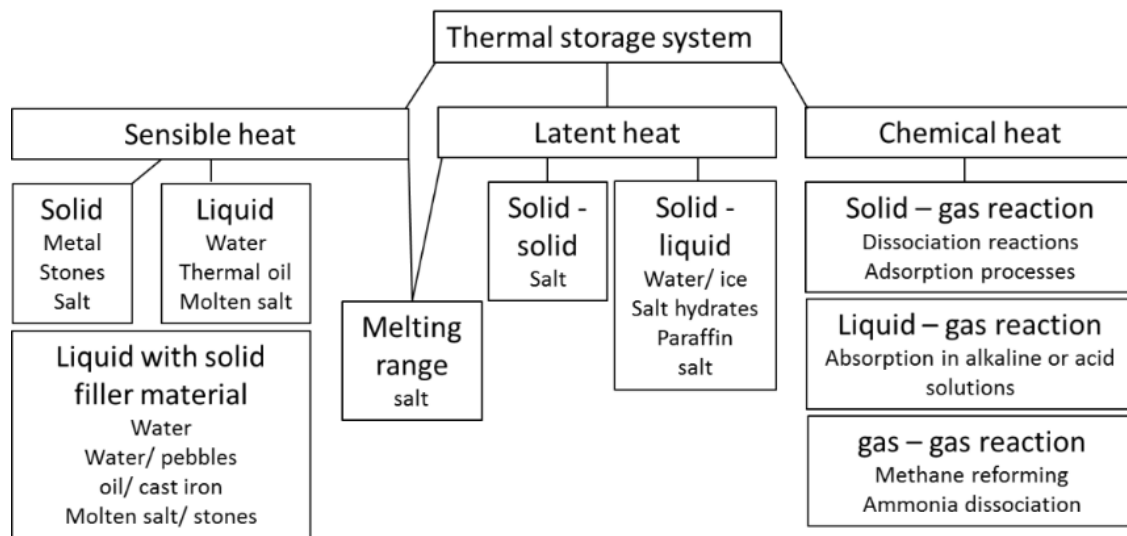


Figure 2.1 Above show the types of thermal energy storage [16].

## 2.2 SENSIBLE

Considering all the energy storage systems, this happens to be the simplest. It is based on heating or cooling of the solid or liquid storage medium, Figure 2. Some storage medium includes water, molten salt, sand, several metals, with water being the cheapest and most popular. Also, the materials used as sensible heat storage media are usually non-toxic. Low operation cost also comes from the direct contact between the heat transfer fluid and the storage medium.

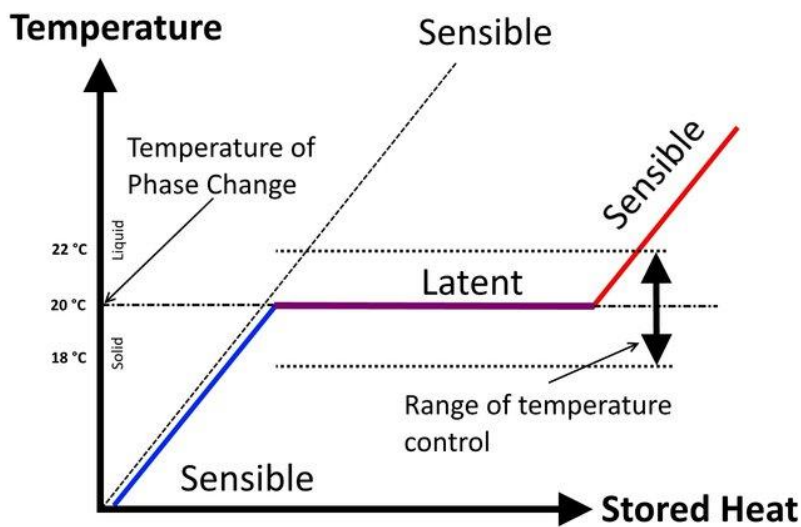


Figure 2.2. this figure shows the dependence of sensible heat on change in temperature and independence of latent heat on temperature change [17].

The amount of stored heat stored in the material is given by the Debye model which depends on the temperature difference between the charge and discharge phase, the mass of the storage material and the specific heat capacity of the storage medium. There exists a direct proportionality in this relation;

$$Q_s = \int_{T_i}^{T_f} mC_p(T)dT = mC_p(T_f - T_i) \quad (7)$$

Where  $Q_s$  is the amount of heat stored in the material in Joules;  $C_p$  which is a function of temperature, is the specific heat capacity of the storage material, in J/(kg.K);  $m$  is mass of the storage material, in kg; and  $T_f$  and  $T_i$  are the final and initial temperatures in K respectively.  $Q_s$  is a function of only temperature. Thus, for a given storage material, temperature is the only independent variable that influences the heat storage of the medium.

According to the Dulong-Petite rule, specific heat per mole of a pure solids (especially heavy elements) is approximately  $3R$ , where  $R$  is the molar gas constant ( $R=8.314$  kJ/kmolK). The molar thermal energy stored in pure substances (solids) is given by;

$$Q_{mol} \approx 3R \cdot \Delta T \quad (8)$$

$Q_{mol}$  is in kJ/kmol and the molar mass is given by  $M$  (kg/kmol).

$$Q_s = \frac{m \cdot Q_{mol}}{M} = \frac{3R \cdot m \cdot \Delta T}{M} \quad (9)$$

The quality of the heat is therefore defined as the amount of the useful heat that can be applied and it all about the temperature. This heat is called exergy, and it is given by;

$$E_x = Q_{12} - \frac{T_a}{T} Q_{12} \quad (10)$$

Where  $T_a$  is the ambient air temperature in Kelvin and  $E_x$  is in Joules.

### 2.2.1 Materials for sensible heat storage

An example of high temperature storage materials for sensible heat is the molten alkali metals such as sodium or potassium. Advantages of these metals such as high thermal conductivities and high thermal stabilities is what makes them suitable in nuclear reactor designs [18]. Nonetheless, the high reactivity of the alkali metals with air is one limitation to its use. Much more abundant sensible heat storage materials used are water, molten salt and thermal oil.

Table 2.2. Illustrates the properties of various solid-liquid materials for sensible heat storage. The table shows that water as a storage medium is a very good competitive due to its high specific heat capacity and ability to absorb low grade heat energy.

**TABLE 2.2 PROPERTIES OF SOLID-LIQUID MATERIALS FOR SENSIBLE HEAT STORAGE [19].**

Material	Density ( $\rho$ ), kg/m <sup>3</sup>	Specific Heat ( $C_p$ ), KJ/kgK	Melting point (°C)	Thermal conductivity (k) at 20°C, W/mK
Water	1000	4.19	0	0.5918
Aluminum	2707	0.896	660	235
Cast iron	7900	0.837	1150	29.3
Brick	1600	0.840	1800	1.04
Concrete	2240	0.880	1000	1.7
Sodium	927	1.385	97.9	85.84
Granite	2640	0.820	1215	1.7 – 4.0
Sand	1555	0.800	1500	0.15 – 0.25

Water is the most used as a storage material in sensible heat storage systems. Hot water tank is one of the common thermal energy storage technologies. Other TES technologies such as Underground thermal energy storage and Packed-Bed thermal energy storage will be discussed in detailed later.

### **2.2.2 Applications**

One of the most common application in sensible heat storage is the water storage tank. Cogeneration and solar energy are common means of energy supply in water storage systems. There have been numerous applications of sensible heat storage technology, including nuclear power plants and even agriculture [18]. Ayyappan S. reported the improvement in a natural convection solar greenhouse dryer using sensible heat storage. The sensible heat materials investigated includes concrete, rock and sand. Depending on the thermal material used, the

technology increased the daytime temperature by 12°C to 16 °C and night time temperature by (3 - 6) °C [19]. Other applications include steam accumulator, thermal oil systems, molten salt systems and graphite energy systems.

### 2.3 LATENT HEAT ENERGY STORAGE

Basically, phase changing materials change their physical state to either store or release energy. For this reason, there is always volume change as well as change in energy storage densities during the charge and discharge phases. As demonstrated in the figure 3 above, the phase change material used must first store or release energy sensibly during the charging or discharging phase. The storage capacity of a PCM is computed by;

$$Q_l = \int_{T_i}^{T_m} mC_{ps}dT + mf\Delta H_l + \int_{T_m}^{T_f} mC_{pl}dT \quad (11)$$

Where  $T_m$  is the melting temperature in °C,  $T_i$  and  $T_f$  are initial and final temperatures respectively in °C,  $m$  is mass of the PCM in kg,  $C_{pl}$  is the specific heat capacity of phase between  $T_i$  and  $T_m$ , in J/(kgK),  $\Delta H_l$  is the latent heat of fusion in J/kg,  $C_{ps}$  is the heat capacity from the phase between  $T_f$  and  $T_m$ , in J/(kgK) and  $f$  is the fraction melted.

Charalambos et al [20], Kinga P. [21], and Ming Lui et al [14] have stated certain properties that an ideal phase changing material should meet in chemical, thermophysical, kinetic and economic properties. These properties, shown in Table 3 determine the performance of the TES system.

Table 2.3. Properties for selecting PCMs.

Chemical Properties	Thermophysical	Kinetic Properties	Economic properties
<ul style="list-style-type: none"> <li>• Long term chemical stability.</li> <li>• No degradation after large charge and discharge cycles.</li> <li>• No corrosiveness</li> <li>• No toxic material released during operation.</li> <li>• Fully reversible cycles.</li> </ul>	<ul style="list-style-type: none"> <li>• High density</li> <li>• Favorable phase equilibrium</li> <li>• High thermal conductivity of both phases.</li> <li>• High specific heat.</li> <li>• Congruent melting.</li> <li>• Small volume changes.</li> <li>• High latent heat of fusion.</li> <li>• Low vapor pressure</li> </ul>	<ul style="list-style-type: none"> <li>• High nucleation rate.</li> <li>• High rate of crystallization.</li> <li>• No supercooling</li> </ul>	<ul style="list-style-type: none"> <li>• Cost effective</li> <li>• Ability to be implemented on a large scale</li> <li>• Readily available.</li> </ul>

### 2.3.1 Classification of phase changing materials

Phase change materials are usually classified into organic, inorganic, and eutectic, Figure 3 [22]. Despite the large number of phase change material which satisfies a wide range of temperatures, it is still necessary that PCM materials receives relevant improvements and research from the efficiency and melting point standpoint. Myriads attempts have been made to compensate poor physical properties with effective and reliable system design; example, we can suppress undercooling by adding nucleating agents into storage media and also, the thermal conductivity of the PCM can be improved by employing metallic fins.

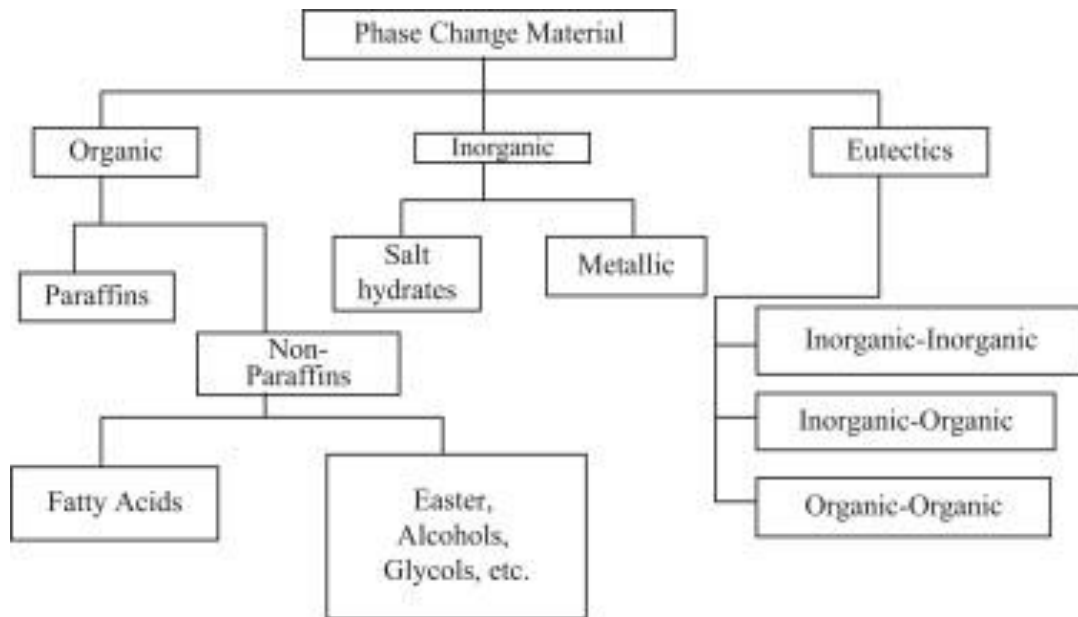


Figure 2.3. Classification of PCM and some examples [22].

In inorganic PCMs, salt hydrates are the most researched. However, its greatest impedance in its development is supercooling and phase separation. Several studies have been done on its morphology and its nucleation rate and it has been observed that, using faster nucleating materials and gelled mixtures improved its properties [23]. This development improves the heat transfer characteristics of the material or mixture but its degradation also increases with time [24]. Sodium acetate trihydrate was studied by Wada et al. and its decrease in heat storage capacity investigated. Sodium phosphate decahydrate was used as a nucleating agent and they reported that, after 500 thermal cycles, the performance of the thickened material showed little degradation [22].



Eutectics are mixtures of two or more substances whose melting and freezing points can be superimposed. They can be grouped based on the type of substance mixed, resulting in organic eutectic, inorganic eutectic or both. Organic eutectics is the combination of organic compounds. Many studies have been done in this type of PCMs. Joshi et al studied ammonium nitrate eutectic for solar heating applications and investigated the enthalpy change for 1100 thermal cycles, which they found to have decreased by just 5% [25][26]. Sari and Zhang et al also studied solid – liquid phase transitions in palmitic, stearic and lauric acids as well as their binary systems using DSC and Fourier transform infrared spectroscopy (FTIR). They concluded that the thermal properties were stable after 100 thermal cycles and the single acids had higher fusion points than the combined mixture [27]. The inorganic eutectics, also known as the salt-based eutectics, thus eutectics made from salts hydrates have also been researched. Notable ones include Kimura and Kai who investigated the thermal stability of these mixtures, their degradation (for 1000 thermal cycles) and for green house purposes [28].

### **2.3.2 CHARACTERIZATION OF LHS MATERIALS**

Differential Scanning Calorimetry (DSC) and Differential Thermal Analysis (DTA), thermo-analytical techniques measure the difference between the heat energy needed to cause a change in temperature between a reference sample and the PCM material under investigation. A typical reference sample used is Alumina ( $Al_2O_3$ ) [24]. Latent heat systems are temperature specific, meaning that they are designed for a specific temperature or temperature range application. For this reason, the DSC or DTA is used to measure the melting temperature of the PCM as the material is heated at a constant rate. This in effect determine the Peak, On-set and End-set temperatures. The area under the melting and peak temperatures is used to calculate the Latent heat of fusion. This technique enables efficient calculation of the energy stored or released by the LHS during charging and discharging respectively. Drop Calorimeter is also used in the determination of the Latent heat of the PCM but this technique is time consuming and has low level of accuracy.

The thermal conductivity, which is directly linked to the heat transfer during the energy transfer process is calculated using the Hot-wire, Laser flash or the Hot disk techniques. The specific heat capacity, an important factor which indicates how much energy can be stored in a given mass of Latent heat material is normally measured using three methods. These methods include the

dynamic, areas and isostep methods. Fourier Transform Infra-Red Spectroscopy (FTIR) and X-ray diffraction techniques are used to determine the chemical degradation of the Latent heat material. This is further used to calculate the durability of the PCM and the LHS as a whole. The test for degradation performed by the FTIR and the XRD include the Aging test, Flammability test and the corrosion and compatibility test. Thermal cyclability is also done to measure the stability of PCM material after several mechanical and thermal cycles, in order to determine usage time of the LHS material before deterioration begins.

### **2.3.3 FACTORS INFLUENCING LHS SYSTEMS**

As stated above, there are several factors that influence the performance and possible commercialization of the latent heat system. Importance and effects of these factors in LHS systems are reported in many studies which have directed the development of the TES systems. Zakir Khan et al investigated the influence of the PCM chamber and its orientation, as well as the employment of fins on the thermo-physical performance of the TES system[29].

#### **2.3.3.1 Temperature Range**

This is the first parameter to consider when designing a Latent Heat System since the working temperature determines its application. As stated above and seen from Figure 2, before latent heat storage is sensible heat. This implies that for a specific application, the sensible heat storage or release should be considered as well. Lots of research have been done on phase change materials and their melting temperatures and has been found to range from -33 °C to beyond 1600 °C [29][30][31][32]. This wide range of temperature and relatively low melting temperatures gives the LHS systems diverse applicability as well as the ability to utilize low grade of heat energy. However in building applications, thermal comfort is of great importance, making PCMs with phase transition temperatures between 16 °C to 25 °C preferred [30]. A research on Al-Si eutectic alloy by Zhengyun et al showed that after 1000 thermal cycles, the melting temperature and the latent heat of the PCM did not change [31]. This demonstrate a good thermal stability and its potential to be used for long term storage applications. Multiple PCM used together has reported to yield constant heat flux which means constant temperature difference which improves the thermal storage performance of the LHS system [29].

### 2.3.3.2 Heat Transfer Enhancement

There are several methods to improve the heat transfer property in PCMs but they are usually classified into three; enhancement by thermodynamic analysis and optimization and using multiple PCM, increasing surface area for heat transfer using fine tubes and encapsulated PCMs, and the addition of Nano-additives and porous media [20].

### 2.3.4 Basic PCM models

Phase change systems have complex structure and behavior making them very difficult to predict. Their boundaries and displacement rate are non-linear in nature during absorption or removal of heat. The Stephen equation is used to describe this process [33];

$$H_l \rho \left( \frac{ds(t)}{dt} \right) = k_s \left( \frac{\partial T_s}{\partial t} \right) - k_l \left( \frac{\partial T_l}{\partial t} \right) \quad (12)$$

Where  $H_l$  is the latent heat of fusion,  $s(t)$  is the surface position,  $k$  is the thermal conductivity,  $T$  is temperature,  $t$  is time,  $\rho$  is the density and  $l$  and  $s$  indexes represent the liquid and the solid phases respectively. Other models such as one by Abdel and Morrison have been developed for describing the behavior of PCMs [34].

## 2.4 SORPTION

When a liquid or gaseous phase of a component actively binds with the surface of a porous material, the process is termed adsorption. This is different from absorption in the sense that adsorption is when a molecule binds two-dimensionally to a matrix where in absorption, the absorbent material penetrates a three-dimensional matrix [35]. This process is an exothermic reaction; thus, energy is released when there is adsorption. This is the useful energy obtained with the sorption process. The energy produced depends on the effectiveness of the binding between the adsorbate and the adsorbent, the size and number of the pores, the storage capacity of the adsorbent among other properties [36]. The reverse occurs when there is desorption. During this process, heat (equal or higher than required for adsorption) is supplied to the adsorbent and this

causes the ejection of adsorbed components (water vapor for this study) from the active sites of the adsorbent surface (see Fig 2.4 below). Hence this is an endothermic process. The desorption process is called the charging phase, where high temperature heat is supplied and the adsorption process is called the discharging phase where air moist air is supplied. The Figure 2.4 below demonstrates the desorption and the adsorption process that occurs during solid sorption. Absorption is similar to adsorption only that the adsorbent is a liquid instead of a solid.

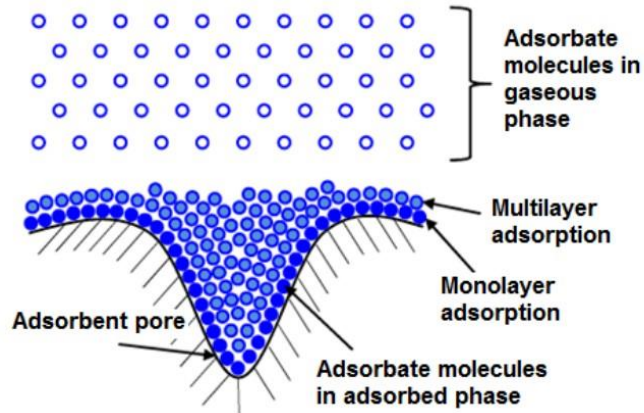


Figure 2.4 diagram showing molecular sorption and solid sorption [117].

### 2.4.1 Opened and closed sorption systems

This basically distinguishes sorption systems based on the mass transfer between the system and the surrounding. They are either closed or opened, for which the closed system is normally an absorption or adsorption systems while the open system is usually a desiccant system [37]. For the opened sorption systems, moist air is supplied to the adsorbent or absorbent which causes the release of heat of sorption. This is also sometimes referred to as humidification process. After the adsorption or absorption process, the humidity of moist air decreases and the temperature increases. The change in humidity is more needed and investigated with absorption process and for the case of adsorption, the temperature rises very high and it is of most interest. During the desorption process for an opened storage system, hot air is supplied to the absorbent or adsorbent to release moisture and heat of condensation. After the desorption process, the adsorbent/absorbent can be stored in its charged state until adsorption. Determination of the thermal energy storage is by separating the adsorption and the desorption processes.

For a closed sorption system, system operating pressure is easily regulated there is no exchange or air between the system and the surrounding. Figure 2.5 below shows water vapor as the adsorbate and the working process of the closed solid sorption process. During the adsorption, heat of sorption must be taken away from the adsorbent at the same time heat of evaporation is supplied to the evaporator. Likewise, during the charging process (desorption), heat of desorption has to be delivered to the adsorbent at the same time heat of condensation is ejected from the condenser. These two processes should continue, least thermodynamic equilibrium is reached and the system stops operation.

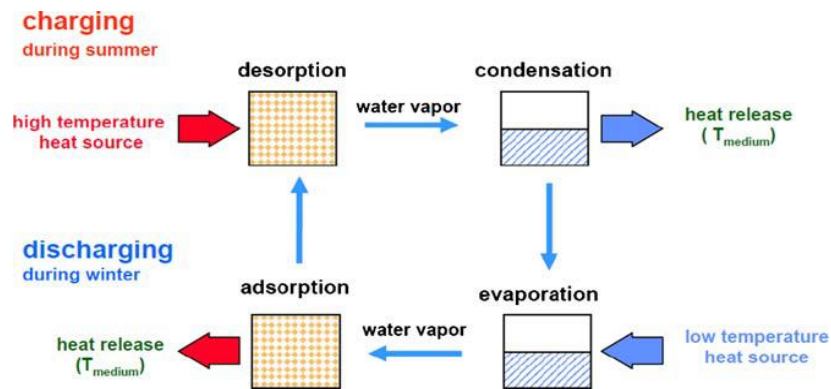


Figure 2.5 Depiction of a closed energy storage system [38].

The major drawback to the closed sorption systems is the vapor and the heat transfer to and the adsorbent/absorber due to their high energy density. One way to solve this problem is to implement advanced heat exchangers. However closed sorption system is able to yield much lower temperatures as higher temperatures than the open sorption systems. Moreover, Michel et al stated that, a comparison between open and closed system indicated that mass transfer is the major limitation for the performance of open systems [39]. Further investigation by Mette et al on zeolite 13X in open sorption concluded that, the heat and mass transfer occurring in the system are strongly coupled [40].

## 2.4.2 Classification of Sorption

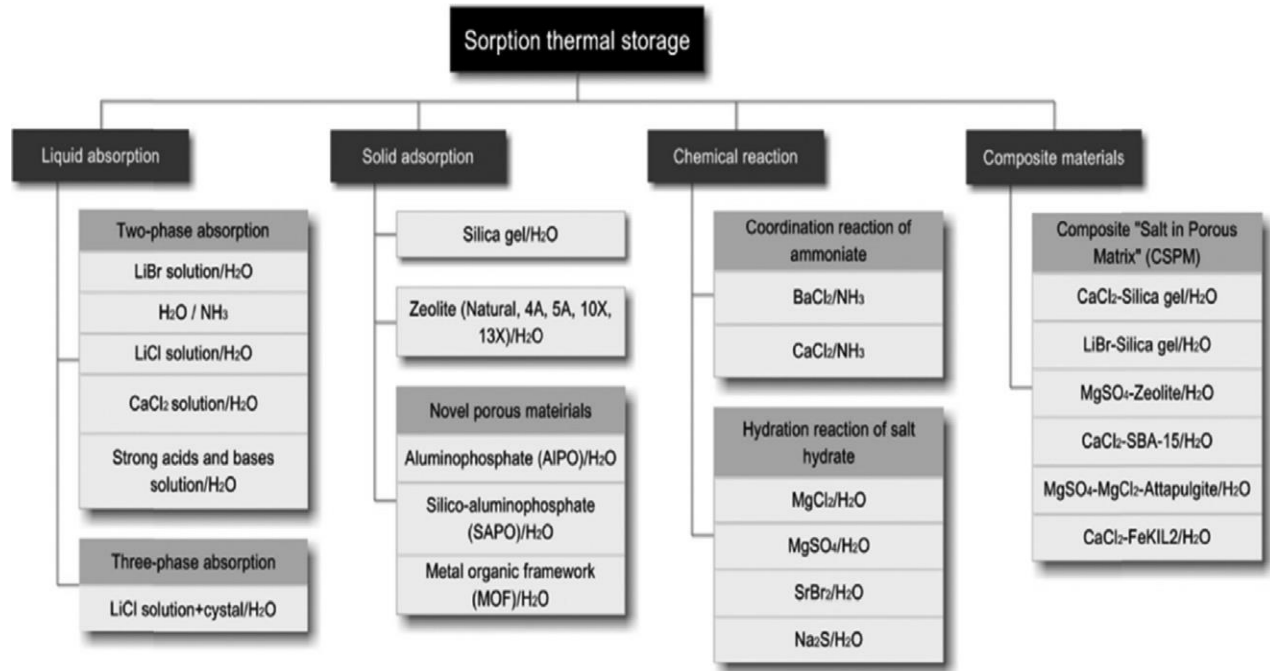


Figure 2.6 Diagram of Sorptive and Chemical thermal energy storage methods [41].

### 2.4.2.1 Absorption

Absorption systems exist only in closed systems and their mode of operation is comparable to the closed adsorption systems, having an evaporator and a condenser in common. One reason is due to the fact that for closed systems, the humidity is of great importance as stated in subsection 2.3 and to also prevent mass loss of the absorbent. Several absorbent materials have been investigated; one being aqueous  $\text{CaCl}_2$ , which combine both sensible heat storage and absorption to attain energy density of  $105 \text{ kWh/m}^3$  [37]. In an absorption process for a  $\text{NaOH}/\text{H}_2\text{O}$  single stage system, charging phase begins by solar heat being supplied to the regenerator which contains the low concentration solution. This causes desorption of water vapor which then flows to the condenser to be condensed and stored in a storage tank. During the discharging phase, this same stored water is sent to the evaporator to be evaporated using a low-grade heat. The water vapor is absorbed by a concentrated  $\text{NaOH}$  which then releases heat since it is an exothermic reaction. This storage process is able to yield storage density between  $170 \text{ kWh/m}^3 - 400 \text{ kWh/m}^3$  [37]. Double stage

systems have also been investigated and it has been noticed to reduce heat needed for charging and improved heat produced during discharging.

### **2.4.2.2 Adsorption**

This method of thermal storage is capable of storing energy for long term purposes as well as supporting intermittent cycle operation. Moreover, adsorption systems are capable of utilizing low grade energy during the charging phase and this has made them attractive and their waste energy utilization widely studied [42]. Absorption systems have noticeable higher COP and cheaper than adsorption systems. This is why adsorption systems have much limited commercialization relative to the absorption systems. However, adsorption systems are capable of utilizing a much lower grade heat for charging and discharging cycles. Adsorption systems are normally grouped into two (based on their interaction effects), one with only physical interactions (physisorption) and the other with chemical interactions (chemisorption).

#### **2.4.2.2.1 Chemical Adsorption**

Chemical adsorption is caused by bond formation between the active sites of the adsorbent surface and the adsorbate. This is a characteristic of atom rearrangement or fracture and or electron transfer. After this interaction, the adsorbent and the adsorbate never keep their initial state. It is an exothermic reaction with very high reaction enthalpies due to the formation of chemical bonds. Nonetheless, the reaction normally occurs more slowly and the needed activation energy is quite high. Since the bond formation between the adsorbate and adsorbent is strongest with the closest atoms (close range atoms), the heat of adsorption of the first monolayer is strongest. Figure 2.7 below depicts Monolayer adsorption on the surface of the adsorbent for a chemisorption process and the Vander Waal graph depicts the sorption energy as we move into the surface of the material. The negative enthalpy shows that it is an exothermic process and it varies inversely with distance from the surface (see Fig. 2.8). High enthalpy of sorption is released from the surface of the adsorbent and drastically drops as we move into the material. This is due to the availability of active sites where bond formation and distortion can occur, which is mainly the surface or near surface region of the adsorbent. As we move into the surface of the adsorbent much weaker bonds are formed. This in a nut shell characterizes why chemisorption processes have high enthalpy of

adsorption and considered normally a monolayer adsorption process. Chemisorption give a Morse potential.

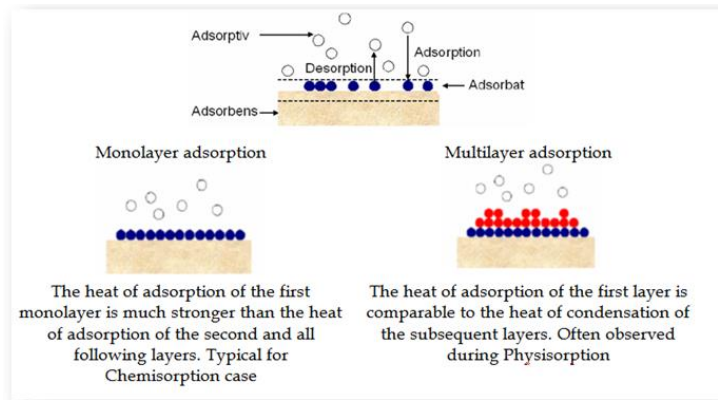


Figure 2.7 a diagram showing monolayer and multilayer adsorption [43].

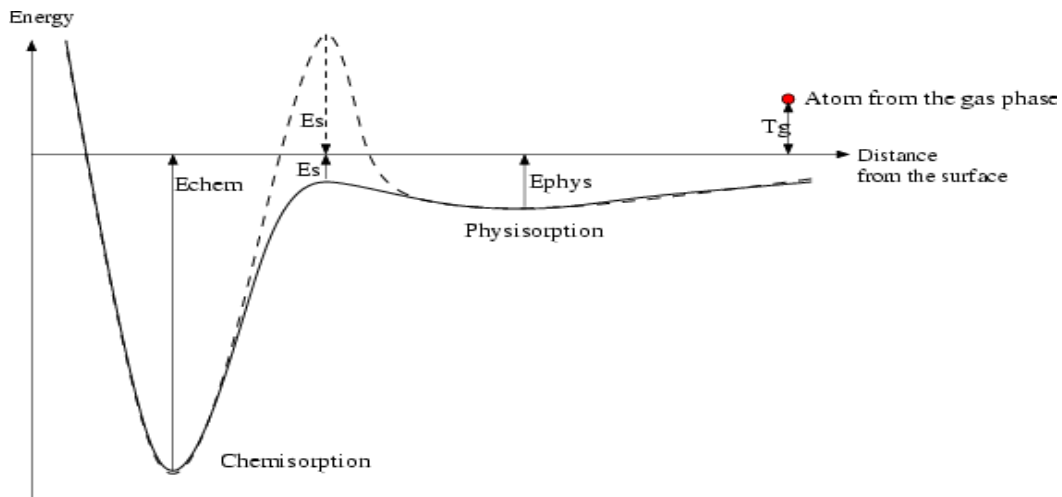


Figure 2.8 Diagram showing chemisorption and physisorption processes and their relation with distance away from the surface [44].

Moreover, chemical adsorption seems not to be affected by small changes in pressure but favors high temperature and pressures. But there is a decrease in the enthalpy of sorption when the



temperature rises beyond certain limits (see Fig. 2.9 below). It is also highly specific to the kind of adsorbate and increases with increasing surface area of the adsorbent.

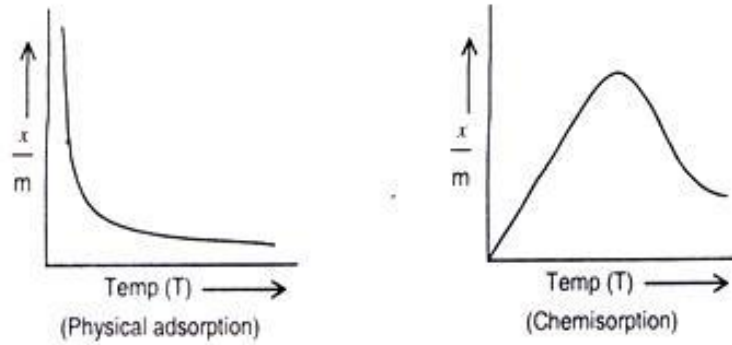


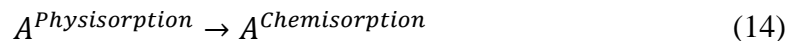
Figure 2.9 Relation of temperature effect on physical adsorption and chemisorption processes [45].

#### 2.4.2.2.1.1 Chemisorption Process

First as the adsorbate comes into contact with the adsorbent mainly through an inelastic collision, it is trapped into the gas-surface potential well if it lacks the energy to leave the surface [46]. This is because the inelastic collision causes momentum loss, which causes the adsorbate to stick unto the surface by the activity of weak forces similar to physisorption.



It then undergoes surface diffusion until it finds a chemisorption potential well where a stronger bond can take place.



The Gibbs energy ( $\Delta G$ ) equation can be applied to study the reaction on the surface of the adsorption and it is given as follows:

$$G(p, T) = U + pV - TS \quad (15)$$

(16)

$$\Delta G = \Delta H - T\Delta S$$

Where  $\Delta H$  is the change in enthalpy in J,  $\Delta S$  is the entropy in J/K, U is internal energy in J, P is pressure in Pa, V is volume in m<sup>3</sup> and T is temperature in K. Thermodynamics shows that for a spontaneous reaction to occur, the Gibbs free energy should be negative ( $\Delta G < 0$ ). And since the adsorbate is initially confined to the surface with minimal mobility, entropy is minimal and enthalpy must be negative which means the reaction is exothermic.

#### **2.4.2.2.2 Physical Adsorption**

Physical adsorption is caused by the weak Van de Waals interactive force between the adsorbate and the active sites of the adsorbent. Physical adsorbents are normally not selective since Van der Waals force are universal, but becomes selective after specific treatments under certain conditions. It has relatively lower enthalpy of adsorption values and occurs with the formation of multilayer on the adsorbent by the adsorbate. Physisorption has an inverse relation with temperature, increase in temperature decreases enthalpy of sorption as show in the Fig. 2.9 above.

Due to its low activation energy, physisorption processes are normally reversible. Like chemisorption, physisorption is an exothermic process which occurs readily at lower temperatures and decreases in sorption enthalpy with increasing temperature. There is also a positive relation between pressure and physisorption processes. Sorption enthalpy increases with increasing pressure and vice versa. Physical adsorption also increases with increasing surface area of the adsorbent and the extent of adsorption is highly dependent on the nature of the adsorbate. Additionally, unlike chemisorption, the heat of adsorption of the first layer in physisorption is highly comparable to that of the second layer.

### 2.4.2.2.1 Physisorption Process

Most adsorptive separation process depend mainly on physisorption rather than chemical adsorption. The sorption heat derived from this process determines the strength of the interfacial bonding between the adsorbent and the adsorbate. As stated above, physical sorption is exothermic just like chemisorption process hence, the Gibbs free energy follows.

There are two major types of forces present during physical adsorption and they include, electrostatic interactions (this comprises of the dipole, polarization and quadrupole interactions) and Van der Waals forces (which is the repulsive or attractive forces). The most prevalent among these forces is the Van Der Waals interaction, with the electrostatic interactive forces contributing only when the adsorbent has an ionic structure. Zeolite, which has ionic structure produces high heat of sorption (25-30 kcal/mol) due to the dipole interaction of the H<sub>2</sub>O molecule and the zeolite adsorbent [47].

#### Repulsion-Dispersion energy

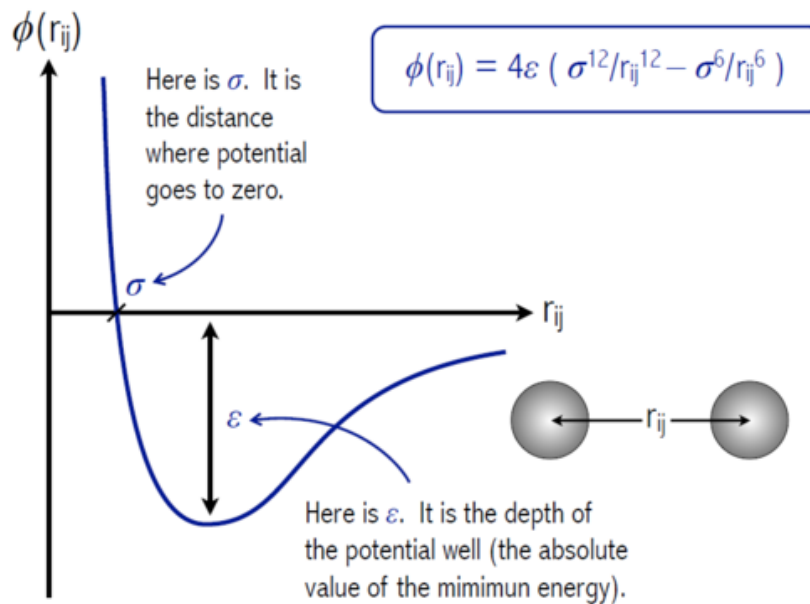


Figure 2.10 Illustration of the Lennard – Jones potential [48].

For two isolated molecules M1 and M2 show in the Figure2.10 above, the attractive potential ( $\phi_A$ ) that exist between them is given by:

$$\phi_A = -\frac{A_1}{r_{1-2}^6} - \frac{A_2}{r_{1-2}^8} - \frac{A_3}{r_{1-2}^{10}} \quad (17)$$

where  $r_{1-2}$  is the distance between the two molecules and  $A_1, A_2, A_3$  are constants. The coupling interactions between instantaneous induced dipole given by the first term of the equation is the most dominant. The second and third terms of the equation are the induced dipole-induced quadrupole interaction and induced quadrupole-induced quadrupole interactions. The short-range repulsive energy is also given by;

$$\phi_R = \frac{B}{r_{1-2}^{12}} \quad (18)$$

Summing both equations (17) and (18) and neglecting higher order terms results in the Lennard-Jones potential ( $\phi_{LD}$ );

$$\phi_{LD} = 4\varepsilon \left[ \left( \frac{\sigma_{1-2}}{r} \right)^{12} + \left( \frac{\sigma_{1-2}}{r} \right)^6 \right] = -\frac{A}{r^6} + \frac{B}{r^{12}} \quad (19)$$

where  $\sigma$  and  $\varepsilon$  are characteristic constants, dependent on the type molecule under study, A and B are  $4\sigma\varepsilon^6$  and  $4\sigma\varepsilon^{12}$  respectively. The Lennard-Jones potential is shown in the diagram above. The two constants  $\sigma$  and  $\varepsilon$  are given as follows;

$$\sigma_{1-2} = \frac{1}{2} (\sigma_1 + \sigma_2), \quad \varepsilon_{1-2} = \sqrt{\varepsilon_1 \varepsilon_2} \quad (20)$$

### *Electrostatic Energies*

Considering ionic adsorbents, there is a significant electric field on the active surface which contributes to the total energy heat adsorbed. A typical example is the zeolite and its total heat of sorption given by contribution from the Lennard-Jones potential ( $\phi$ ), dipole interactions ( $\phi_d$ ), field gradient quadrupole interaction ( $\phi_Q$ ) and the polarizations ( $\phi_p$ ).

$$\phi_d = -\mu E \quad (21)$$

$$\phi_p = -\frac{1}{2} \alpha E^2 \quad (22)$$

$$\phi_Q = -\frac{1}{2} Q \frac{\delta E}{\delta r} \quad (23)$$

E is the electric field, Q is the quadrupole moment,  $\mu$  is the dipole and the  $\alpha$  is the polarizability. Q can be further determined by the equation;

$$Q = \frac{1}{1} \int q(\rho, \theta) (3 \cos^2 \theta - 1) \rho^2 dV \quad (24)$$

Where  $q(\rho, \theta)$  is the local charge density and it is integrated over the whole volume of molecule, hence for an adsorbent which is ionic in nature, the overall potential is given as the summation of all interacting energies:

$$\phi = \phi_A + \phi_R + \phi_P + \phi_d + \phi_s + \phi_Q \quad (25)$$

The first two terms give the Lennard-Jones potential and  $\phi_s$  is the sorbate-sorbate interaction.

### 2.4.3 Sorption Materials

#### 2.4.3.1 Absorption materials and systems

Lithium bromide/water and water-ammonia are the two major absorption systems and extensive work has been done on them [49][50][51]. Both absorptions systems have their advantages and disadvantages. The H<sub>2</sub>O/NH<sub>3</sub> has evaporative temperature below 0 °C but it is very toxic. Another disadvantage is that, there is a need of a column of rectifier when operating at high temperatures [49]. The H<sub>2</sub>O/NH<sub>3</sub> system can have an outflow temperature as low as -60 °C due to the fact that

NH<sub>3</sub> is a refrigerant [37]. Li/H<sub>2</sub>O absorption system on the other hand is non-toxic and environmentally friendly, has relatively low operation pressures, has high coefficient of performance (COP) and large latent heat of vaporization. However, this system is expensive and there exist a high risk of congelation [52]. Although both have similar operating principles, Li/H<sub>2</sub>O are mostly suitable for air-conditioning purposes and H<sub>2</sub>O/NH<sub>3</sub> for refrigeration applications. High temperature is needed during the discharging phase for a NaOH/H<sub>2</sub>O system. However, low grade heat (150 °C) can be used to charge the system and the energy density of the system can be as high as 900MJ/m<sup>3</sup> [53]. Other absorption materials and systems including metal chloride solutions such as LiCl and CaCl<sub>2</sub> have been implemented in open dehumidification and absorption storage systems [54]. Further research stated that it was not economical for seasonal storage due to its high cost.

#### **2.4.3.2 Adsorption Materials**

The sorption material used for the energy storage is the core of the storage system, thereby having the largest effect on the net efficiency, cost and repeatability of the system. Myriad sorption materials have been studied with certain properties taking preference. These includes low charging temperatures, high sorption capacity, Non-toxic material, environmentally friendly, non-corrosive, low cost, good mechanical and thermal stability, high energy storage density and good heat and mass transfer [36][55].

##### **2.4.3.2.1 Chemical adsorbents**

The working mechanism of chemical adsorbents is by valence force interaction between the adsorbate and the surface of the adsorbent at favorable conditions. In general, chemical adsorbents have more efficient adsorption kinetics (thus they have higher rates of adsorption) than physical adsorbents [55][56]. However, chemical adsorbents undergo agglomeration and swelling which impedes the heat and mass transfer performance of the TES system. Moreover, it has lower stability due to chemical change of the adsorbent without the possibility of returning to its initial state [57]. For this this reason it is difficult to employ chemical adsorbents where cycle repeatability is needed.

## **Salt hydrates**

This is a huge group of chemical adsorbents and they include Calcium hydrates ( $\text{CaCl}_2 \cdot 4\text{H}_2\text{O}$ ), Iron III chloride ( $\text{FeCl}_3 \cdot 6\text{H}_2\text{O}$ ), Calcium bromide ( $\text{CaBr}_2 \cdot 6\text{H}_2\text{O}$ ), just to mention a few. Salt hydrates are inorganic crystals that have water molecules bonded to it in a definite ratio. The bonding of the water molecules is to a metal complex or to a metal center. A common example of a salt hydrate is the cobalt chloride which changes color from blue to red upon hydration. The water that bonds to these hydrates is called water of hydration. These salts hydrate form when a saturated salt solution crystallizes at a given temperature and pressure. Salt hydrates, due to their promising long-term usage have attracted attention as candidates for TES systems.

## **Metal Hydrides**

The reaction of hydrogen with other elements can be grouped into four major types of hydrides; metal hydrides, salt hydrides, non-metal molecular hybrids, and the covalent polymerized hybrids. For a metal hydride to form, a hydrogen atom must enter the crystal lattice of a parent metal in a reaction with a transition metal. These usually have very high chemical activity and low electronegativity. Salt hydrides (example  $\text{LiH}$ ,  $\text{CaH}_2$ ) are formed by the reaction of the group I and II with hydrogen [58][59]. Salt hydrides have a larger density than metal hydrides and even pure metals. This is because unlike salt hydrides, metal hydrides expands during adsorption [60]. Most research with best performance for Metal hydrides used hydrogen as its adsorbate [60].

## **Metal Chlorides**

A coordinating compound is formed from a complexation reaction between a refrigerant and a metal chloride. Some metal chlorides include but not limited to barium chloride, magnesium chloride, calcium chloride and copper chloride [61]. For a coordinate bond to occur, the central atom bonds with a lone pair of electrons from a ligand [62]. The strength of this coordinate bond formed infer the behavior of adsorbate adsorbent pair and their performance in a TES system. Most metal chlorides have a good performance with ammonia as the adsorbate. However metal chlorides

have a major drawback which is agglomeration. This impedes performance of the system with metal chloride as adsorbent due to less efficient heat and mass transfer.

## **Metal Oxides**

Oxygen is usually the adsorbate in a system where metal oxide serves as an adsorbent. Just like Metal chlorides, agglomeration also occurs when metal oxides are used as adsorbent. Nevertheless, the performance of the adsorption by the adsorbent is dependent on the unsaturated degree of coordination, surface bond direction of the adsorbent, the coordination number of the metal ion, the active center arrangement, symmetric characteristics of the ligand, among other things [60][62].

### **2.4.3.2.2 Physical adsorbents**

Due to certain stringent requirements for effective adsorption capacity, the required pore diameters ranges from few Angstroms to few tens of Angstroms. This includes advanced adsorbents such as zeolites or other aluminosilicates to more traditional ones such as silica gel, alumina and activated carbon. The major differences between the two kinds of adsorbents is the mean micropore distribution and the micropore size. However, zeolites have no distribution of pore size, its crystalline structure controls the micropore size. This is why zeolites is sometimes classified as a separate class of adsorbent and usually have high heats of adsorption similar to that of chemisorption.

## **Activated Alumina**

When bauxite ( $\text{Al}_2\text{O}_3 \cdot 3\text{H}_2\text{O}$ ) or its monohydrate is exposed to high temperatures, dehydration followed by recrystallization occurs, forming a porous high surface area aluminum oxide called activated alumina. This material has an amphoteric nature and exhibits much stronger surface polarity than silica gel. The adsorption capacity of silica is higher than activated alumina at room temperature. The affinity for water for both adsorbates is also similar at room temperature. However, at elevated temperatures the capacity of silica falls below that of activated alumina.



## **Activated Carbon**

Activated carbon is usually produced by first thermally decomposing carbonaceous material followed by carbon dioxide or steam activation at temperatures in the range of 700 °C to 1000 °C [63]. During pyrolysis (incomplete combustion), tarry carbonization products which are formed are released by activation which thereby open the pores. The micropores of the activated alumina is caused by microcrystalline graphite which are randomly stacked together. The pore size distribution is highly dependent on the conditions for pyrolysis and activation. Due to the fact that carbon surface has a high degree of nonpolar nature, carbon adsorbents are usually organophilic and hydrophobic. Hence its applications in water purification and solvent recovery systems. Activated carbons employed in gaseous phase is usually have smaller pores than that employed in liquid phase. Jribi et al investigated adsorption isotherms and kinetics of CO<sub>2</sub> onto activated carbon with gravimetric apparatus at pressures from 4 – 7 MPa and temperatures from 30 °C to 70 °C, and concluded that there was an agreement with measurements made with the volumetric apparatus [64]. Research shows that the hydrocarbon transport in activated carbon adsorbent is mostly by surface flow and Knudsen flow [65]. Microwave assisted reduction and oxidation with nitric acid was used to modify activated carbon and the adsorption isotherms and energy was measured by Xin et al. They reported that in low relative humidity, the activated carbon had increased adsorption capacity of water and the desorption activation energy with increased oxidation [66].

## **Carbon Molecular Sieves**

Generally, the adsorbate adsorbed is independent on the size of the adsorbent when it comes to activated carbon. However, increase in research in this adsorbent has made it possible to reduce the micropore size and its distribution such that, they tend to act as molecular sieves [67]. Various methods have been used to synthesis carbon molecular sieves with one of the most prominent method being the vapor deposition method. This involves the deposition of pyrolytic carbon at the tip (mouth) of the pore, reducing the entrance of the pore for a desired adsorbate size. Agents such as benzene, methane, cyclohexene, acetylene and methyl pentane have been widely used in carbon deposition with benzene yielding the best results [68][69]. Using oxidation and other thermal treatments with precursor materials such as hard coal or anthracite, pore diameters in a range of 4 to 9 Å can be achieved [47]. Their high selectivity, low cost and high chemical resistance has made

them good candidates for gas separations, as such they have been widely used in this field [70][71][72]. Xiong et al studied the level of upgrade of coal mine methane with carbon molecular sieves and concluded that, coal mine methane would benefit from reaching optimal balance between adsorption equilibrium and kinetics when the adsorbent is used [71].

## **Zeolites**

They are aluminosilicates which are hydrated and are formed from interlinked tetrahedra of silica ( $\text{SiO}_4$ ) and alumina ( $\text{AlO}_4$ ). Zeolites, usually called the boiling rock, have water molecules trapped in between them and based on the formation process or synthesis process used, they form a myriad of crystalline structures. About 40 different zeolites are found naturally in nature and these include the mordenite, clinoptilolite, faujasite, chabazite among others [73]. Among the dozens of zeolites synthesized, the most common one is the zeolite A which has so many applications such as drug delivery to detergents. The Alumina and silica which are interconnected together by means of an oxygen atom, forming a lattice containing pores. Unlike other adsorbent with a distribution of pore sizes, zeolites have almost precise pore dimension and this sets them apart. In the zeolite framework of secondary building blocks and polyhedral, each aluminum introduces one negative charge ion of which and exchangeable cation will be needed to balance it. The properties of the exchangeable cation determine the adsorptive properties of the zeolite. Zeolites generally have about 3300 J/kg to 4200 J/kg sorption heat and a regeneration temperature range of 250 °C to 300 °C [55].

Considering the structure of Zeolite A, shown in Figure 2.11a below, the cell consists of four-membered oxygen rings connecting eight sodalite cages at the corners of a cube. There are about 24 tetrahedral units in each cell with about 12 univalent exchangeable cations, due to the almost 1:1 ratio of Silica to Alumina in zeolite A. faujasite and zeolite X and Y all have a similar structure with a unit cell containing 192 silica ( $\text{SiO}_4$ ) and alumina ( $\text{AlO}_4$ ) tetrahedral units and 8 cages and shown in below (see Fig. 2.11). The difference in the X and Y zeolites are in the ratio of silica to alumina, which is larger for Y than X. This directly shows the effect on the number of exchangeable univalent cations which is larger for X than for Y [74]. The structure has 6 membered oxygen atoms which connects the sodalite tetrahedral unit lattice. It is reported in literature that when loading with adsorbent the equilibrium distribution may change. For this reason, mixing

cationic forms and ion exchange can revamp selectivity and adsorption. Mordenites, as mentioned above are usually naturally occurring but can also be synthesized. The silica to alumina ratio of mordenite is usually 5, but the alumina can greatly be decreased without significant loss of crystallinity through acid leaching. Unlike zeolite A, X, Y and faujasite, mordenite is unidimensional with the channel consisting of 12 membered oxygen rings. Due to its unidimensional characteristic, a small amount of irrelevant material can greatly affect its adsorptive property, hence they are mainly applied in adsorbent of nonhydrocarbon gases where there is mostly no intracrystalline coke formation.

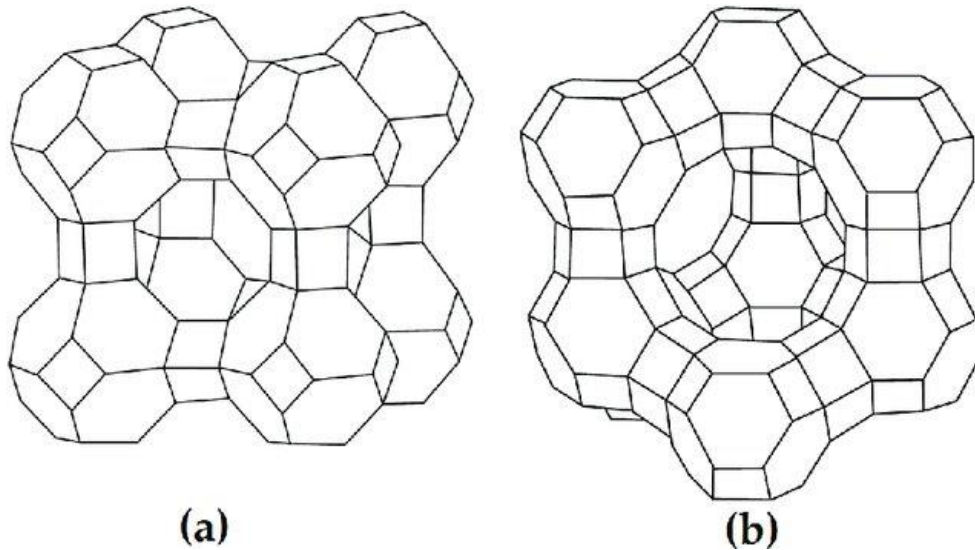


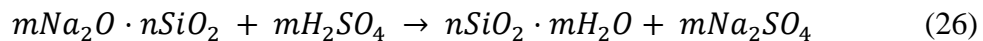
Figure 2.11 Zeolite A and b) faujasite, zeolite X and Y [75].

Mette et al reported the kinetic and adsorption isotherms of zeolite 13X and concluded that it has very fast adsorption kinetics and high water uptake which implies high energy storage density and high thermal power output during adsorption [40]. A study on open adsorption with zeolite as the adsorbent was undertaken by Zettle et al and they concluded that, the process was able to yield an adsorption heat up to 12KWh, with temperature lift up to 36K based on the inlet air conditions [76]. Johannes et al also designed a high energy density zeolite for thermal energy storage. The reactor was able to produce 2250 W for 6 hours [77]. The equilibrium isotherms for N<sub>2</sub> and CO<sub>2</sub>

on potassium chabazite was measured and the paper concluded that potassium chabazite showed and alteration in its thermodynamic behavior, which favors CO<sub>2</sub> adsorption over N<sub>2</sub> adsorption [78]. The research also compared potassium chabazite adsorption, lithium chabazite and sodium chabazite and concluded that for N<sub>2</sub> adsorption, volume filling was better suited for sodium and lithium chabazites. Due to high regeneration temperatures of the zeolites, low grade cannot be used.

#### 2.4.4 SILICA GEL

Silica gel, just like alumina is an amorphous material and is porous and highly active. Silica gel is a highly polar compound and is much softer than silicate glass or quartz. Due to very high specific surface area of silica gel, usually 300 m<sup>2</sup>/g to over 1000 m<sup>2</sup>/g, the gels have very high capacity for adsorption [79]. For this reason, they are used for adsorbing gases and for liquid absorption, though certain low-grade silica gels rupture when exposed to liquid water. If the pore size of the silica gel is increased, there is a decrease in the specific surface area of the silica gel (< 300 m<sup>2</sup>/g), thereby significantly decreasing its adsorption capacity [79]. There are the fine pore size (1.5 to 2.0 nm) and the coarse pore size (4.0 to 5.0 nm) silica gels, although certain methods such as immersing a wet gel in a basic solution can be used to increase the pore sizes to 30 nm [80][79]. Silica gel normally dissolves in strong alkali and hydrofluoric acid. Although there exist several synthesis routes, it is normally manufactured by adding sulfuric acid to sodium silicate (water glass). After the reaction, the process is followed by gelling, washing, desalination, amidation, drying and screening. The reaction is given by:



Where m and n are constants. The water content present which exists as hydroxyl bonds is usually about 5 w%. During the drying step, there is particle agglomeration and pore size creation is dependent on the original particle size. Another thing that can affect the pore size creation is the pH during drying and the availability of cations during the precipitation. Thereby it becomes imperative to control the pH and the cations present to be able to tune the pore size. Pathak et al demonstrated that sorption decreases with increasing ionic strength when they studied the sorption of europium (III) on silica gel [81].

The formation of bonds occurs when neighboring hydroxyl groups join to form water (which is removed), and the resultant is a complex structure. However, the proportion of hydroxyl groups present shows the extent of polarity of the silica gel surface to certain molecules such as water, amines, alcohols and unsaturated hydrocarbons to mention a few. Saturated hydrocarbons on the other hand are hardly adsorbed and this selectivity is why silica gel is also used for the Arosorb process, in the separation of aromatics from naphthene and paraffins [82].

Comparison between the equilibrium water isotherms for silica gel, zeolites and alumina shows that the intracrystalline micropore of the zeolites is completely filled during saturation and this is observed to be similar to all zeolites. This is due to a well-defined micropore size with zeolites, where there is no pore size distribution. Isotherms for alumina and silica gel on the other hand shows a different behavior. Due to the existence of pore size distribution in silica gel and alumina, they show a sustained increase in loading with water vapor pressure. As the pressure of water vapor increases the multilayer adsorption of the surface coalesce to form capillary condensation, increasing the pore size. Therefore, the equilibrium isotherm can give an information on the pore size distribution. Figure 2.12 shows that although CaO, zeolites and other molecular sieves shows very high adsorption rates of water molecules at low relative humidity, silica tend to have the highest overall adsorption capacity at low temperatures [83]. The figure also depicts a steep rise and almost a constant amount of water vapor adsorbed irrespective of the relative humidity for adsorbents such as the molecular sieves and CaO. This shows the no pore size distribution characteristic of these adsorbents.

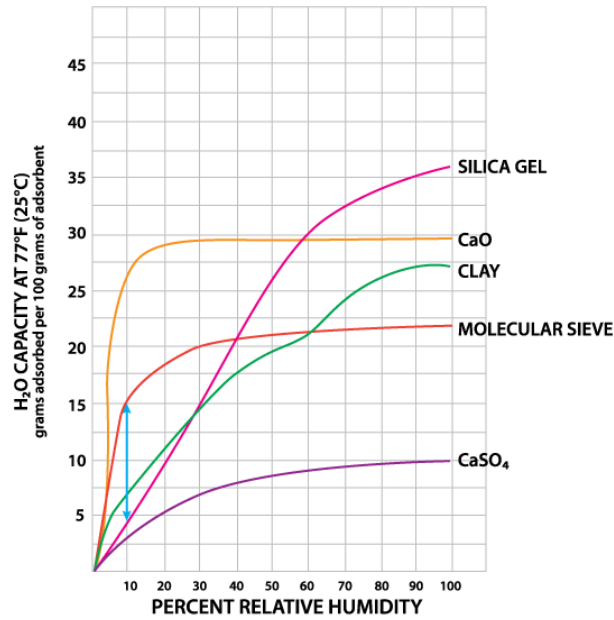


figure 2.12 shows the adsorption rates for silica gel and other adsorbents. it shows the amount of water vapor adsorbed at a given relative humidity [83].

The combined content of water in silica gel is about 0.04 to 0.06 g<sub>vap</sub>/g after heating at 350 °C [84]. If the silica gel loses this water content it becomes hydrophobic, losing its adsorption capacity. The regeneration temperatures of silica gel, montmorillonite and most molecular sieves is illustrated in the Fig. 13 below. The regeneration temperature for silica gel is about 130 °C to 160 °C. It also shows a steep drop in adsorption capacity as temperature increases, for this reason silica gel is best used at room temperatures (25 °C). Molecular sieves on the other hand have high adsorption capacities even at high temperatures.

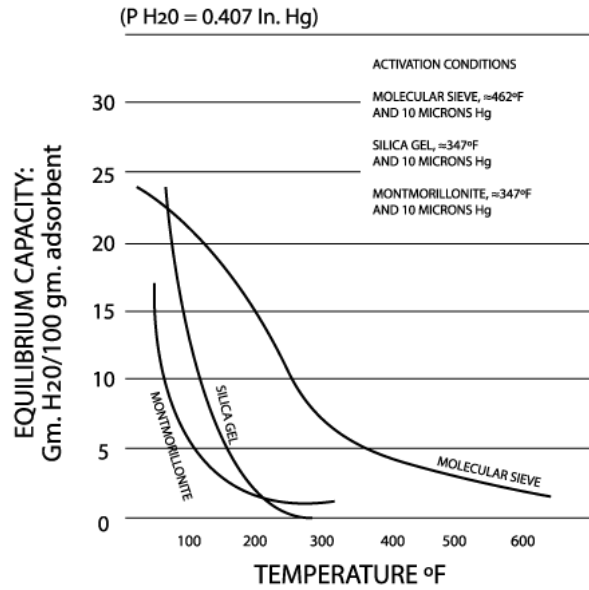


Figure 2.13. Relation between adsorption capacity and temperature [83].

Myriad studies have been performed on silica gel and their performance as an adsorbent in an energy storage system. This encompasses studies from silica gel properties and well as improvement on silica gel sorption energy efficiencies. Yuri et al studied the kinetics of water adsorption on silica grains using a TG differential step method with a pressure range of 6.5 mbar to 34 mbar and 29 °C to 64 °C temperature range. With three grain sizes chosen (0.3 – 0.325 mm, 0.355 – 0.425 mm, 0.8 – 1 mm), they concluded that the influence of temperature, particle size and pressure on the adsorption kinetic studies can be described by the Fickian diffusion model [85]. The apparent diffusivity in the pores of the silica gel was reported to be  $(3.7 - 4.7) \times 10^{-7} \text{ m}^2/\text{s}$ . The pre-exponential factor and the apparent activation energy was also reported to be  $2.9 \times 10^{-4} \text{ m}^2/\text{s}$  and 41.5 KJ/mol respectively [85][86]. In another study, the use of Langmuir – Freundlich isotherm as the adsorption isotherm and the linear driving force (LDF) to approximate the adsorbate uptake, the kinetics of hydrocarbon adsorption on silica gel and activated carbon was investigated. It was reported that, while the hydrocarbon transport in activated carbon is by Surface and Knudsen flow, the transport in silica gel was observed to be mostly Knudsen flow [65]. They also reported that for the three chosen hydrocarbons (methane, ethane and propane), the experimental coefficient correlated well using the following equation:

$$k = \left( \frac{15 \epsilon_p D_{e,ave}}{R_p^2} \right) \left( \frac{C_{af}}{q^* \rho_p} \right) \quad (27)$$

Where  $\epsilon_p$  is the particular adsorbent void fraction,  $D_{e,ave}$  (0.0085 and 0.0018 cm<sup>2</sup>/s for activated carbon and silica gel respectively) is the micropore diffusivity (cm<sup>2</sup>/s), radius of macropore (cm),  $C_{af}$  is the gas-phase concentration of adsorbate at the inlet (mol/cm<sup>3</sup>),  $q^*$  is the equilibrium adsorbed phase concentration (mmol/g) and  $\rho_p$  is the density of the adsorbent. Furthermore, Xia et al reported on the adsorption equilibrium of water on silica gel using the weight method. The pressure set was from 300 Pa to 20000 Pa and temperature from 25 °C to 90 °C, and the data obtained were fitted to Freundlich equation, the Dubinin – Astakhov equation and the modified Freundlich equation [87]. They concluded that the experimental result was in best agreement with the modified Freundlich equation [87]. These equations are discussed in detail. Large deviation was also observed for DA equation and Freundlich equation for low water uptakes when the experimental data was fitted with it. However, Ng et al concluded that the Henry-type equation was suitable for investigating the adsorption isotherm characteristics of Silica-gel/water working pair at adsorption chiller conditions [88]. They also concluded that, type RD silica gel and type 3A silica gel should be used for cyclic operations since both can achieve about 95% regeneration within 250 s. And for low grade heat, type 3A silica gel is the better choice as the adsorbent [88].

Many other researches have been done to compare experimental data to numerical data. J. P. Oliver compared the experimental results obtained from the adsorption isotherms of argon on silica gel to numerical results obtained from using density functional theory (DFT) modelling at temperatures in range of 77 K to 95 K [89]. The paper concluded that the DFT model and the experimental data for the heat of adsorption were in good agreement [89]. Adsorption isotherms of silica gel composites have also been studied extensively in respect to increase adsorption capacity, cycle repeatability, cost, adsorption energy as well as overall efficiency of the heat storage system. A composite of CaCl<sub>2</sub> in silica gel and its adsorption isotherms was studied by Aristov et al. Using the Polyani invariant principle, they concluded that the equation well described the entire experimental data with the possibility of calculate isobars, isosteres, and isotherms of water at a given temperature and pressure [90].



#### 2.4.4.1 Parameters that affect adsorbents performance.

There are a number of adsorbent characteristics that affects the adsorption of the adsorbate on the adsorbent surface are summarized as follows;

##### 2.4.4.1.1 Adsorbent size

This determines the pressure drop required to maintain a given output in a fixed-bed operation and the rate of adsorption depends on the adsorbent size. The rate of adsorbate adsorbed by the adsorbent is dependent on the adsorbent size ( $d_p$ ).

##### 2.4.4.1.2 Porosity

Specific pore volume is the volume per unit mass adsorbed, and it is an independent variable when considering the adsorbent energy density.

$$V_{pore} = \frac{\varepsilon_p}{\rho_p} = \frac{1}{\rho_p} - \frac{1}{\rho_s} \quad (28)$$

$$\varepsilon_p = 1 - \frac{\rho_p}{\rho_s} \quad (29)$$

Where  $V_{pore}$  is the specific pore volume ( $\text{cm}^3/\text{g}$ ),  $\varepsilon_p$  is the total porosity which is a dimensionless number,  $\rho_p$  is the particle density and  $\rho_s$  is the true solid density.

The particle density ( $\rho_p$ ) is usually determined by a mercury pycnometer. The sample is evacuated and exposed to mercury at atmospheric conditions, which causes the mercury to penetrate the pores of the sample. A ratio of the particle weight to the particle volume is equal to the relation of the pycnometer without the sample ( $W_m$ ) and that of the pycnometer with the sample ( $W_s$ ), filled with mercury after the evacuation ( $W_p$ ) and this is given by:

$$\rho_p = \frac{\text{Particle weight}}{\text{Particle volume}} = \frac{W_s}{\left[ \frac{W_m - W_p + W_s}{\rho_{Hg}} \right]} \quad (30)$$

where  $\rho_{Hg}$  is the density of the mercury at a given temperature.

It is difficult to find the true solid densities of some porous bodies due to the fact that they have well confined space which is not accessible from the outside. In the case direct measurement is used to measure the true solid density. In place of mercury, another liquid can be used to penetrate the porous to measure the particle density. Another method which works on  $PV = \text{constant}$  at a constant  $T$  called the helium densitometer can be used to measure the particle density.

#### **2.4.4.1.3 Pore size distribution**

With the exception of molecular sieves and other advanced porous adsorbents which have a well-defined pore size with almost no pore size distribution, most adsorbents have the size of their pores distributed in a certain range. Based on the range the pore sizes are normally considered as macropores ( $d_{\text{pore}} > 500 \text{ \AA}$ ), mesopores ( $20 \text{ \AA} < d_{\text{pore}} < 500 \text{ \AA}$ ) and micropores ( $d_{\text{pore}} < 20 \text{ \AA}$ ) [91]. Although the adsorbent capacity and the rate of the adsorbate uptake is hugely determined by the pore size distribution, the exact relation linking this is still unclear. The three most common method for measuring the pore size distribution are the mercury porosity measurement, nitrogen adsorption or desorption measurement and the molecular probe method.

##### **2.4.4.1.3.1 Mercury porosity measurement**

In the mercury porosity measurement, a pressure,  $P$ , is applied to the mercury surrounding the porous body (adsorbent), which causes the mercury to penetrate the pores whose radii ( $r$ ) are larger than a particular  $r$ . The equation is given by;

$$r = - \frac{2 \sigma \cos \theta}{P} \quad (31)$$

where  $\sigma$  is the surface tension of the mercury at a given temperature, and  $\theta$  is the contact angle between the surface of the sample and mercury which is usually measured at  $140 \text{ }^\circ\text{C}$ . Pressure penetration volume relation is used to calculate the pore size distribution. A typical mercury porosimeter will generate pressure as high as  $3000 \text{ kg/cm}^2$ , which enables determination of pore size distribution to  $r = 25 \text{ \AA}$ . Nevertheless, this method is usually used to determine macropore sizes in the range of  $d_{\text{pore}} > 100 \text{ \AA}$  [91][84].

#### 2.4.4.1.3.2 Nitrogen adsorption/desorption measurement

Nitrogen is adsorbed on the adsorbent surface and capillary condensation also takes place when nitrogen adsorption method is performed at 77.34 K. The size of the pore where the condensation occurs and the thickness of the adsorbed layer on the surface is dependent on the partial pressure of the nitrogen. The pore size distribution can then be derived from the adsorption isotherm by relating the size of the pore where the condensation occurs and the adsorbed layer thickness. The Halsey's relation and the kelvin's radius gives the relation:

$$t = 4.3 \left[ \frac{5}{\ln \left( \frac{P_s}{P} \right)} \right]^{\frac{1}{3}} \quad (32)$$

$$r_k = \frac{-9.53}{\ln \left( \frac{P}{P_s} \right)} \quad (33)$$

where  $t$  is the thickness of the adsorbed layer on the surface in Å, and  $P_s$  is the saturation pressure,  $P$  is the partial pressure, and  $r_k$  is the capillary condensation radius in Å. The contact angle of nitrogen ( $\theta$ ) is given as  $\cos \theta = 1$ .

The adsorption isotherm is determined by the constant volume method or the gravimetric method which is then used to determine the pore size distribution using the Dollimore method. When the pore size is close to the adsorbate's molecular size, the Kelvin equation no longer works, hence the nitrogen method cannot be used to determine the pore size distribution. Nitrogen adsorption/desorption can be used to determine pore size distribution in the range of  $15 \text{ \AA} < d_{\text{pore}} < 250 \text{ \AA}$  [91].

#### 2.4.4.1.3.3 Molecular probe method

This is used to determine the effective pores sizes of adsorbents with molecular sieving abilities. For activated carbons, since the micropores are considered to be two dimensional, the thickness of the molecules determines the ability of the adsorbent to adsorb the adsorbate.

#### 2.4.4.1.4 Specific surface area

Since adsorption is a surface phenomenon, adsorption capacity is highly dependent on the surface area of the adsorbent. The specific surface area ( $S_g$ ) has a great effect on the kinetics of adsorption and even greater effect on the adsorption capacity. The specific surface area can be calculated using the volume of the monomolecular layer of the gas adsorbed at standard temperature and pressure. Specific surface area can be determined using the standard Brunauer, Emmett and Teller (BET) method and it is given as:

$$S_g = \frac{\alpha V_m N_A}{V} \quad (34)$$

where  $V$  is the molar volume of  $N_2$  at STP,  $V_m$  is the volume of the monomolecular layer of the gas adsorbed at standard conditions,  $N_A$  is the Avogadro's constant ( $6.023 \times 10^{23}$  molecules/mol) and  $\alpha$  (in  $cm^2$ ) is the projected surface area of the adsorbate molecule. Depending on the close 2D packing of spherical particles,  $\alpha$  is given as:

$$\alpha = 1.091 \left( \frac{M}{N_A \rho_L} \right)^{\frac{2}{3}} \quad (35)$$

where  $M$  is the adsorbate molecular weight, and  $\rho_L$  (in  $g/cm^3$ ) is the density of the adsorbate at its liquid state at the particular temperature. The Table 2.4 below shows few characteristics of some common adsorbents.

Table 2.4 Characteristics of some common adsorbents [88][92][91][93].

<b>Adsorbent</b>	<b>Silica Gel</b>	<b>Activated Alumina</b>	<b>Zeolites</b>	<b>Activated Carbons</b>
Porosity	0.4 – 0.7	0.5 – 0.77	0.2 – 0.5	0.4 – 0.7
Density (kg/m <sup>3</sup> )	700 - 800	650 – 1000	1100 – 1570	600 - 900
Specific surface area (m <sup>2</sup> /g)	300 - 1000	200 - 390	200 – 600	0.5 – 1200
Porous volume (ml/g)	0.35 – 0.45	0.5 – 0.6	0.28	0.15 – 0.5
Pore size (nm)	1 - 14	1.5	0.2 - 8	2 - 50

## 2.4.5 ADSORPTION WORKING PAIRS

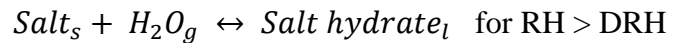
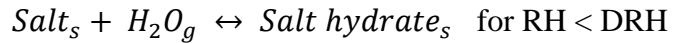
### 2.4.5.1 Chemical adsorption working pairs

Chemical reaction without sorption and chemical reaction with sorption are normally similar. As discussed above, a coordinate compound is formed when a ligand such as H<sub>2</sub>O or NH<sub>3</sub> donate a lone pair of electrons to the central atom which is usually a metal ion (such as Mg or Na) [62]. However, chemical adsorption working pairs is also a function of hydrogenation, oxidization and complexation reactions. Some chemical adsorption working pairs includes metal oxides /oxygen, salt hydrate/water, metal chlorides/ammonium and metal hydrides/hydrogen working pairs.

#### 2.4.5.1.1 Salt hydrates/water working pair

Hygroscopic salts which are basically salts that adsorb water are usually employed as adsorption working pairs in a sorption energy system. During the process, hydration reaction occurs to cause a release of energy. Some salts hydrates include sodium sulfide (Na<sub>2</sub>S), magnesium chloride (MgCl<sub>2</sub>), magnesium sulphate (MgSO<sub>4</sub>), zinc chloride (ZnCl<sub>2</sub>), calcium chloride (CaCl<sub>2</sub>), sodium hydroxide (NaOH), strontium bromide (SrBr<sub>2</sub>) and potassium hydroxide (KOH) among others [62]. The product of the hydration reaction is either salt hydrates with higher amount of water molecules or a saturated salt solution. The latter form occurs when there is a high relative humidity

(RH) or pressure and this process is called deliquescence. So in general deliquescence occurs when the partial pressure of water vapor in air is greater than the vapor pressure of the solution that is formed [94]. The threshold relative humidity for deliquescence to occur at a given pressure and temperature is called the deliquescence relative humidity (DRH). The two form of equations are presented as follows:



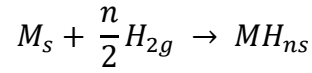
Where the subscripts s and l represent solids and liquids respectively. During operation of the sorption system, deliquescence can pose as a problem due to the ability to foster corrosion of metal components and the prevention of hydration reaction. Lewis Greenspan reported that the DRH of LiBr and LiCl are 6.2% and 11.3% at 30 °C, which means that it is relatively easier for their solids to form solution in most conditions. Hence such salt hydrates should not be used for hydration reactions in sorption systems [95]. Lahmidi et al stated that with temperatures below 80 °C, SrBr<sub>2</sub> can be regenerated, and this seems promising for short term energy storage system [96].

#### **2.4.5.1.2 Metal oxides/oxygen working pair**

A metal can adsorb either an atomic oxygen or a molecular oxygen, when the oxygen enters the unit lattice of the metals, forming a metal oxide. However, the type of metal and the temperature, pressure and other conditions determine whether an atomic oxygen is adsorbed or a molecular oxygen is adsorbed. During the desorption process, the heat applied causes some oxygen molecules to be released and some transforms into a stable form inside a metal which will need an activation energy to be released.

### 2.4.5.1.3 Metal hydrides/hydrogen working pair

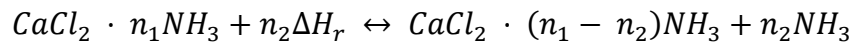
This is more of a resorption process rather than an adsorption process. The reaction is as follows:



Where n is a constant. Porous metal hydrides and metal matrix with alloys such as Fe, Al and Ni usually have very high sorption heat and adsorption capacity. Nonetheless, the reaction occurs at temperatures which are a little higher than the environmental conditions. What makes the metal hydrides/hydrogen working pair sorption system attractive is that they have high heat of sorption, fast reaction rates, high storage density and are optimal for very high temperature applications which cannot be obtained by other working pairs [60]. On the other hand, hydrogen is flammable and explosive, and the metal hydrides are expensive. And this puts a huge limitation on the commercialization of the TES system.

### 2.4.5.1.4 Metal chlorides/ammonia working pair

This group is the most used together with ammonia as a working pair due to the fact that their application spans wide range of temperatures (from 48 °C using NH<sub>4</sub>Cl to 334 °C using NiI<sub>2</sub>) [72]. An example of the chemical reaction is as follows:



Where  $\Delta H_r$  is the enthalpy of the reaction in (J/mol),  $n_1$  and  $n_2$  could be 2, 4 and 8. Their advantages include high adsorption capacity, wide variety of halides to cover a wide temperature range and relatively higher working pressure to the atmospheric pressure for better mass transfer.

Stitou et al investigated the thermochemical process for solar air conditioning using barium chloride (BaCl<sub>2</sub>)/ammonia as the working pair. The paper reported an average yearly efficiency of 0.4 – 0.5, a daily cooling capacity of 20 kWh and COP of 0.3 – 0.4 with a 20 m<sup>2</sup> solar collector which produces 60 °C to 70 °C [97]. Bao et al designed resorption refrigeration system for cold storage and long-distance refrigeration applications using ammonium chloride and manganese chloride as low temperature and high temperature adsorbents. Ammonia was used as the adsorbate. Within a range of a source temperature of 140 – 170 °C and refrigeration temperature of 15 – 5°C,

a COP of 0.3 – 0.31 was reported. The specific cooling power was also reported to be between 87 W – 125 W per kg of  $\text{MnCl}_2$  [98].

#### **2.4.5.2 Physical adsorption working pairs**

As discussed above, physical adsorption does not involve significant electron interactions. Nevertheless, they are a combination of Van Der Waals force of interaction, orientation forces, dispersion forces and Debye Forces and electrostatic forces. Many adsorbents have Van Der Waals force being the most prevalent. A working pair is chosen for the best performance in the interaction between the adsorbate and the adsorbent. In literature, the most researched physical adsorption working pair includes silica gel/water, zeolite/water, activated carbon/ammonia and activated carbon/methanol [60].

Activated carbon/ammonia and activated carbon/ (methanol and methane) working pairs.

Due to large adsorption quantity and lower adsorption heat (1800 kJ/kg to 2000 kJ/kg), activated carbon/methanol tend to be one of the most common research working pairs [60]. Despite this, the process of adsorption for activated carbon/ammonia and activated carbon/methanol are akin to each other. The porous volume is 0.15 – 0.5 ml/g, with the micropore surface area of about 95% the surface of the activated carbon, and this is where the adsorption occurs. The energy consumed during the desorption is dependent on the adsorption capacity and the adsorption heat. Hence, good adsorption capacity and low adsorption heat values will be much advantageous to the coefficient of performance. Activated carbon/methanol are employed as a working pair with solar energy as the source heat for two reasons; lower desorption temperatures (100 °C) and stability of the working pair at temperatures below 120 °C [60]. Nonetheless, temperatures above 120 °C will cause the methanol to decompose into other compounds. One major disadvantage of using the activated carbon/methanol working pair is that pressures lower than atmospheric pressures is needed which is quite difficult to manage.

Activated carbon/ammonia on the other hand has higher working pressures which make it much easier to manage and gives it a better mass transfer characteristic, although both activated carbon/methanol and activated carbon/ammonia have similar adsorption heat. Another advantage of activated carbon/ammonia is the ability to withstand higher temperatures of about 200 °C during



the charging phase without the fear of degradation. The major draw backs to this working pair is, relatively lower adsorption capacity, toxicity, and the incompatibility of ammonia and some metals.

Suzuki Motoyuki studied an improved form of activated carbon which is the activated carbon fiber has been developed to have very large surface area ( $1380 \text{ m}^2/\text{g}$ ) and it is known to have heat of sorption capacity 1 – 3 times that of activated carbon [99]. A composite of activated carbon fiber / $\text{CaCl}_2$  was studied by wang et al and they concluded its adsorption capacity is about  $1.7 \text{ g/g}$  [100][101]. In an activated carbon/methane working pairs, Farzard et al reported that the best isotherm to fit the experimental adsorption and desorption data is the TVFM isotherm [102].

#### **2.4.5.2.1 Zeolite/water working pair**

The unit structure of zeolite and the various types of zeolite have been briefly discussed in section 2.4.3 above. It is this structure and pores that determines the amount of water adsorbed by the zeolite. Zeolite adsorption heat is in the range of  $3300 - 4200 \text{ kJ/kg}$ , which is more than twice that of activated carbon/ammonia or activated carbon/methanol [55]. From the Fig. 2.13 above, zeolites just as many molecular sieves can withstand very high temperatures without significantly degrading. Therefore, the zeolite/water working pair can be desorbed at high temperatures such as  $200 \text{ }^\circ\text{C}$ . However, due to the fact that the coefficient of performance (COP) is highly dependent on the desorption temperature and adsorption heat, the COP for the zeolite is relatively lower than the activated carbon/methanol working pair for a low heat source. Due to overall better performance of the zeolite/water, a higher heat source gives higher COP. Due to the low working pressure of zeolite/ water working pair, the mass transfer is relatively low and it is impossible to produce evaporation temperatures below  $0 \text{ }^\circ\text{C}$ . These are the two major disadvantages of the zeolite/water working pair. Moreover, the cycle time for the working pair is relatively longer compared to most working pairs. Dawoud et al studied the adsorption of a zeolite water/ working pair with an evaporator inlet temperature between  $10 \text{ }^\circ\text{C}$  and  $40 \text{ }^\circ\text{C}$  and adsorbate flowrate in the range of  $0.5$  to  $2 \text{ l/min}$ , and found the storage density in the range of  $80$  to  $92 \text{ kWh/m}^3$  [103]. Moreover, the storage power density increased from  $144$  to  $165 \text{ kWh/m}^3$ . They also concluded that lower adsorbate flow rate translated to higher output temperatures, and higher adsorbate flowrates produced more effective and faster heat outputs. With cation exchange in zeolites, Li cation

exchange in zeolite was found to increase the storage density from 149 – 225 Wh/kg [104]. Dicaire and Tezel investigated activated alumina /zeolite 13X adsorbent composite with water as the adsorbate and the observed a maximum energy density of 200 kWh/m<sup>3</sup> [105][102].

#### **2.4.5.2.2 Silica gel/water working pair**

With a surface area of 800 m<sup>2</sup>/g, the adsorption heat of the silica gel/water working pair is about 2380 kJ/kg to 2510 kJ/kg [88]. Another important thing about the silica gel/water working pair is the desorption temperature which is usually well below 90 °C and above 50 °C [106][60]. Wang et al worked on a silica gel/water adsorption chiller with a low-grade heat source and found the COP and the refrigeration capacity to be 7.15 and 0.38 KW respectively [107]. At very high temperatures the silica gel may lose all of its hydroxyl group on the surface of the gel, in effect losing its adsorption characteristic as discussed earlier. Moreover, adsorption by silica gel/water system is highly dependent on temperature, hence, higher pressures are needed for high level of adsorption, which is a drawback when employed in closed systems. Furthermore, there is a very low temperature lift for a given range of adsorption capacity. Another disadvantage of silica gel/water working pair is producing evaporative temperatures below 0 °C is quite improbable. Jaehning et al studied experimental prototype of closed sorption systems with temperature range of 25 °C to 85 °C and obtained a heat storage density of about 50 kWh/m<sup>3</sup> which is lower than water, which has a storage density of 70 kWh/m<sup>3</sup> [104][108]. Therefore, the short-term energy storage with silica gel/water working pair is not very competitive. Nonetheless, long term silica gel/water system may have much higher storage densities than water. This thesis goes further on sorption thermal energy system that utilizes silica gel/water working pair, and it aims to design a system, test the repeatability of the system as well as the efficiency of the system. Silica gel /water adsorption pair in a solar adsorption chiller was designed by Zisheng et al. The adsorption refrigerator coefficient of performance, the thermal efficiency of the solar collector and the solar coefficient of performance of the system are 0.44, 0.36 and 0.16 respectively[109]. They also reported a COP of 0.63 and cooling capacity of 17.9 kW when cooling water inlet temperature, hot water inlet temperature, and the chilled water outlet temperature was 25.4 °C, 79 °C and 13.7 °C respectively [109].

## **2.5 Kinetics of Sorption and Adsorption Models**

### **2.5.1 Adsorption isotherms**

To design any sorption system, the right adsorbent/ absorbent must be selected, which streams from the calculated equilibrium isotherms. Several adsorption isotherms for various sorption materials have been investigated numerically and experimentally in literature [110]. These isotherms describe the interactive mechanisms between the adsorbate and the adsorbent by taking into account the equilibrium characteristics of the adsorbent materials. Additionally, the information obtained from adsorption equilibria can be used to study the equilibria of multi component systems, the kinetics of adsorption of single and multicomponent systems [111]. In this section we introduce few adsorption isotherms including once used in calculations and fitting of experimental curves. These include the Langmuir isotherm, Freundlich isotherm, Dubinin-Radushkevich isotherm, Toth isotherm and the Brunauer – Emmett – Teller (BET) isotherm.

### **2.5.2 Langmuir Isotherm Model**

This model assumes that at equilibrium, there is a persistent bombardment of adsorbate molecules unto the surface of an adsorbent with corresponding desorption of the adsorbate from the same surface in order for a zero state of accumulation of the adsorbate on the surface to be maintained [93]. Three assumptions are made for this model and they are as follows:

1. The surface of the adsorbate is homogeneous. The energy required for adsorption of adsorbate is constant at all sites.
2. Adsorption of adsorbate occurs at well-defined localized sites of the adsorbent surface.
3. Each site will accommodate only one atom or molecule there is no interaction between adjacent molecules.

This follows the kinetic principle that the rate of adsorption is equal to the rate of desorption. The rate of adsorption is equal to the accommodation coefficient multiplied by the striking rate of the surface.

*At Equilibrium; Adsorption rate = Desorption rate*

$$K_a p_v (X_0 - X) = K_d X \quad (36)$$

$$y = \frac{X}{X_0} = \frac{b p_v}{1 + b p_v} \quad (37)$$

$$b = \frac{K_a}{K_d} \quad (38)$$

Where  $K_a$  and  $K_d$  are the adsorption and desorption constants respectively, fractional surface coverage,  $y$ ,  $X_0$  is the maximum amount to that can be adsorbed by the adsorbent,  $X$  is the amount adsorbed,  $b$  depicts the adsorption equilibrium constant and  $p_v$  is the vapor pressure. This parameter expresses the relation between heat of adsorption ( $\Delta H$  [kJmol<sup>-1</sup>]) and the adsorbent temperature ( $T_s$ ) by the Hoof equation as;

$$b = b_0 \exp\left(\frac{\Delta H}{RT_s}\right) \quad (39)$$

$R$  is the universal gas constant and  $b_0$  is the adsorption affinity constant.

### **2.5.3 Isosteric Heat of Adsorption**

Isosteric heat happens to be one of the most fundamental quantities evaluated in adsorption studies. It is the ratio of the infinitesimal change in the enthalpy of the adsorbate to that of the amount adsorbed by the adsorbent [112]. The importance of this is that, it gives the proportion of heat that is released to the surrounding and the proportion released to the solid adsorbent [93]. This causes rise in the temperature of the solid sorbent which results in slowing down the adsorption kinetics, since the mass (adsorbate) uptake is regulated by the cooling rate of the particle. The isosteric heat is computed from the van't Hoff thermodynamic equation:

$$\frac{\Delta H}{RT^2} = -\left(\frac{\partial \ln p}{\partial T_s}\right)_X \quad (40)$$

As stated in subsection 2.5.2, it is stated that the adsorption process is an exothermic reaction. Thus, equation above, increasing the temperature causes the decrease in affinity constant. For the adsorption to occur, the Gibbs free energy should decrease, which results in a negative  $\Delta H$ .

## 2.5.4 Freundlich Isotherm

The Langmuir isotherm best describes monolayer absorption at low vapor pressures. In case of heterogenous surface, the Freundlich isotherm defines the surface heterogeneity and the active sites and their corresponding energies. Additionally, the isotherm describes adsorption between water uptake,  $X$ , (in kg of adsorbate/kg of adsorbent), vapor pressure at saturation,  $p_s$  and vapor pressure,  $p_v$  at the adsorbent temperature. The homogeneity of the surface ( $\frac{1}{n}$ ) is identified between 0 and 1. For a given  $1/n$  where  $1/n > 1$ , the adsorption is unfavorable, when  $(0 < 1/n < 1)$ , the adsorption is favorable and when  $1/n = 1$ , the process is irreversible [113]. The Freundlich isotherm is modelled based on the phenomenon that the surface of the adsorbent is patch wise. This implies that all site with the same adsorption energy forms one patch and each patch is independent from the other. There is also no interaction between patches. The constant  $n$  is a temperature dependent parameter and the Freundlich equation is given as follows:

$$X = X_o \left( \frac{p_v}{p_s} \right)^{\frac{1}{n}} \quad (41)$$

The linearized form of the isotherm is given as follows:

$$\ln(X) = \ln(X_o) + \frac{1}{n} \ln \left( \frac{p_v}{p_s} \right) \quad (42)$$

The major limitation of the Freundlich isotherm model is that, it is not valid for extremely low and high vapor pressures with maximum uptake.

### 2.5.5 Dubinin isotherms

This isotherm is a semiempirical equation that is used to model the adsorption mechanism with Gaussian energy distribution usually on heterogeneous adsorbent surface [114]. The Dubinin-Radushkevich Isotherm model centers the assumptions that there exists a multilayer behavior that characterizes the Van der Waal's forces and can describe the physisorption processes [35]. This isotherm has been reported to be temperature dependent by Gunay et al [115] and it actively describes adsorption onto microporous adsorbent surfaces [113]. Nevertheless, the downside of this model is that it shows unrealistic asymptotic character and it only works for a range of intermediate adsorbate amounts. The Dubinin-Radushkevich is expressed as:

$$\ln(X) = \ln(X_0) - \beta E^2 \quad (43)$$

$$\epsilon = RT \ln\left(1 + \frac{1}{X}\right) \quad (44)$$

$\epsilon$  is the Polanyi potential,  $E$  is the mean adsorption Energy and  $\beta$  is the Dubinin-Radushkevich constant and  $T$  is the absolute temperature.

A modified form of the Dubinin-Radushkevich isotherm model was developed to make computations and interpretation easier. This resulted in the assumption that the adsorbed phase density remains constant [116]. The resulting equation is termed the D – A equation and it is given as follows:

$$X = X_0 \exp \left\{ -D \left( \ln \left( \frac{p_s}{p_v} \right) \right)^n \right\} \quad (45)$$

$D$  is the coefficient of affinity which depends on the microstructure of the adsorbent material and on the adsorbate – adsorbent pair. The pitfall of the D – A equation is that, it is not able to predict adsorption isotherm at low relative pressures due to zero slope at zero loading [116][117].

## 2.5.6 Toth Isotherm

The Toth isotherm is an empirical Langmuir isotherm which has been modified to reduce the error between the predicted and experimental values [35]. The isotherm is able to predict with a good accuracy at low and high adsorbate amounts, as well as heterogeneous adsorption surface where Langmuir and Freundlich models are not able to predict accurately. The equation is expressed as:

$$X = \frac{b_0 p_v \exp\left(\frac{\Delta H}{RT_s}\right)}{\left\{1 + \left[\frac{b_0 p_v}{X_0} \exp\left(\frac{\Delta H}{RT_s}\right)\right]^\tau\right\}^{\frac{1}{\tau}}} \quad (46)$$

$\tau$  is the adsorbent structural heterogeneity parameter and at  $\tau = 1$ , the equation reduces to the Langmuir isotherm model. This isotherm equation has been used to model several heterogeneous systems and multilayer adsorption [118][119].

## 2.5.7 Brunauer – emmet – teller (bet) isotherm

Comparing the BET model to the Langmuir isotherm, they are bot similar on the assumption that the adsorption of adsorbates in onto specific adsorption sites [91]. The difference between the two model is that, the BET model allows the build up of different adsorbate layers on different fractions of the adsorbent surface. Additionally, the parts that are covered with bilayer, monolayers and are empty are held constant.

$$k_0 a_0 p = A_1^* e^{\frac{-E_1}{RT}} a_1 \quad (47)$$

$$a_1 = \frac{k_0}{A_1^*} e^{\frac{E_1}{RT}} a_0 p = \alpha_0 a_0 \quad (48)$$

Where  $\alpha_0$  is given by;

$$\alpha_0 = \left(\frac{k_0}{A_1^*}\right) e^{\frac{E_1}{RT}} p \quad (49)$$

In the same way, the constant  $a_1$  can be used to derive  $a_2$  and so on;

$$k_0 a_0 p + A_2^* e^{\frac{E_2}{RT}} a_2 = k_1 a_1 p + A_1^* e^{\frac{-E_1}{RT}} a_1 \quad (50)$$

Comparing;

$$A_2^* e^{\frac{E_2}{RT}} a_2 = k_1 a_1 p \quad (51)$$

where

$$\gamma = \left( \frac{k_1}{A_2^*} \right) e^{\frac{E_2}{RT}} p \quad (52)$$

If  $v_s^*$  is given as the adsorbate volume necessary for monolayer coverage per unit area, then the total adsorbate adsorbed  $v_s$  is given as:

$$v_s = v_s^* \sum a_i = v_s^* \sum_{i=1}^n i B_2 \gamma^i a_0 \quad (53)$$

Where  $B_2$  is:

$$B_2 = \frac{\alpha_0}{\gamma} ; \quad a_1 = B_2 \gamma^i a_0 \quad (54)$$

expressed into:

$$\frac{v_s}{v_s^*} = \frac{B_2 a_0 \gamma \frac{d}{d\gamma} \left[ \left( \frac{1 - \gamma^{II}}{1 - \gamma} \right) \gamma \right]}{a_0 \left[ 1 + B_2 \gamma \left( \frac{1 - \gamma^{II}}{1 - \gamma} \right) \right]} \quad (55)$$

Rearranging the equation yields:



$$\frac{v_s}{v_s^*} = \left( \frac{B_2 \gamma}{1 - \gamma} \right) \frac{[1 - (n + 1)\gamma^n + n\gamma^{n+1}]}{[1 + (B_2 - 1)\gamma - B_2\gamma^{n+1}]} \quad (56)$$

If the adsorbate pressure reaches the saturated vapor pressure  $p_s$ , there will be condensation and the ratio  $\frac{v_s}{v_s^*}$  will approach infinity, which results in (gamma)  $\gamma=1$ . The resulting equation are given as follows:

$$1 = \left( \frac{k_1}{A_2^*} \right) e^{\frac{E_2}{RT}} p_s \quad (57)$$

$$\text{and, } \gamma = \frac{p}{p_s} \quad (58)$$

y yields:

$$y = \frac{X}{X_0} = \frac{v_s}{v_s^*} = B_2 \frac{\frac{p}{p_s}}{\left( 1 - \frac{p}{p_s} \right) \left[ 1 - \left( \frac{p}{p_s} \right) + B_2 \left( \frac{p}{p_s} \right) \right]} \quad (59)$$

This equation 52 is the special case of the general BET equation with  $n = \infty$ . One of the most prominent application of the BET model is to determine the surface area for adsorption of nitrogen [91][120].

## 2.5.8 Adsorption Rate

The rate at which the adsorbent takes up the adsorbate is given by

$$\frac{dX}{dt} = K_m(X_o - X) \quad (60)$$

Where  $K_m$  is the mass transfer coefficient of adsorption and is given by;

$$K_m = (15D_s/R_p^2) \quad (61)$$

From this relation activation energy  $E_a$ , can be obtained from the surface diffusivity ( $D_s$ ) by

$$D_s = D_{s0} \exp \left[ \frac{-E_a}{RT} \right] \quad (62)$$

$D_{s0}$ , is a pre-exponential term with the value of  $2.54 \times 10^{-4} \text{ m}^2/\text{s}$ , R is gas constant,  $R_p$  is the radius of silica gel particles.

## 2.6 Energy balance

Average temperature out;

$$T_{out.avg} = \frac{\sum_{i=1}^n T_{out}^i}{n} \quad (63)$$

Average temperature lift

$$T_{lift} = T_{out.avg} - T_{in} \quad (64)$$

The total energy balance is calculated as the sum of heat obtained by convection, sensible, losses and sorption heat which is equal to zero:

$$P_{sorption} - P_{convection} - P_{sensible} - P_{losses} = 0 \quad (65)$$

$$\left[ \frac{\dot{m}_{v,in} - \dot{m}_{v,out}}{M} \Delta H \right] - [(\dot{m}_a C_{p,a} + \dot{m}_{v,out} C_{p,v}) T_{out} - (\dot{m}_a C_{p,a} + \dot{m}_{v,in} C_{p,v}) T_{in}] \quad (66)$$

$$- \left[ \sum_{i=1}^3 \rho C_p A \frac{\Delta T_{ci}}{\Delta t} \Delta L \right] - \left[ \sum_{i=1}^3 \frac{T_{Bi} - T_{Wi}}{R} \Delta L \right] = 0$$

Where subscripts v, a, c, B, W, represents water vapor, air, middle of the bed, bed and wall.  $\dot{m}$ ,  $C_p$ ,  $T_{in}$ ,  $T_{out}$ ,  $t$ ,  $R$ ,  $\rho$  represents the mass flow rate, the specific heat capacity, temperature at the inlet and outlet, time, heat resistance and density respectively.

The first term on the left of equation (66) represents the power produced during adsorption, the second term represents the power lost through air flow through the bed, the third term represents the amount used to heat up the adsorbent, and the last term represents the loss through the sorption tube.

The power derived from sorption is calculated for  $n$  cycles and a graph of power to the number of cycles is plotted to study the number of cycles until significant deterioration of adsorbent or system begins.

### 3 DESIGN OF THERMAL STORAGE SYSTEM

Efficiencies of sorption materials as heat storage systems have remained low due to factors listed and elaborated in section 2. To attain competitive efficiencies of these materials, systems must be built to effectively utilize the properties of the adsorbent materials. This section presents the design of a sorption tube and an energy storage system which undergoes two phases: the charging phase, where energy is stored and a discharging phase, where the energy is given off in terms of heat. Additionally, the system specification, detailed drawings, and material selected for 3D printing of sorption tube are discussed.

#### 3.1 FUNCTIONAL ANALYSIS

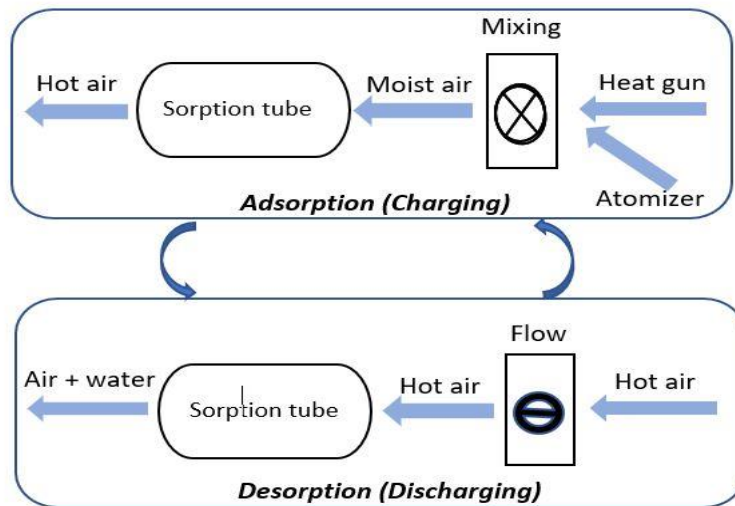


Figure 3.1. Functional architecture of proposed storage system

Figure 3.1 above presents the functional analysis for the design. The figure shows the interconnection between the adsorption phase and the desorption phase as well as the system architecture. The system is divided based on the major components, which are, the heat gun and atomizer section, upstream and downstream flow ducts and control valves and the sorption tube.

## **Heat gun**

The heat gun will function in both the adsorption and desorption phases. Thereby, it is required to be able to deliver warm air of 30 °C and hot air of 70 °C. Also, since it will be the source of flow, it is required to have specified flow rate which can be adjustable. The heat gun connects to the system through a Y-pipe which is positioned uniaxially to the sorption tube.

## **Atomizer**

The atomizer is only needed in the adsorption phase to deliver fine atomized water molecules for effective mixing. It is connected to the system by positioning it in a y fashion using the y-pipe tube (see Fig. 3.1).

## **Upstream and downstream flow ducts and control valves**

Flow duct for the atomizer is made long enough to obtain fully developed mist as specified by the manufacturer before it meets with the flow from the heat gun. Moreover, the upstream flow duct is also specified to obtain homogeneous mixing before entering the sorption tube. The downstream flow ducts will also be made long enough for to obtain accurate measurements from flow without fluctuations. The ducts are chosen to give the possibility of fitting into the y-pipe and the sorption tube. The ducts will allow the insertion for measurements of flowrate, temperature and relative humidity.

## **Sorption Tube**

This houses the adsorbent material thus; it is where the exothermic reaction takes place. It is designed to give the possibility of taking the measurements of the relative humidity and temperature at the inlet, outlet and at the bed. It should also allow the attachment of the upstream and downstream flow ducts.

## PROPOSED DESIGN

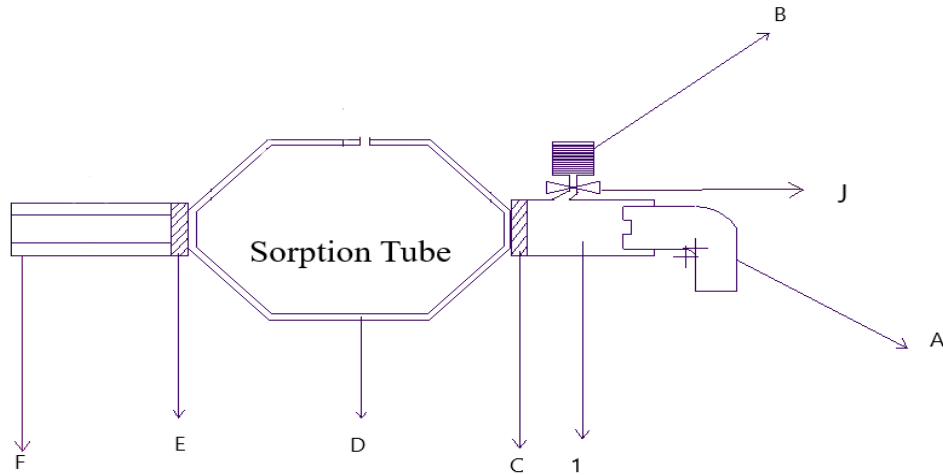


Figure 3.2. A schematic diagram illustrating the proposed design

The process of adsorption integrates the atomizer (B), the heat gun (A), the upstream and downstream ducts (1 and F), control valves (C, E) and the sorption tube (D). Both the atomizer and the heat gun are turned on simultaneously while the inlet valve remains closed to ensure homogeneity of mixing. Adsorption of moisture from the atmosphere is also ensured by closing the outlet valve. The relative humidity and temperature during the mixing are carefully monitored. After mixing, the outlet and inlet valves are opened for adsorption to occur. Due to the fact that the adsorption is exothermic, heat is released which flows downstream the ducts by it being transferred to the heat transfer fluid and also stored as sensible heat. The desorption phase constitutes all components of the system without the atomizer. During this phase, the heat gun blows hot air through the adsorbent bed, where it causes the release of moisture from the adsorbent. The flow velocity at the inlet and outlet as well as the temperature and relative humidity at the inlet, outlet and bed are monitored.

## 3.2 System specification

### 3.2.1 Moist air calculation

For a desired relative humidity, inlet flow rate and temperature, the amount of moisture is calculated to select the heat gun and the atomizer to give these conditions after mixing. The psychrometric chart (see Appendix B) is used to calculate these conditions during heating and mixing.

Air at room temperature was measured to have a relative humidity ( $\phi_a$ ) of 0.34. The specific humidity and the pressures of water vapor can be obtained from the Mollier diagram using relative humidity and the temperature. The calculation to obtain desired relative humidity, specific humidity and temperature for effective water absorption by the sorption tube is divided into two steps; heating and mixing.

#### 3.2.1.1.1 HEATING

Heating: This is achieved by heating the air using the heat gun. The minimum and maximum temperatures of the heat gun is specified by the producer. Most heat guns have a minimum temperature of 30°C.

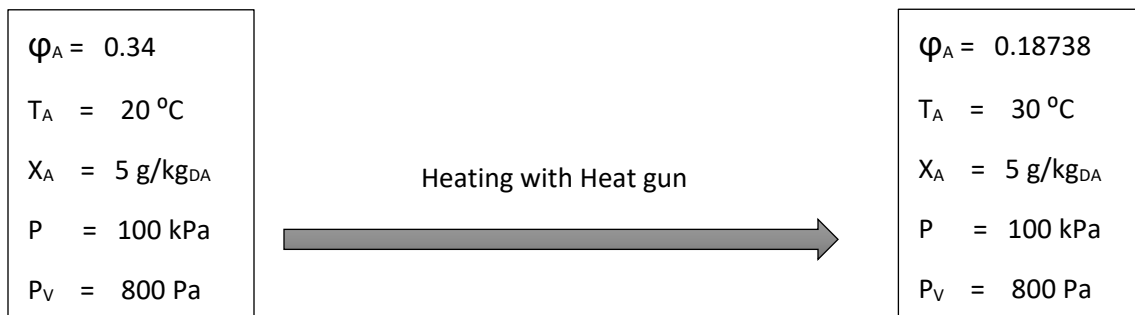


Figure 3.3. This shows the Mollier diagram for stages moist air

The diagram above shows the process of heating the air with the heat gun at a temperature of 30°C. Although the specific humidity remains the same, the relative humidity is reduced. This leads to the next stage, the mixing process.

### 3.2.1.1.2 MIXING

The mixing conditions is achieved either by mixture with another gas or atomizing. The humidifier or atomizer used have specific parameters such as the flow rate, nozzle diameter, angle of flow and the minimum and maximum relative humidity which are given by the producer. This is done by addition of water droplets or by mixture of two gases.

The calculation derived from the Dalton's model for both processes given  $R_{da} = R/M_A$  and  $R_V = R/M_V$  as specific gas constants of dry air and vapor respectively are as follows;

$$\dot{m}_{da} = \frac{p_{da}V}{R_{da}T} \quad (67)$$

$$\dot{m}_V = \frac{p_V V}{R_V T} \quad (68)$$

$$R = \frac{m_A R_{da} + m_V R_V}{m} \quad (69)$$

$$R = \sigma_A R_{da} + \sigma_V R_V \quad (70)$$

For *mixing with water droplets*, a desired relative humidity, temperature and the specific humidity for optimum absorption by the silica gel is chosen and this is used to calculate the water flowrate of the atomizer. The flow rate of the water from the atomizer is given by the following relation;

$$\dot{m}_M = \dot{m}_A + \dot{m}_{H_2O} \quad (71)$$

$$\dot{m}_{H_2O} = \dot{m}_{da}(X_M - X_A) \quad (72)$$



Where  $X_A = \dot{m}_A/\dot{m}_{da}$ , is the specific humidity of air,  $X_M = \dot{m}_M/\dot{m}_{da}$  is the specific humidity after mixing and  $\dot{m}_{H_2O}$  is the mass flow rate of water. This flow rate is used to select the kind of atomizer needed to create the desired relative humidity and temperature in the sorption tube.  $\dot{m}_M$  is the mass flow rate of mixture,  $\dot{m}_{da}$  is the mass flow rate of dry air, and  $\dot{m}_A$  is the mass flow rate of air.

From the above calculations, a humidifier or atomizer should have flowrates between 1 l/h to 3.5 l/h. A heat gun that can also blow at room temperature will be needed for the discharge phase

### 3.2.2 Sorption Tube design Calculation and 3D printing

Since cycle repeatability tests will be performed, the tube is supposed to be able to withstand moderate temperatures (70 °C) and pressures (60 kPa maximum), have accessibility to the inside as well as to have a high fatigue life and good creep resistance. Moreover, it should resist corrosion which could be caused by the moisture, and also enable the filling of the sorption tube through the inlet.

The sorption tube was designed with the ASME BPVC code and ABS + carbon fibers composite material was chosen for the tube design due to good heat resistivity, low water adsorption at saturation, high temperature material, good fracture toughness, high strength, have high processability and flow characteristics. Nevertheless, the presence of the carbon fibers reduces the heat insulation property of the sorption tube due to the high heat conductivity of carbon fibers.

#### *Shell Thickness*

$$t_s \geq \frac{PR}{SE - 0.6P} \quad (73)$$

Where  $t_s$  is the thickness of the shell, P is the maximum working pressure, S is the maximum allowable stress, E is the weld efficiency and R is the radius.

### *Hemispherical Head Thickness*

$$t_h \geq \frac{PR}{2SE - 0.2P} \quad (74)$$

### *Nozzle Thickness*

$$t_n \geq \frac{PR_n}{SE - 0.6P} \quad (75)$$

Where  $t_h$  is the hemispherical head thickness,  $t_n$  is the nozzle thickness and  $R_n$  is the radius of the nozzle.

Due to the fact that 3D printing techniques produces materials and objects with comparatively low strength values as well as other properties, the calculated thickness of the vessel is increased. There were other constraints such as the bonding, length per section, and diameter. For this reason, the materials selected, the tube diameter and tube length were adjusted.

## **SPECIFICATION TABLE**

**TABLE 3.1 SPECIFICATION AFTER CALCULATION.**

Device	Flow Rate Capability Range [m <sup>3</sup> /h]	Tip Diameter [mm]	Tip Length [mm]	Temperature Capability Range [°C]
Heat Gun	1.5 – 15	28.5 – 31.75		30 – 70

Device	Flow Rate Capability Range [l/h]	Body Diameter [mm]	Water Droplets Diameter [μ]	Working Temperature [°C]
Sprinkler	0.1 – 0.35	< 32	20 – 200	80 <

Ducts	Total Length [mm]	Outer Diameter [mm]	Inner Diameter [mm]	Working Temperature [°C]
Upstream Duct	300 – 400	32	25.4	80 <
Downstream Duct	200 <	32	25.4	80 <
Y-channel Duct	180 <	32	25.4	80 <

Object	Material	Length [mm]	Internal Diameter [mm]	Thickness [mm]	Working Temperature [°C]	Working Pressure [kPa]
Sorption Tube	ABS + Carbon fiber	360	90	3	120 <	< 60

### 3.2.3 SELECTED CONCEPT

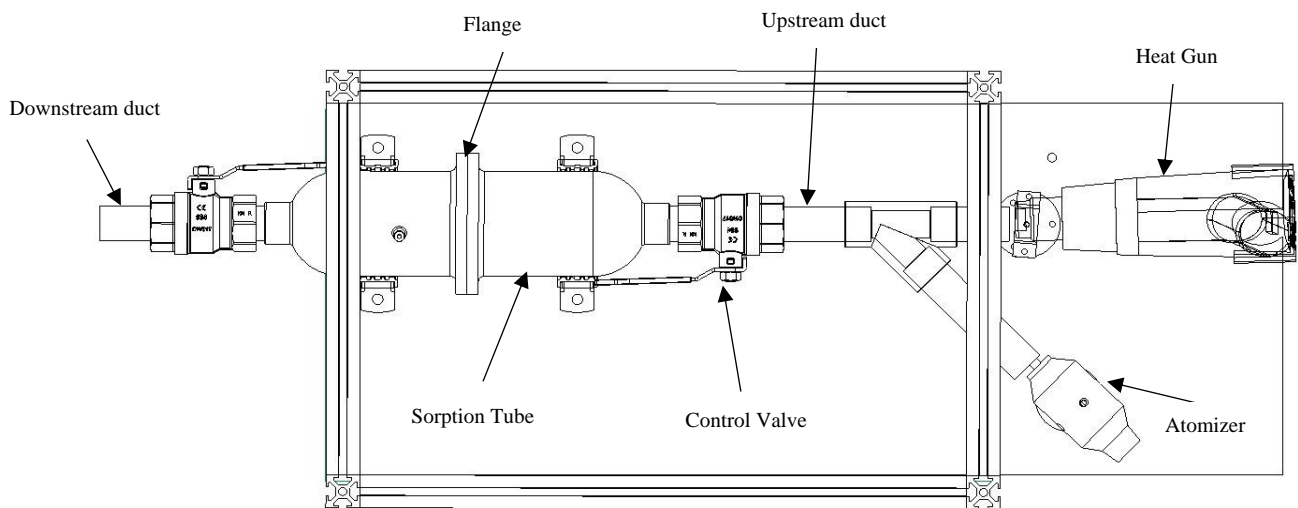


Figure 3.4. 2D drawing of the system

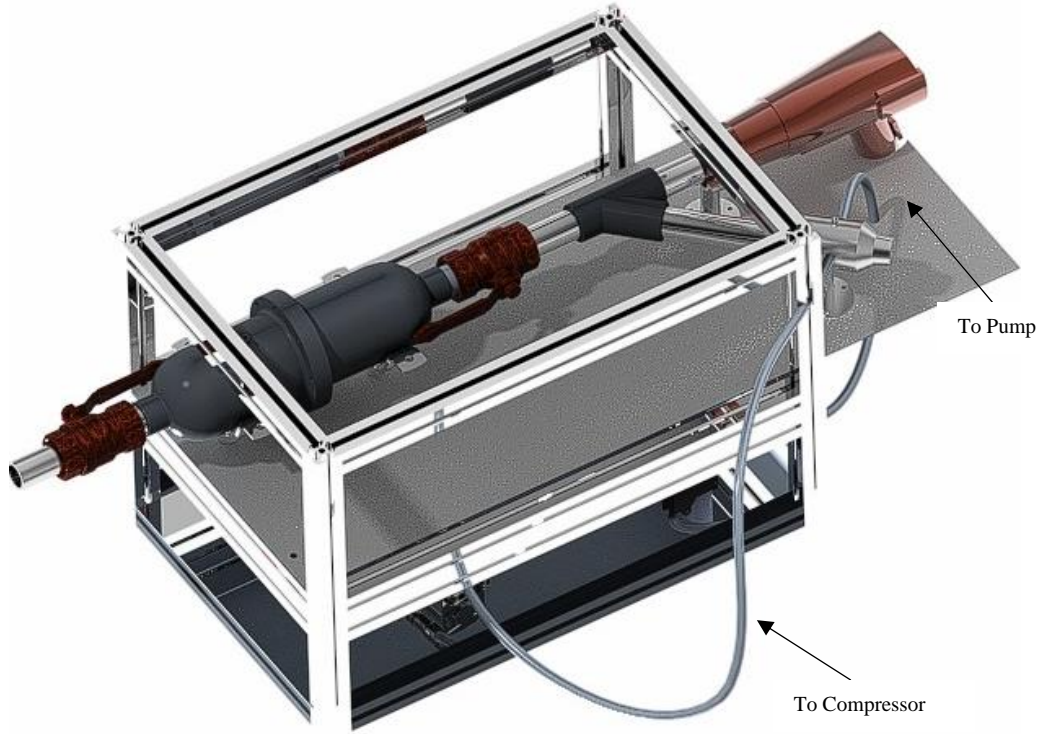


Figure 3.5. 3D drawing of system.

Figure 4 and 5 shows the 2D and 3D of the heat storage system, indicating the main components of the system; the downstream and upstream ducts, the sorption tube, heat gun and the atomizer. The tubes to the compressor and the pump which controls the flow rate are shown. Appendix contains parts and assembly of detailed drawings.

## 4 EXPERIMENTAL DESIGN

This section focuses on the research part of the study. It involves testing of the energy storage system, study of the process repeatability using a low heat grade and velocity effects on the adsorption and desorption phases.

### 4.1 EXPERIMENTAL SETUP

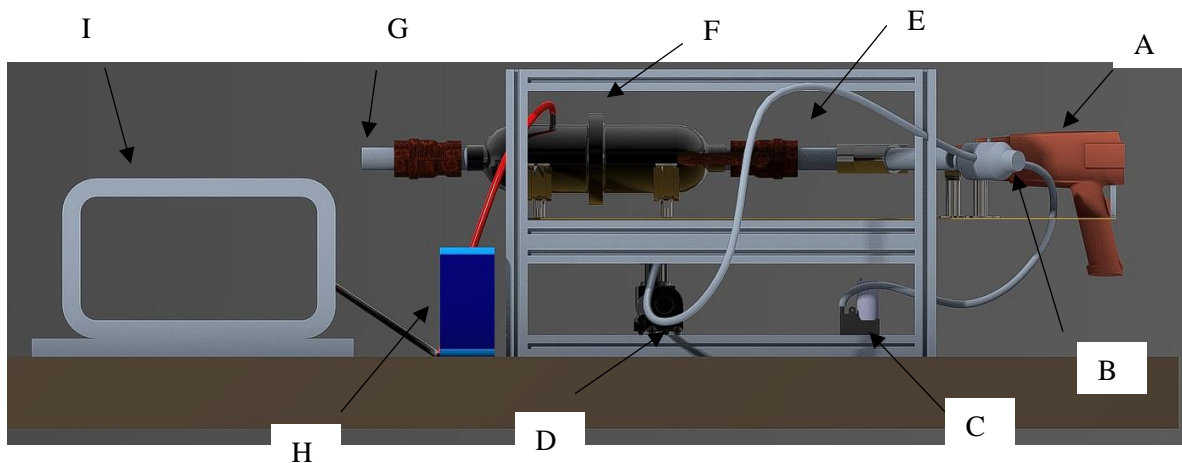
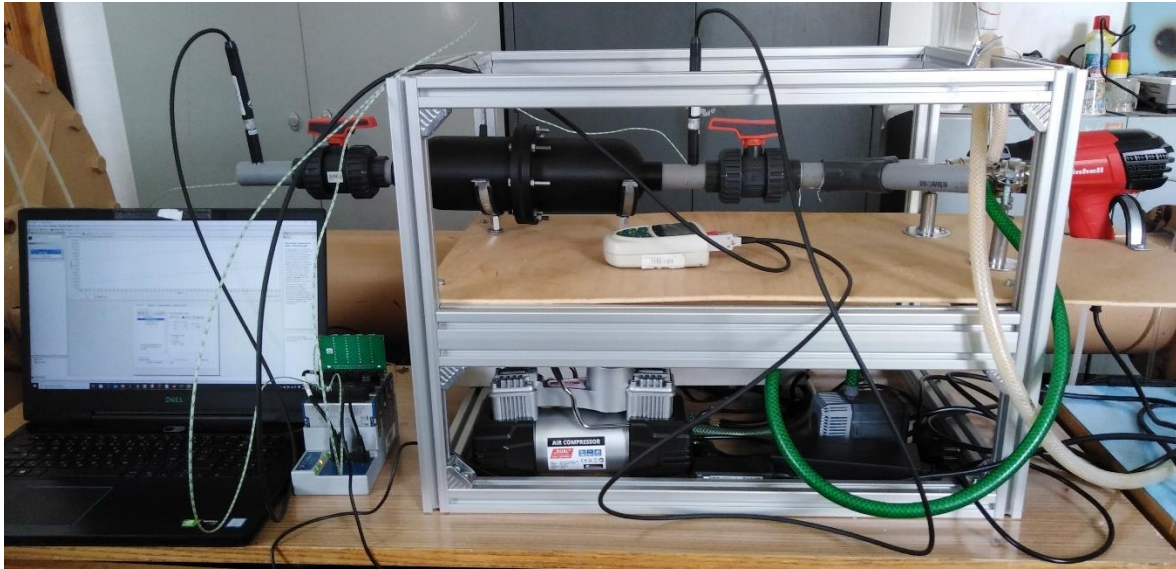


Figure 4.1. Depicts the experimental set up where the heat gun (A), upstream duct (E), sorption tube (F), downstream duct (G), pump (C), atomizer (B), compressor (D), data acquisition device (H) and computer (I).

The sorption tube, data acquisition instrument and energy storage system are setup in Fig. 4.1. The sorption tube is filled with the silica gel with bed porosity of about 0.4. The tube is also connected to control valve which control the flow of moist air in and out of the bed. The system has a width of 0.35 m and length of 0.9 m, with the heat gun and the atomizer positioned 45° away from each other by means of a 45° Y-channel joint. The heat gun is also position in a uniaxial direction to the sorption tube. Data is obtained at three different positions; at the upstream duct, the bed and at the downstream duct. The atomizer is also connected to a compressor and a pump to control the flow rates.

#### 4.1.1 Material Properties of Silica gel

The silica gel used in this study was obtained from Traiva company. Its corresponding properties given by the manufacturer is listed in table 4.1 below. Yuri et al [86][85] reported similar properties with apparent diffusivity, the pre-exponential factor and the activation energy being  $(3.7 - 4.7) \times 10^{-7}$ ,  $2.9 \times 10^{-4} \text{ m}^2/\text{s}$  and 41.5kJ/mol respectively.

Table 4.1 showing properties of the silica gel at T = 23 (+2) °C obtained from Manufacturer.

Property	Value
$\phi=0.2$	11.0% of water absorbed
$\phi=0.5$	25.5% of water absorbed
$\phi=0.9$	36.0% of water absorbed
Regeneration Temperature [°C]	130 – 160
pH	4 – 6
Pore diameter [nm]	2 – 3
Pore Volume [ml/g]	0.35 - 0.45
Thermal conductivity [W/mK]	0.63
Bulk Density [g/cm <sup>3</sup> ]	620 - 700
Active surface [m <sup>2</sup> /g]	800

#### 4.1.2 Adsorption Phase

Silica gel of mass 0.8 g is weighed by means of a mass balance and placed into the sorption tube. During the adsorption phase, the atomizer and the heat gun are started while the inlet and outlet valves remain closed to prevent adsorption of moisture from the atmosphere. The compressor together with the pump is fed to the atomizer to deliver fine atomized water at a flow rate of 0.045 l/h. The air flow rate from the heat gun was also set to 3.0 m<sup>3</sup>/h. Several tests were carried out to ensure a constant inlet condition of 70% relative humidity at 25 °C and flow rate of 3.0 m<sup>3</sup>/h. After this, the inlet valve and outlet valves were opened and the adsorption of moisture was allowed to take place. Data on the humidity, temperature and flowrate at the bed and outlet were recorded while the inlet conditions are carefully monitored and kept constant. The data was recorded at a time interval of 15 mins for a total of 165 mins (cycle repeatability testing).

After testing the system's ability with 135 mins duration to adsorb the silica gel and a lower flow velocity of 2.6 m<sup>3</sup>/h, a five-cycle test was performed in a 165 minutes duration to check the performance of the silica gel using a low-grade heat during the desorption phase. After this, a test on the effect of the flow rate on the adsorption is also examined.



Figure 4.2a figure showing silica gel after adsorption.

### 4.1.3 Desorption Phase

The desorption phase comprises of all the components of the storage system with the exception of the atomizer. At this phase, the heat gun is set to a flowrate of 3.5 m<sup>3</sup>/h and a temperature of 70 °C. The low temperature is to represent the system working with a low-grade heat. The hot air is allowed to flow through the bed and desorb the water vapor. The inlet, outlet and bed temperature, relative humidity and flowrates are recorded. The data was recorded at an interval of 15 mins for a total of 165 mins.

### 4.1.4 Regeneration of Silica gel

The silica gel was regenerated (temperature of 150 °C) after the experiment to restore it back to its initial storage capacity and performance after the 5-cycle operation. Several regeneration tests were also performed to measure the amount of moisture retained in the silica gel with increasing temperature.

## 4.2 Adsorption Isotherm and parameters for calculation

The Langmuir, Freundlich, and the D – A models were fitted with the experimental data obtained from the manufacturer.

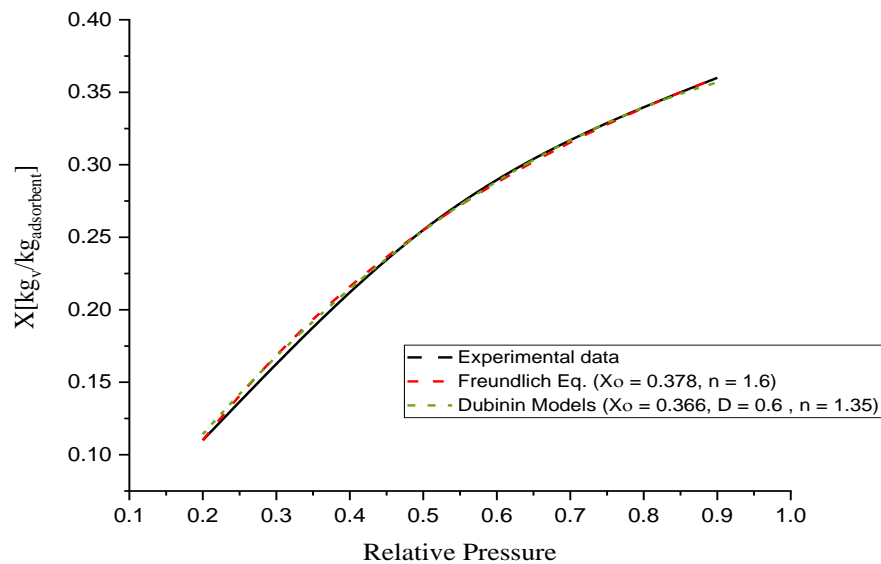


Figure 4.3 A graph showing data fitting of experimental data of water adsorption by silica gel.



Table 4.2. Parameter obtained after fitting the experimental data.

Models	Xo	n	D
Langmuir	0.549	1.365	-
Freundlich	0.378	1.6	-
Dubinin	0.366	1.35	0.6

Figure 4.1 above illustrates how the various models (Freundlich and D – A models) is above to fit the experimental data. Langmuir isotherm fit the data relatively poorly with an  $R^2$  value of less than 0.8. However, the Freundlich isotherm and the D – A model was able to fit the data relatively better, with the D – A model having the best fit. This means that the maximum adsorption capacity of the silica gel approaches that given by the D – A model (0.366 kgv/kg<sub>silica gel</sub>). Hence, the activation energy used is one obtained using the D – A model.

Table 4.3. Parameters used for the analysis of the system.

Symbol	Parameter	Value
$C_{ps}$	Specific heat capacity of silica gel	924 J/kg/K
$C_{pw}$	Specific heat capacity of water	4180 J/kg/K
$C_{pv}$	Specific heat capacity of vapor	1866 J/kg/K
$\Delta H$	Isosteric heat of adsorption	2.27e6 J/kg
$E_a$	Activation energy	4.08e4 J/mol
$D_{s0}$	Pre-exponential term	2.54e -4
$R_p$	Adsorbent particle radius	1e – 3 m
R	Universal gas constant	8.314 J/mol/K
$\tilde{V}$	Air flow rate	3.0 m <sup>3</sup> /h

## 5 RESULTS AND DISCUSSION

### 5.1 Adsorption and Desorption Test with low grade heat.

#### *Adsorption*

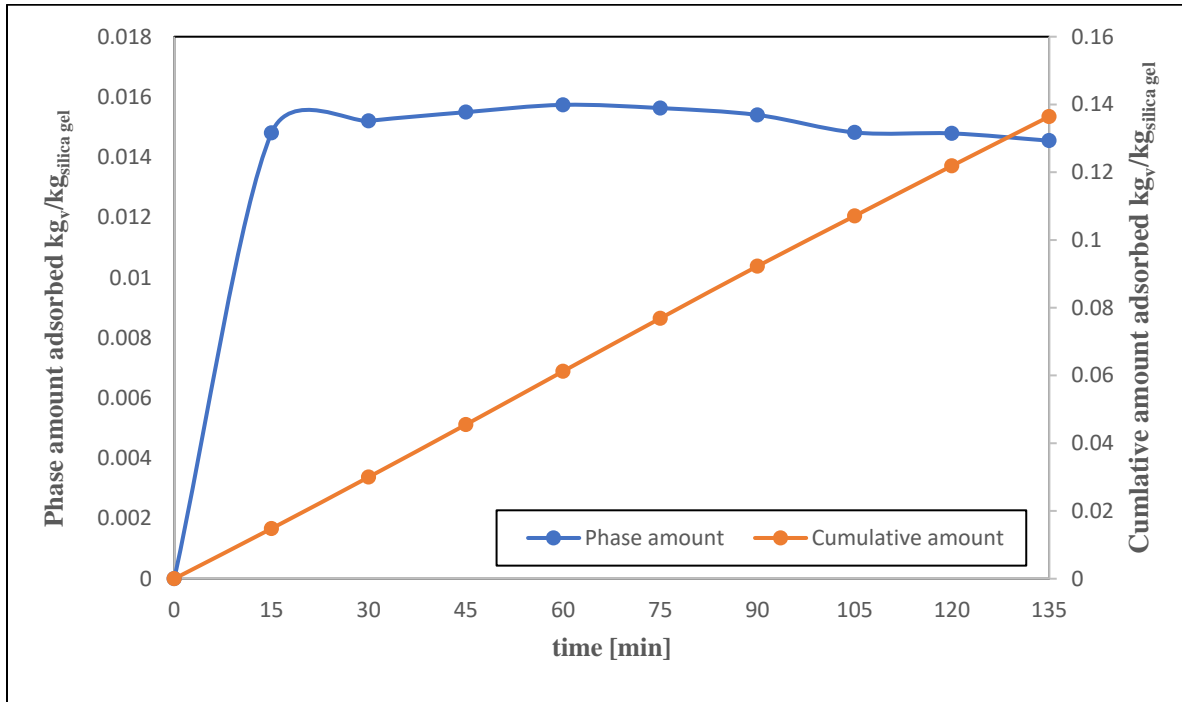


Figure 5.1 Illustration of the phase and the cumulative amount of moisture adsorbed per kg of silica gel.

With system adsorption testing conditions such as 70 % inlet relative humidity, 25 °C inlet temperature and 1.3 m/s flow velocity, the phase amount and cumulative amount are shown for an adsorption time of 135 minutes (see Fig. 5.1). In the figure, the phase amount adsorbed resides between 0.014 – 0.016 kg<sub>v</sub>/kg<sub>silica gel</sub> for the whole 135 mins duration. However, there is a beginning of a slight decline at time 90 min. This show a high tendency of continuous high adsorption for an extended time period before a large decline begins. Furthermore, this is more evident in the cumulative amount adsorbed shown. The relation of the cumulative amount to time is almost linear with a gradient of 0.001 kg<sub>v</sub>/kg<sub>silica gel</sub> per min for the given adsorption time. Thus, there is going to be a much higher increase for an extended time before the graph levels off to the maximum.

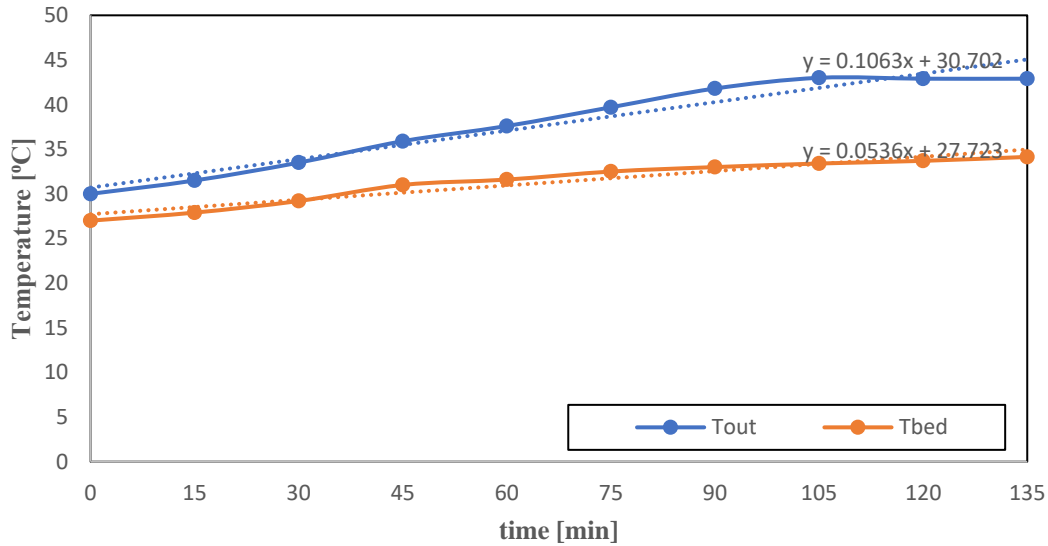


Figure 5.2 Depicting the temperature out of the sorption tube and that of the bed.

The temperature out of the sorption tube increases at a rate of  $0.1063 \text{ }^\circ\text{C}/\text{min}$  as shown in Fig. 5.2 above. The rise continues until time 105 min where the outlet temperature remains almost constant at  $42.9 \text{ }^\circ\text{C}$  for the remaining time. However, the bed temperature is much lower than the temperature out, as it rises to a temperature of  $34 \text{ }^\circ\text{C}$  at a rate of  $0.0536 \text{ }^\circ\text{C}/\text{min}$ . The difference between the inlet and the bed temperatures widens as time increases. This shows that more heat is given as convective heat than sensible heat with increasing time. Hence, this should be considered when using both the design, silica gel and the operation conditions for the purpose of space heating.

### *Desorption*

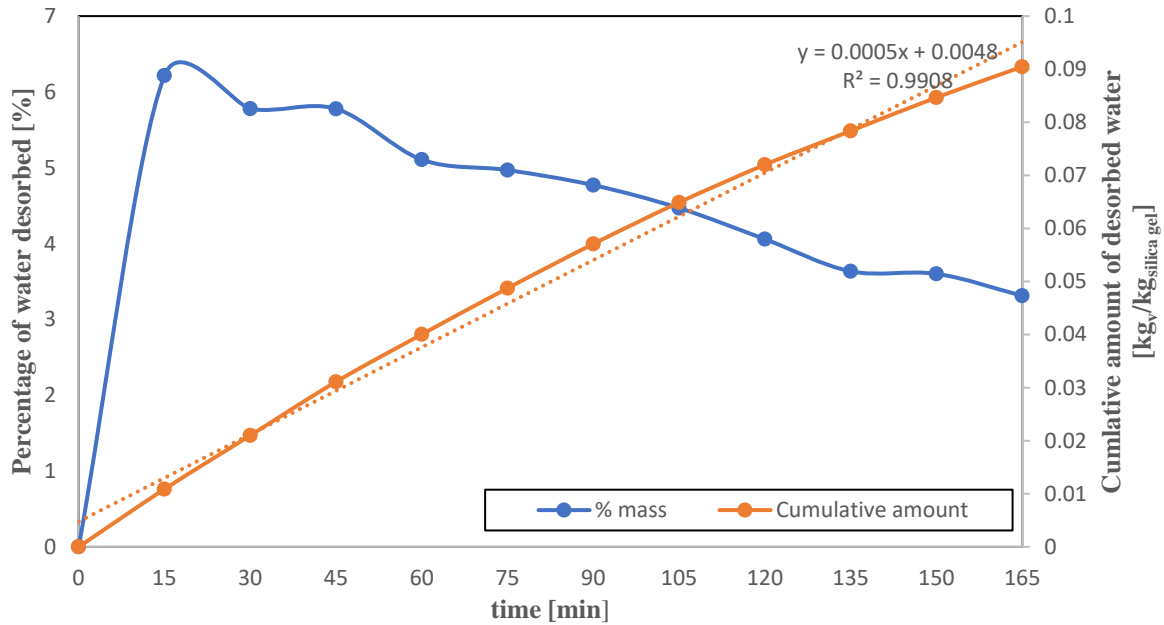


Figure 5.3 Illustration of the desorption of silica gel with time.

The desorption was done with a temperature of 70 °C and inlet flow rate of 3.5 m<sup>3</sup>/h (see Fig. 5.3S). Its effect on the amount of moisture desorbed in 165 mins from the silica gel is shown. It is seen that about 6 % of the moisture in the silica gel is desorbed in the first 15 mins. After this, the percentage mass desorbed decreases to a rate of 0.0195 %/min, which continues until the 165 mins where the percentage desorbed reaches 3.3 %. Consequently, there is a relatively high cumulative amount desorbed in the duration adsorption at the rate of 0.0005 (kg<sub>v</sub>/kg<sub>silica gel</sub>)/ min. However, the cumulative amount desorbed seem to be steering towards leveling off (thus reaching a point where there is no longer desorption by the operating desorption conditions). The total amount desorbed reached 0.09 kg<sub>v</sub>/kg<sub>silica gel</sub> at the end of the 165 mins which corresponds to 52 % of the mass adsorbed during the adsorption phase. This means that, the low-grade heat of 70 °C and flowrate of 3.5 m<sup>3</sup>/h is not enough to completely desorb the silica gel to reach its full adsorption capacity. This is evident in the reason why the adsorption of moisture during the cyclic test kept on reducing.

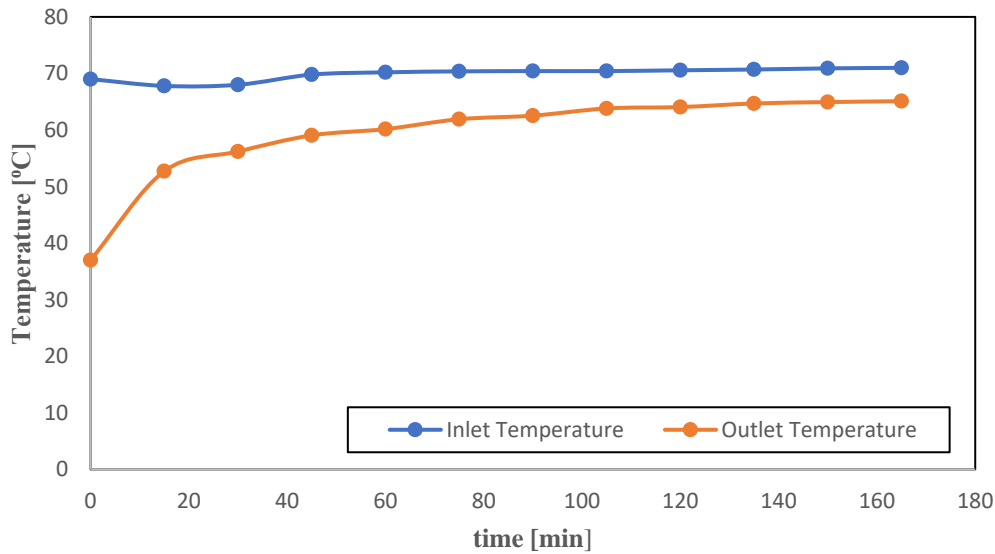


Figure 5.4 Showing the temperature profile for the inlet and outlet temperatures during desorption.

The corresponding inlet and outlet temperature during the desorption phase are plotted against time in **Fig. 5.4** above. A rise in the outlet temperature while the inlet temperatures are kept constant at 70 °C is observed. During the first 15 minutes, the temperature rise is about 14 °C, which is followed by a steady rise but a lower rate for the whole desorption duration. The rise of the outlet temperature is observed to be inverse to the rate of amount of water desorbed. Thus, as the amount of moisture that is desorbed decreases with time, the outlet temperature increases.

## 5.2 Adsorption Test For 5 Cycles using Low grade heat

### Adsorption

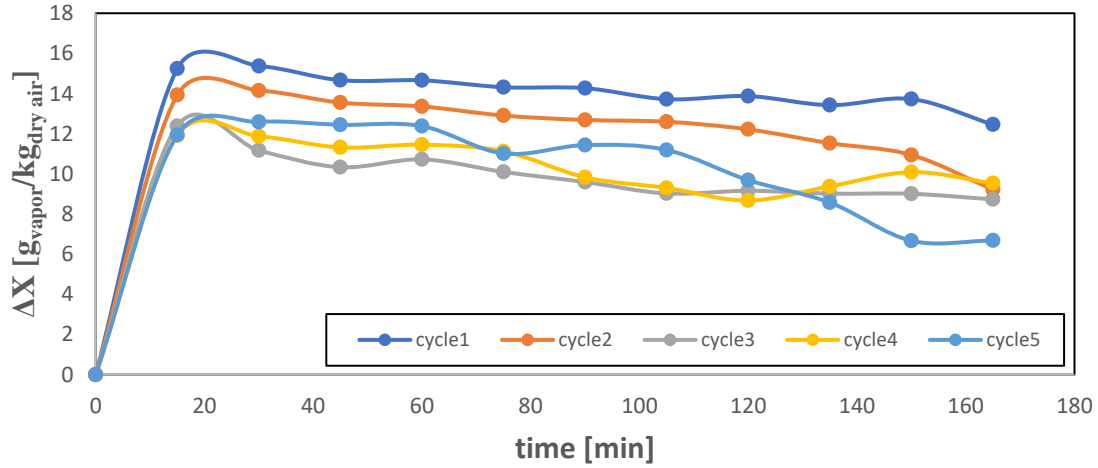


Figure 5.5. Adsorption of moisture in the bed for all cycles

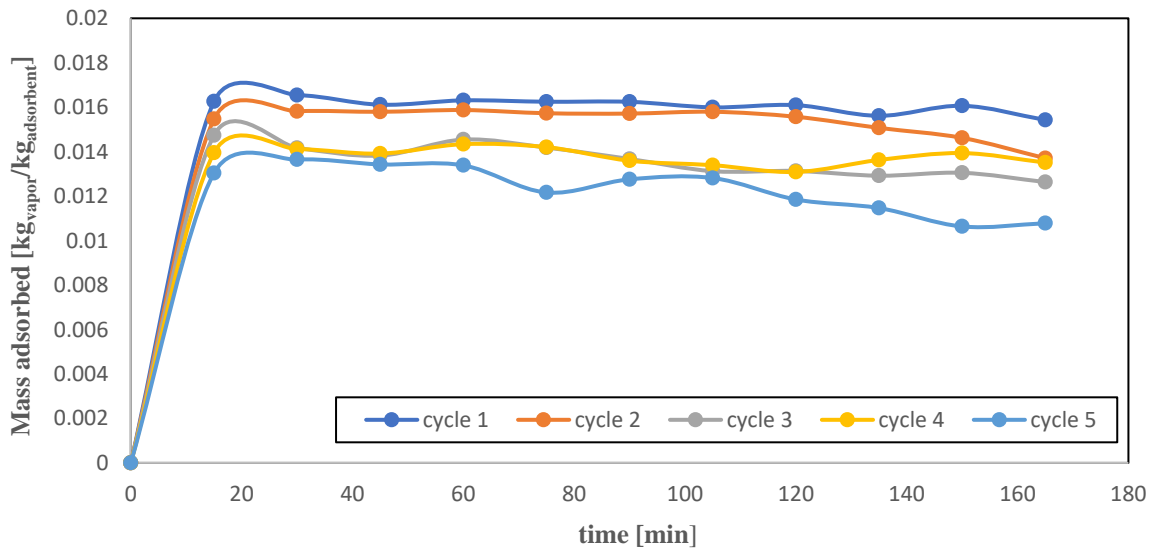


Figure 5.6. Phase mass adsorbed

Figure 5.6 above show the change in specific humidity with time which is used to calculate the mass of water vapor accumulation in the sorption tube with time. The difference in the specific humidity was calculated from relative humidity and temperature difference between the inlet and the outlet of the sorption tube. The first cycle demonstrated the highest capacity for the given duration of 165 mins, followed by the subsequent cycles with cycle 3, 4 and 5 developing a situation based on accuracy measurement for each cycle, the specific humidity decreases at an average rate of  $0.02 \text{ g}_{\text{vapor}}/\text{kg}_{\text{dry air}}/\text{min}$ . Nonetheless, this rate is slow indicating there is a potential for more adsorption with an increased adsorption duration above 165 mins. Moreover this is evident in several researches, which have clearly indicated adsorption with similar inlet condition for over 7 hour duration [106][100]. With better distinction in adsorption of water vapor for the last 3 cycles. Additionally, the water adsorption is almost constant for cycles 1 and 2 from time 40 mins to 105 mins before it starts to decline.

Given the inlet conditions of  $3 \text{ m}^3/\text{h}$  flowrate, 70% relative humidity and temperature of  $25 \text{ }^\circ\text{C}$ , the specific humidity decreases slightly with increasing number of cycles. This decrease is because the desorption temperature used ( $70 \text{ }^\circ\text{C}$ ) in the time duration of 165 mins is not sufficient to completely desorb the silica gel and return it to its initial adsorption capacity. Hence, the water molecules that is left in the silica gel reduces the adsorption capacity of the silica gel as well as gives slower adsorption kinetics during subsequent adsorption. This is expected because the regeneration temperature prescribed by the manufacturer is between ( $130 \text{ }^\circ\text{C} - 160 \text{ }^\circ\text{C}$ ) [121]. Moreover, research from Ng and Jahnig et al [88][104] shows that show that the regeneration temperature of silica gel is usually between  $90 \text{ }^\circ\text{C}$  to  $160 \text{ }^\circ\text{C}$  at a time duration of at least 5 hours. The difference between the first and the fifth cycles is about  $3.1 \text{ g}_{\text{vapor}}/\text{kg}_{\text{dry air}}$  during the first 20 mins. The difference increases further with duration, where it reaches  $6 \text{ g}_{\text{vapor}}/\text{kg}_{\text{dry air}}$  at the end of the 165 mins. Moreover, this is expected to increase with increasing time [106].

Figure 5.6 shows a change of about  $0.003 \text{ kg}_{\text{vapor}}/\text{kg}_{\text{silica gel}}$  to  $0.006 \text{ kg}_{\text{vapor}}/\text{kg}_{\text{silica gel}}$  from cycle 1 to cycle 5. This further corresponds to a decrease of about 18 % to 37 % after the 5 cycles. This means that with similar desorption conditions, and as the number of cycles increases, the phase amount of moisture adsorbed will decrease gradually until regeneration temperature and times prescribed in literature or by the manufacturer is performed.

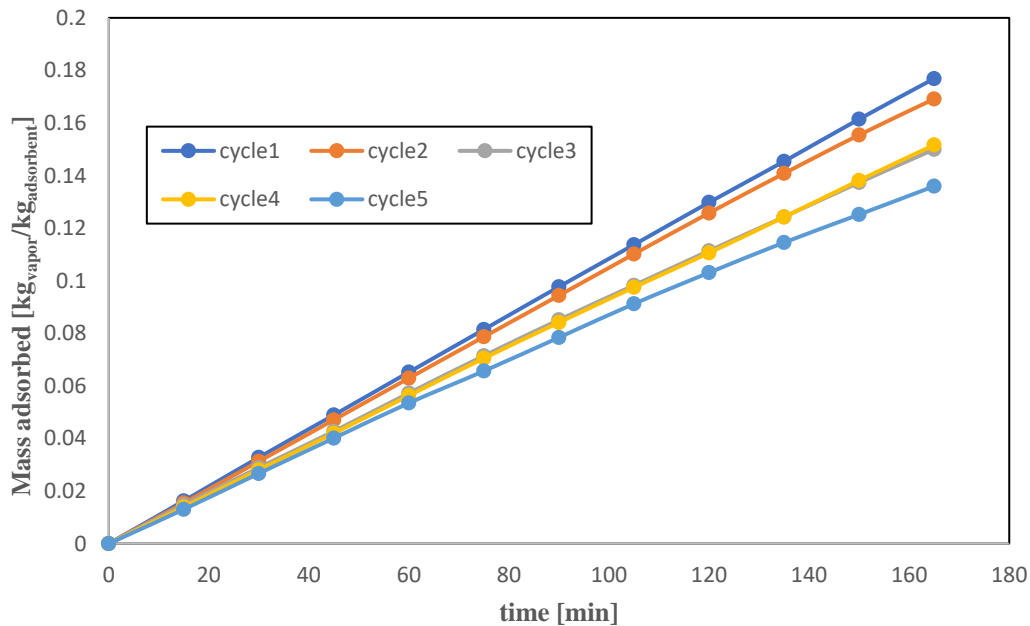


Figure 5.7. Cumulative mass adsorbed over 165 mins.

Figure 5.7 above illustrates the amount of moisture that is adsorbed in a given time period of 165 mins. The highest amount adsorbed is observed with the cycle 1 but decreases as the number of cycles increases. The graph for cycles 1 and 2 indicates linearity, meaning that the maximum adsorption is not yet reached. Hence, there is a tendency to continue to increase with increasing time before it approaches a constant value. Bending towards the maximum should be clearer for a period of over 10 hours. Mohammed et al [122] demonstrated with a 5 g of RD-2060 silica gel with 0.3 – 0.79 mm particle size for 35 mins that the silica gel approaches constant value after a given time. On the other hand, the amount of silica gel used in the study was relatively small. Howbeit, Amorim et al [106] reported that for a 650 g of silica gel with diameter 4 mm, flow velocity of 0.5 m/s, 70 % relative humidity and 26 °C inlet temperature, the phase amount of the adsorbed moisture reached 0 kg<sub>vapor</sub>/kg<sub>silica gel</sub> after 20 hours. This means that there was no more adsorption after 20 hrs. Nevertheless, there was about 27 % more amount of moisture adsorbed in 165 mins for this work than was reported by Amorim et al, which may be a consequence of higher flow velocity (1.4 m/s) used for this work. Therefore, we expect to observe the curve leveling off sooner than the 20 hours.



Furthermore, concerning the cycle repeatability, there was about  $0.03 \text{ kg}_{\text{vapor}}/\text{kg}_{\text{silica gel}}$  difference in cumulative adsorption between cycles 1 and 5 at the end of the 165 mins. This loss is equivalent to 9 % loss in the adsorption capacity of the silica gel after the 5 cycles.

### *Temperature*

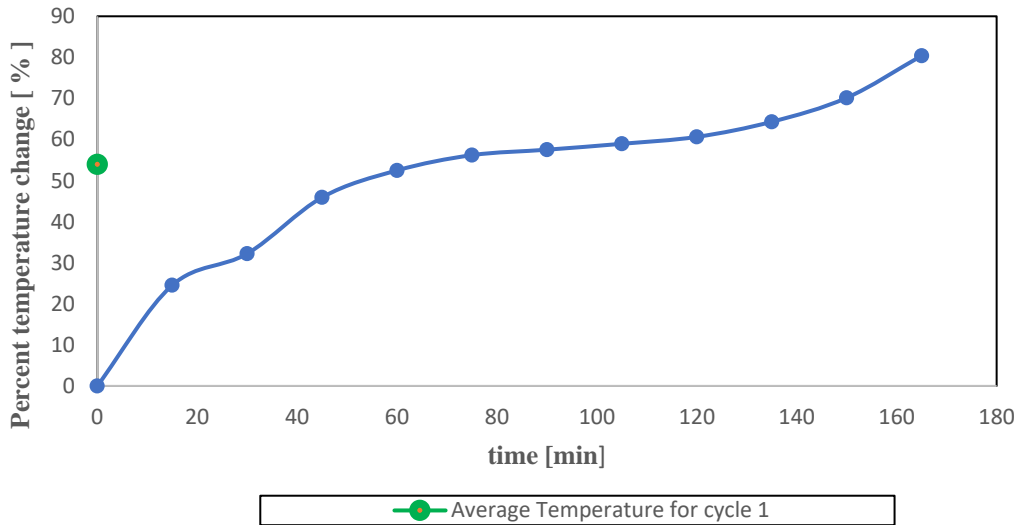


Figure 5.8. A graph showing temperature out and average temperature lift

The temperature at the outlet of the sorption bed is plotted against time (see Fig. 5.8). The percent temperature is expressed as a temperature difference between the outlet and the inlet temperatures, divided by the inlet temperature. The results show that, for about 60 mins, there was a steady rise in the temperature, and an almost steady temperature was observed for another 60 mins. A steady rise followed until the highest temperature of  $45 \text{ }^\circ\text{C}$  was reached for the adsorption time, equivalent to 80 % increase relative to the inlet temperature of  $25 \text{ }^\circ\text{C}$ . The heating capacity is expected to continuously increase with increasing the adsorption time before a constant temperature or a decline in temperature is reached. For 0.8 Kg of silica gel used and adsorption conditions,  $13 \text{ }^\circ\text{C}$  of temperature lift was obtained. Deshmukh et al reported an average of  $25 \text{ }^\circ\text{C}$  temperature lift with a closed system with 350 kg of silica gel and flowrate of  $0.029 \text{ kg/s}$  in a period of 6 hours.

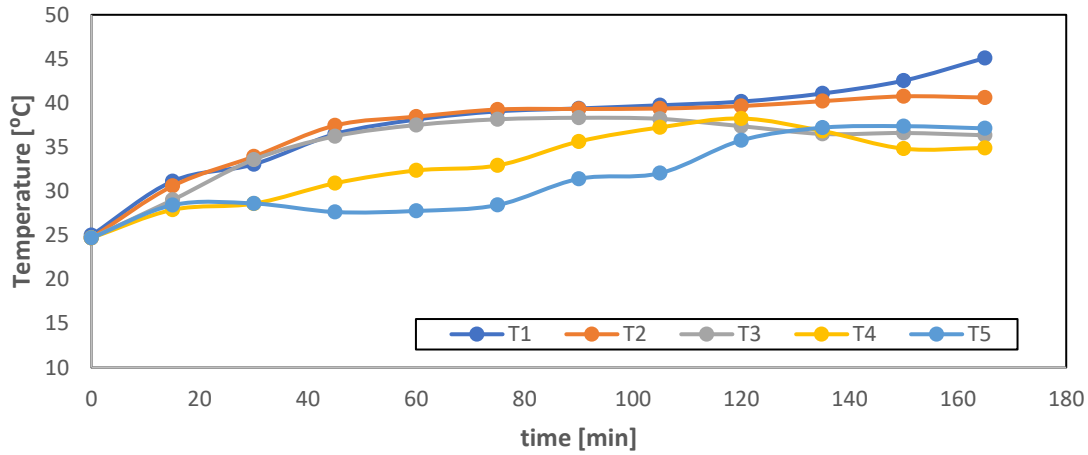


Figure 5.9. Output temperatures for all cycles

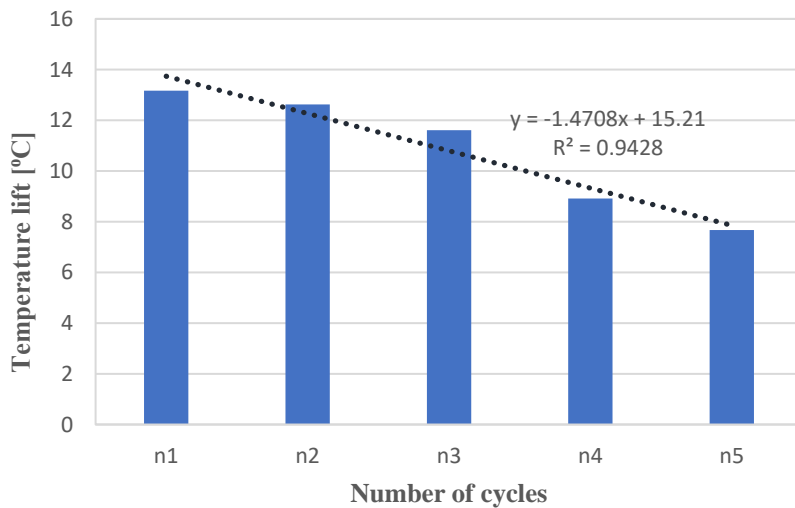


Figure 5.10. Average temperature lift to the number of cycles

Figure 5.10 compares the temperature out of subsequent cycles relative to cycle 1. Cycles 1, 2 and 3 take similar paths for the first 100 mins, where they rise to 37.5 °C and remain almost constant for about 40 mins. With the behavior of the temperature graph of cycle 1 explained above compared to cycle 2, the rise in the temperature for cycle 2 remained almost constant, while cycle 3 began to decrease at time 105 mins before remaining constant. Cycles 4 and 5 kept a steady rise from time 30 mins for a duration of 105 mins with the temperature of cycle 4 being about 4 degrees

higher than cycle 5. After 135 mins, the order interchanges where the temperature for cycle 5 becomes 2 degrees higher than that for cycle 4. Thus, the outlet temperature for cycles 4 and 5 take a long time to reach their peak before they decline or remains constant. These changes seen in the outlet temperature for all the cycles is due to the convective heat transfer characteristic in the bed. Thus, the amount of heat energy produced in the bed and the flow characteristics in the bed affects the temperature at the output of the bed. Additionally, as the number of cycles increases, lower outlet temperatures are recorded and this is evident in the decrease in average temperature lift with number of cycles. The relatively lower temperature recorded is due to lower rate adsorption and exothermic reaction in the bed, hence lower energy produced. Furthermore, for a given  $R^2$  value of 0.94, the rate of decrease in the temperature lift as the number of cycles increases is 1.47 °C/cycle.

**Power and Energy**

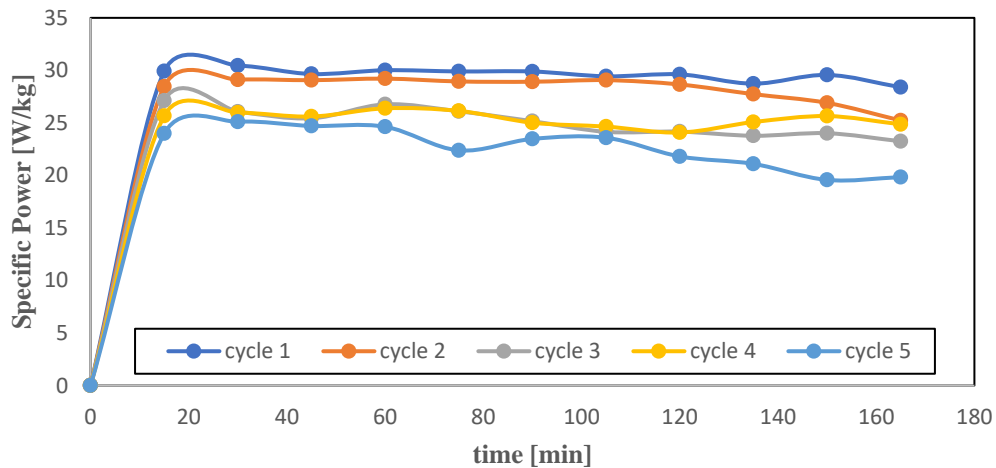


Figure 5.11 Comparison of reaction power generated at a given time for all cycles

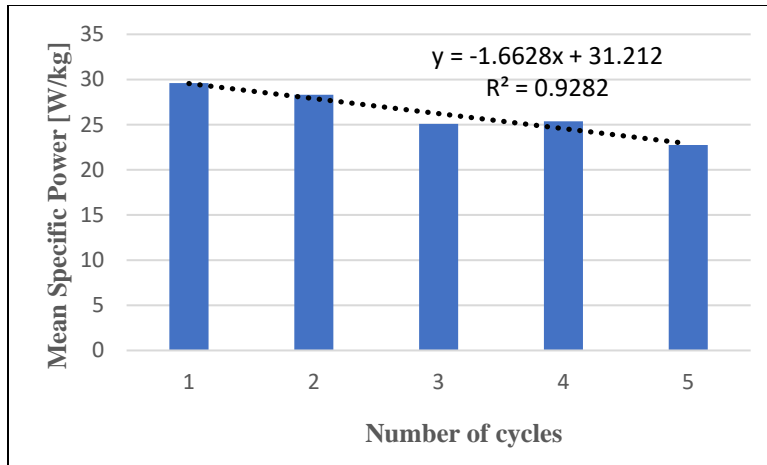


Figure 5.12 Change in Mean Specific Power Over Five Cycles

The power generated through the process and the mean specific power produced for all cycle are shown in Fig. 5.11 and 5.12 respectively. There seem to be a strong correlation between Fig. 5.11 and that with adsorbed moisture by the bed. Since the amount of moisture adsorbed in each cycle varies inversely with time, the generated power decreases with time as well due to less and slower occurrence of the exothermic reaction. The minimum and maximum specific power for the five cycles was observed to occur at cycle 5 and cycle 1 with values of 19.5 W/kg and 30.4 W/kg respectively. M. Gaeni [123] observed similar specific power compared to one delivered by cycle 1, when zeolite was used as the adsorbent material which similar inlet operating conditions. The average specific power produced decreases as the number of cycles increases, with a 6.8 W/kg reduction in mean specific power reduction after 5 cycles. This is equivalent to about 22.5 % loss in the mean specific power after the 5 cycles. For an  $R^2$  value of 0.928, the rate of reduction in the power density was 1.66 W/kg per cycle. The mean specific power for cycle 1 was 29.5 W/kg and this is comparable to an open system with zeolite adsorbent which was reported by Johannes et al to be 27.5 W/kg at similar operating conditions [77].

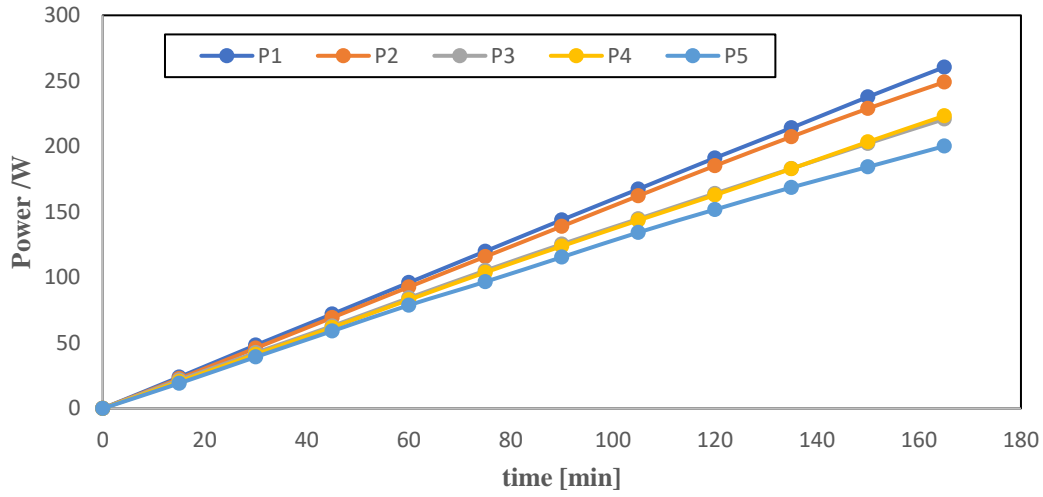


Figure 5.13. Cumulative Power of reactive heat generation

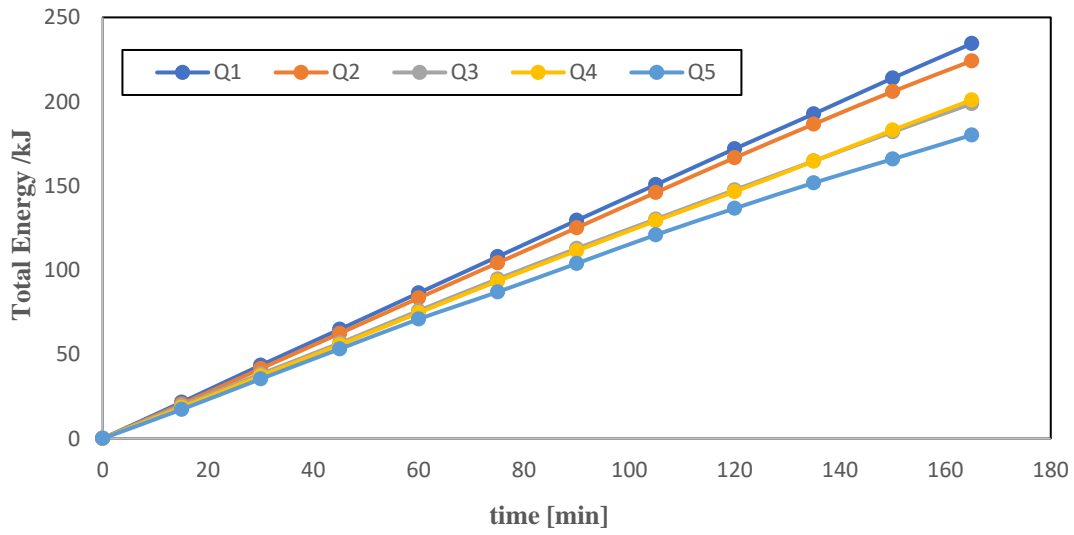


Figure 5.14. Total energy produced

The cumulative power and energy as shown in Fig. 5.13 and Fig. 5.14 also follow the same trajectory as the cumulative mass adsorbed over the adsorption period. The highest and lowest power produced in the sorption bed is during cycle 1 and cycle 5 with about 260 W and 200 W respectively. This about a 60 W loss after a 5-cycle operation which corresponds to 23 % loss. In spite of the fact that there seem to be a linear relation for the power produced with time for cycle 1 (P1) and 2 (P2) in Fig. 5.13, the power produced for cycle 3,4 and 5 shows the beginning of leveling, while with P5 being more prominent. Thus, the power produced by cycle 5 (P5) approaches its maximum before it declines or remains constant. The total energy produced shown in Fig. 5.14 follows the same trajectory. The total energy produced after the adsorption phase is 234 kJ for the first cycle (which is equivalent to 292 kJ/kg) and it decreases to 180 kJ (which is equivalent to 225 kJ/kg) after the 5 cycles.

### 5.3 Effect of Flow Velocity on Adsorption and Desorption Phases

There is an effect of the flowrate on the adsorption and desorption cycles. This effect spans across the amount of moisture adsorbed or desorbed as well as the rise in the temperature at the outlet of the bed. For the adsorption, a flow velocity of 1.25 m/s is compared with 0.9 m/s and for the desorption phase, a flow velocity of 1 m/s is compared with 1.6 m/s.

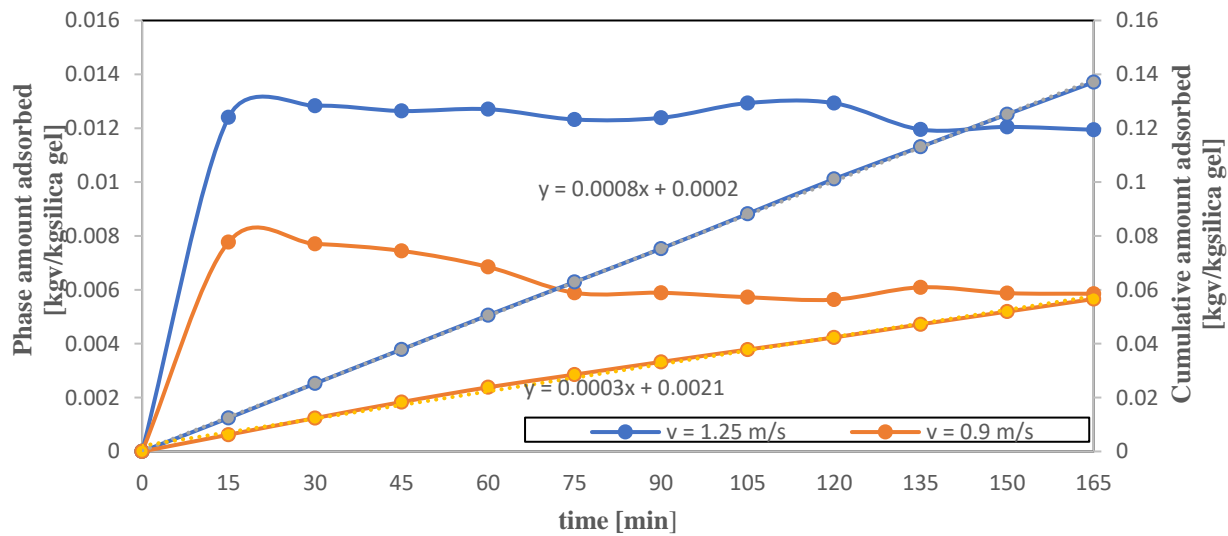


Figure 5.15 A diagram showing amount of water adsorbed for different flowrates.

From **Fig. 5.15** above, the phase amount adsorbed and cumulative amount adsorbed for 165 minutes time duration is plotted for inlet velocities of 1.25 and 0.9 m/s. The figure shows that, for an inlet velocity of 1.25 m/s, the adsorption resides between 0.0129 – 0.0119 kg<sub>v</sub>/kg<sub>silica gel</sub> while slightly decreasing. For an inlet velocity of 0.9 m/s the phase amount adsorbed started at 0.0077 kg<sub>v</sub>/kg<sub>silica gel</sub> and ended at 0.0058 kg<sub>v</sub>/kg<sub>silica gel</sub>. The rate of decrease is also seen to be higher for v=0.9 m/s than for v=1.25 m/s. Consequently, the cumulative amount adsorbed for v = 1.25 m/s at the end of the adsorption phase is about 2.3 times higher than for v = 0.9 m/s. This is also evident in the rate of increase which is 0.0003 [kg<sub>v</sub>/kg<sub>silica gel</sub>]/min for v = 0.9 m/s and 0.0008 [kg<sub>v</sub>/kg<sub>silica gel</sub>]/min for v=1.25 m/s. It can be deduced that, higher flowrates cause higher rates of adsorption, which yields more amount of moisture adsorbed.

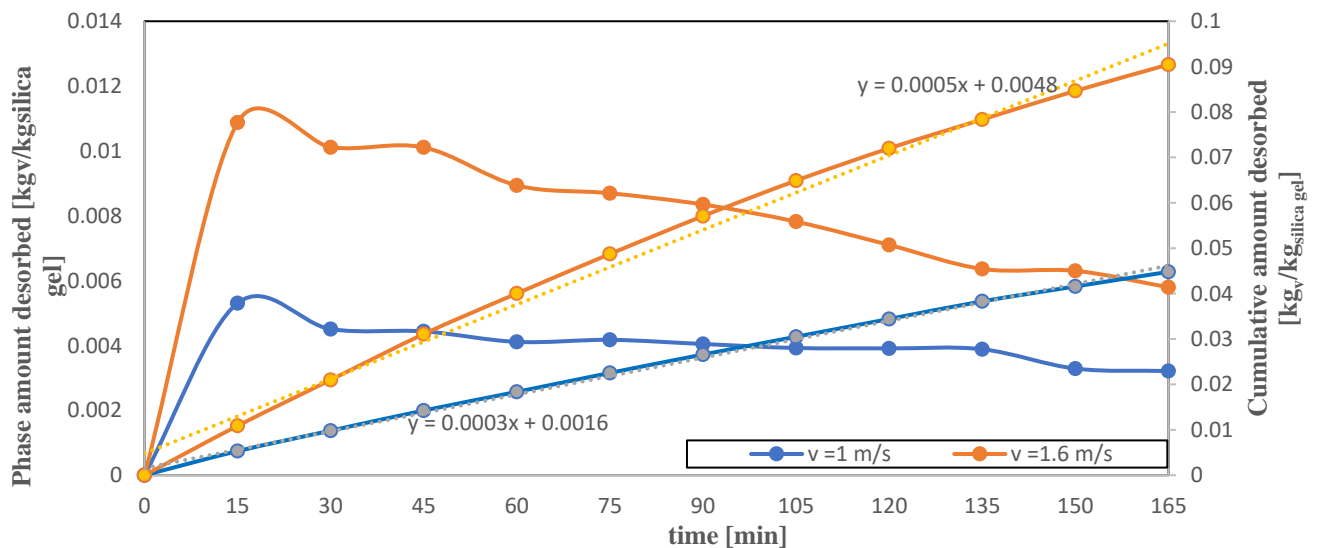


Figure 5.16. A diagram showing the amount of water desorbed using different flowrates.

For the desorption phase, shown in Fig. 5.16, the amount of moisture desorbed using two inlet velocities of 1 m/s and 1.6 m/s are compared. The graph shows a monotonic decrease in the phase amount adsorbed for both velocities, with the decrease for the v = 1.6 m/s having a much more steeper slope. The phase amount desorbed for v = 1.6 m/s begins at 0.0108 [kg<sub>v</sub>/kg<sub>silica gel</sub>] and ends at 0.0057 [kg<sub>v</sub>/kg<sub>silica gel</sub>] The phase amount desorbed for v = 1 m/s starts at 50 % less desorption

compared to  $v = 1.6$  m/s. As a result, the total cumulative amount desorbed for  $v = 1.6$  m/s is 49.5 % higher than the cumulative amount adsorbed for  $v = 1$  m/s at the end of the desorption phase. Furthermore, the rate of desorption for  $v = 1.6$  m/s is  $0.0005$  [kg<sub>v</sub>/kg<sub>silica gel</sub>]/min which is 40 % higher than the desorption rates for  $v = 1$  m/s. Hence, higher flowrates are able to desorb much faster and at a higher rate than for lower flowrates.



## 6 CONCLUSION

In a nutshell, this thesis was to design an energy storage system to be used in a research study of the testing of the adsorption capacity of silica gel as well as the cycle repeatability for the silica gel. Based on this, the energy storage system was designed (see section 3) with specific requirements. The adsorbent material chosen was silica gel based on certain favorable advantages it has (see section 2.4). In the aim to set up a working energy system, a sorption tube was designed for an efficient flow based on specified flowrates and temperatures from the heat gun and the atomizer. The atomizer and all other components are positioned to ensure maximum performance during operation (see section 3). Several tests were carried out to specify the operating conditions. The experimental data of the silica gel obtained from the manufacturer was fitted against adsorption model such as the Langmuir, Freundlich and D – A isotherms to obtain the maximum adsorption capacities (see section 4). Based on the fitting and regression analysis, the D – A model and the Freundlich model gave the better performance with the D – A model being the best among them. Hence, the D – A model was chosen for the determination of the maximum adsorption capacity and activation energy of the silica gel. Adsorption and desorption cycles were set with an operating time of 165 mins. The tests carried out includes the testing of the system, cycle repeatability test with low grade heat for regeneration and the effect of flowrates on the adsorption and desorption of the silica gel. The results for the testing of the system show that there is a high rate of adsorption of  $0.001 \text{ [kg}_v\text{/kg}_{\text{silica gel}} / \text{min}]$  for a given 2.15 hrs. A very high outlet temperature which was 72 % more of the inlet temperature was also obtained with a gradient of  $0.1063 \text{ [}^\circ\text{C/min]}$ . The results for desorption phase with low grade heat showed that, just about 52 % of the amount of moisture adsorbed could be desorbed with a low-grade heat of  $70 \text{ }^\circ\text{C}$  for the duration of 165 mins. For the cycle repeatability study with a low-grade heat, a five-cycle test was performed and the results showed a decrease in adsorption as number of cycles increased. This is due to the low-grade heat used during the desorption phase, which is not able to sufficiently desorb the moisture adsorbed. The average temperature lift for the first cycle was  $13 \text{ }^\circ\text{C}$ , where it decreased as the number of cycles increased at a rate of  $1.47 \text{ }^\circ\text{C/cycle}$ . Furthermore, a mean specific power of  $29.5 \text{ W/kg}$  was obtained for cycle 1, with a 22.7 % loss in the specific power at the end of the 5 cycles, with an energy density of  $(292 - 225) \text{ kJ/kg}$  after 165 mins. It was also observed that, higher flowrate aid in higher adsorption and desorption rates while lower flowrates aid in lower desorption and adsorption rate.

## 7 REFERENCES

- [1] IRENA INTERNATIONAL RENEWABLE ENERGY AGENCY. *Global Energy Transformation: A Roadmap to 2050* [online]. 2019. ISBN 978-92-9260-059-4. Dostupné z: <http://irena.org/publications/2018/Apr/Global-Energy-Transition-A-Roadmap-to-2050%0Awww.irena.org>
- [2] U.S. EIA. Annual Energy Outlook 2019 with projections to 2050. *Annual Energy Outlook 2019 with projections to 2050* [online]. 2019, **44**(8), 1–64. ISSN 1387-1811. Dostupné z: doi:DOE/EIA-0383(2012) U.S.
- [3] CHIDAMBARAM, L. A., A. S. RAMANA, G. KAMARAJ a R. VELRAJ. Review of solar cooling methods and thermal storage options. *Renewable and Sustainable Energy Reviews* [online]. 2011, **15**(6), 3220–3228. ISSN 13640321. Dostupné z: doi:10.1016/j.rser.2011.04.018
- [4] MORENO, Pere, Cristian SOLÉ, Albert CASTELL a Luisa F. CABEZA. The use of phase change materials in domestic heat pump and air-conditioning systems for short term storage: A review. *Renewable and Sustainable Energy Reviews* [online]. 2014, **39**, 1–13. ISSN 13640321. Dostupné z: doi:10.1016/j.rser.2014.07.062
- [5] SHARMA, Atul, V. V. TYAGI, C. R. CHEN a D. BUDDHI. Review on thermal energy storage with phase change materials and applications. *Renewable and Sustainable Energy Reviews* [online]. 2009, **13**(2), 318–345. ISSN 13640321. Dostupné z: doi:10.1016/j.rser.2007.10.005
- [6] BIN, Zhu. „Solid oxide fuel cell (SOFC) technical challenges and solutions from nano-aspects". *International journal of energy research* [online]. 2009, **31**(August 2007), 135–147. ISSN 0363907X. Dostupné z: doi:10.1002/er
- [7] AL-ABIDI, Abduljalil A., Sohif BIN MAT, K. SOPIAN, M. Y. SULAIMAN a Abdulrahman Th MOHAMMED. CFD applications for latent heat thermal energy storage: A review. *Renewable and Sustainable Energy Reviews* [online]. 2013, **20**, 353–363. ISSN 13640321. Dostupné z: doi:10.1016/j.rser.2012.11.079

- [8] DE GRACIA, Alvaro a Luisa F. CABEZA. Numerical simulation of a PCM packed bed system: A review. *Renewable and Sustainable Energy Reviews* [online]. 2017, **69**(July 2016), 1055–1063. ISSN 18790690. Dostupné z: doi:10.1016/j.rser.2016.09.092
- [9] PALOMBA, Valeria, Salvatore VASTA a Angelo FRENI. Experimental testing of AQSOA FAM Z02/water adsorption system for heat and cold storage. *Applied Thermal Engineering* [online]. 2017. ISSN 13594311. Dostupné z: doi:10.1016/j.applthermaleng.2017.06.085
- [10] VASTA, Salvatore, Vincenza BRANCATO, Davide LA ROSA, Valeria PALOMBA, Giovanni RESTUCCIA, Alessio SAPIENZA a Andrea FRAZZICA. Adsorption heat storage: State-of-the-art and future perspectives. *Nanomaterials* [online]. 2018, **8**(7). ISSN 20794991. Dostupné z: doi:10.3390/nano8070522
- [11] GIL, Antoni, Marc MEDRANO, Ingrid MARTORELL, Ana LÁZARO, Pablo DOLADO, Belén ZALBA a Luisa F. CABEZA. State of the art on high temperature thermal energy storage for power generation. Part 1-Concepts, materials and modellization. *Renewable and Sustainable Energy Reviews* [online]. 2010, **14**(1), 31–55. ISSN 13640321. Dostupné z: doi:10.1016/j.rser.2009.07.035
- [12] SAMAN, W., F. BRUNO a E. HALAWA. Thermal performance of PCM thermal storage unit for a roof integrated solar heating system. *Solar Energy* [online]. 2005, **78**(2), 341–349. ISSN 0038092X. Dostupné z: doi:10.1016/j.solener.2004.08.017
- [13] HIMPEL, Michael, Stefan HIEBLER, Christian SCHWEIGLER a Martin HELM. Long-Term Test Results from a Latent Heat Storage Developed for a Solar Heating and Cooling System [online]. 2016, (January 2015), 1–8. Dostupné z: doi:10.18086/eurosun.2010.16.08
- [14] LIU, Ming, Wasim SAMAN a Frank BRUNO. Review on storage materials and thermal performance enhancement techniques for high temperature phase change thermal storage systems. *Renewable and Sustainable Energy Reviews* [online]. 2012, **16**(4), 2118–2132. ISSN 13640321. Dostupné z: doi:10.1016/j.rser.2012.01.020
- [15] FUJII, I., K. TSUCHIYA, M. HIGANO a J. YAMADA. Studies of an energy storage system by use of the reversible chemical reaction:  $\text{CaO} + \text{H}_2\text{O} \rightleftharpoons \text{Ca}(\text{OH})_2$ . *Solar Energy* [online]. 1985, **34**(4–5), 367–377. ISSN 0038092X. Dostupné z: doi:10.1016/0038-

092X(85)90049-0

- [16] PFLEGER, Nicole, Thomas BAUER, Claudia MARTIN, Markus ECK a Antje WÖRNER. Thermal energy storage - overview and specific insight into nitrate salts for sensible and latent heat storage. *Beilstein Journal of Nanotechnology* [online]. 2015, **6**(1), 1487–1497. ISSN 21904286. Dostupné z: doi:10.3762/bjnano.6.154
- [17] SKOVAJSA, Jan a Martin ZALESK. The use of the photovoltaic system in combination with a thermal energy storage for heating and thermoelectric cooling. *Applied Sciences (Switzerland)* [online]. 2018, **8**(10). ISSN 20763417. Dostupné z: doi:10.3390/app8101750
- [18] EDWARDS, Jacob, Hitesh BINDRA a Piyush SABHARWALL. Exergy analysis of thermal energy storage options with nuclear power plants. *Annals of Nuclear Energy* [online]. 2016, **96**, 104–111. ISSN 18732100. Dostupné z: doi:10.1016/j.anucene.2016.06.005
- [19] AYYAPPAN, S., K. MAYILSAMY a V. V. SREENARAYANAN. Performance improvement studies in a solar greenhouse drier using sensible heat storage materials. *Heat and Mass Transfer/Waerme- und Stoffuebertragung* [online]. 2016, **52**(3), 459–467. ISSN 14321181. Dostupné z: doi:10.1007/s00231-015-1568-5
- [20] ELIAS, Charalambos N. a Vassilis N. STATHOPOULOS. A comprehensive review of recent advances in materials aspects of phase change materials in thermal energy storage. *Energy Procedia* [online]. 2019, **161**, 385–394. ISSN 18766102. Dostupné z: doi:10.1016/j.egypro.2019.02.101
- [21] PIELICHOWSKA, Kinga a Krzysztof PIELICHOWSKI. Phase change materials for thermal energy storage. *Progress in Materials Science* [online]. 2014, **65**, 67–123. ISSN 00796425. Dostupné z: doi:10.1016/j.pmatsci.2014.03.005
- [22] RATHOD, Manish K. a Jyotirmay BANERJEE. Thermal stability of phase change materials used in latent heat energy storage systems: A review. *Renewable and Sustainable Energy Reviews* [online]. 2013, **18**, 246–258. ISSN 13640321. Dostupné z: doi:10.1016/j.rser.2012.10.022
- [23] SHARMA, S.D. a Kazunobu SAGARA. Latent Heat Storage Materials and Systems: A

- Review. *International Journal of Green Energy* [online]. 2005, **2**(1), 1–56. ISSN 1543-5075. Dostupné z: doi:10.1081/ge-200051299
- [24] LASER, T. Zu W. Hausotter: Fibromyalgie--ein entbehrlicher Krankheitsbegriff? *Versicherungsmedizin / herausgegeben von Verband der Lebensversicherungs-Unternehmen e.V. und Verband der Privaten Krankenversicherung e.V.* 1998, **50**(4), 154–156. ISSN 09334548.
- [25] JOTSHI, C. K., C. K. HSIEH, D. Y. GOSWAMI, J. F. KLAUSNER a N. SRJNIVASAN. Thermal storage in ammonium alum/ammonium nitrate eutectic for solar space heating applications. *Journal of Solar Energy Engineering, Transactions of the ASME* [online]. 1998, **120**(1), 20–24. ISSN 15288986. Dostupné z: doi:10.1115/1.2888041
- [26] FARID, Mohammed M., Amar M. KHUDHAIR, Siddique Ali K. RAZACK a Said AL-HALLAJ. A review on phase change energy storage: Materials and applications. *Energy Conversion and Management* [online]. 2004, **45**(9–10), 1597–1615. ISSN 01968904. Dostupné z: doi:10.1016/j.enconman.2003.09.015
- [27] SARI, Ahmet, Hayati SARI a Adem ÖNAL. Thermal properties and thermal reliability of eutectic mixtures of some fatty acids as latent heat storage materials. *Energy Conversion and Management* [online]. 2004, **45**(3), 365–376. ISSN 01968904. Dostupné z: doi:10.1016/S0196-8904(03)00154-7
- [28] KIMURA, Hiroshi a Junjiro KAI. Phase change stability of sodium acetate trihydrate and its mixtures. *Solar Energy* [online]. 1985, **35**(6), 527–534. ISSN 0038092X. Dostupné z: doi:10.1016/0038-092X(85)90121-5
- [29] KHAN, Zakir, Zulfiqar KHAN a Abdul GHAFOR. A review of performance enhancement of PCM based latent heat storage system within the context of materials, thermal stability and compatibility. *Energy Conversion and Management* [online]. 2016, **115**, 132–158. ISSN 01968904. Dostupné z: doi:10.1016/j.enconman.2016.02.045
- [30] KARAMAN, Sedat, Ali KARAIPEKLI, Ahmet SAR a Alper BIÇER. Polyethylene glycol (PEG)/diatomite composite as a novel form-stable phase change material for thermal energy storage. *Solar Energy Materials and Solar Cells* [online]. 2011, **95**(7), 1647–1653.

ISSN 09270248. Dostupné z: doi:10.1016/j.solmat.2011.01.022

- [31] WANG, Zhengyun, Hui WANG, Mei YANG, Wenwen SUN, Guangfu YIN, Qinyong ZHANG a Zhifeng REN. Thermal reliability of Al-Si eutectic alloy for thermal energy storage. *Materials Research Bulletin* [online]. 2017, **95**, 300–306. ISSN 00255408. Dostupné z: doi:10.1016/j.materresbull.2017.07.040
- [32] CÁRDENAS, Bruno a Noel LEÓN. High temperature latent heat thermal energy storage: Phase change materials, design considerations and performance enhancement techniques. *Renewable and Sustainable Energy Reviews* [online]. 2013, **27**, 724–737. ISSN 13640321. Dostupné z: doi:10.1016/j.rser.2013.07.028
- [33] DUTIL, Yvan, Daniel R. ROUSSE, Nizar Ben SALAH, Stéphane LASSUE a Laurent ZALEWSKI. A review on phase-change materials: Mathematical modeling and simulations. *Renewable and Sustainable Energy Reviews* [online]. 2011, **15**(1), 112–130. ISSN 13640321. Dostupné z: doi:10.1016/j.rser.2010.06.011
- [34] SARBU, Ioan a Calin SEBARCHIEVICI. A comprehensive review of thermal energy storage. *Sustainability (Switzerland)* [online]. 2018, **10**(1). ISSN 20711050. Dostupné z: doi:10.3390/su10010191
- [35] AL-GHOUTI, Mohammad A. a Dana A. DA'ANA. Guidelines for the use and interpretation of adsorption isotherm models: A review. *Journal of Hazardous Materials* [online]. 2020, **393**(November 2019), 122383. ISSN 03043894. Dostupné z: doi:10.1016/j.jhazmat.2020.122383
- [36] ZHANG, Yannan a Ruzhu WANG. Sorption thermal energy storage: Concept, process, applications and perspectives. *Energy Storage Materials* [online]. 2020, **27**(February), 352–369. ISSN 24058297. Dostupné z: doi:10.1016/j.ensm.2020.02.024
- [37] CABEZA, Luisa F., Aran SOLÉ a Camila BARRENECHE. Review on sorption materials and technologies for heat pumps and thermal energy storage. *Renewable Energy* [online]. 2017, **110**, 3–39. ISSN 18790682. Dostupné z: doi:10.1016/j.renene.2016.09.059
- [38] LEFEBVRE, Dominique a F. Handan TEZEL. A review of energy storage technologies with a focus on adsorption thermal energy storage processes for heating applications.

- Renewable and Sustainable Energy Reviews* [online]. 2017, **67**, 116–125. ISSN 18790690. Dostupné z: doi:10.1016/j.rser.2016.08.019
- [39] MICHEL, Benoit, Pierre NEVEU a Nathalie MAZET. Comparison of closed and open thermochemical processes, for long-term thermal energy storage applications. *Energy* [online]. 2014, **72**(September 2018), 702–716. ISSN 03605442. Dostupné z: doi:10.1016/j.energy.2014.05.097
- [40] METTE, Barbara, Henner KERSKES, Harald DRÜCK a Hans MÜLLER-STEINHAGEN. Experimental and numerical investigations on the water vapor adsorption isotherms and kinetics of binderless zeolite 13X. *International Journal of Heat and Mass Transfer* [online]. 2014, **71**, 555–561. ISSN 00179310. Dostupné z: doi:10.1016/j.ijheatmasstransfer.2013.12.061
- [41] DEEPRESOURCE. *Chemical and Sorptive Thermal Storage Methods* [online]. 2019. Dostupné z: <https://deepresource.wordpress.com/2019/05/12/chemical-and-sorptive-thermal-storage-methods/>
- [42] PAN, Q. W., R. Z. WANG, L. W. WANG a D. LIU. Design and experimental study of a silica gel-water adsorption chiller with modular adsorbers. *International Journal of Refrigeration* [online]. 2016, **67**, 336–344. ISSN 01407007. Dostupné z: doi:10.1016/j.ijrefrig.2016.03.001
- [43] LYUBCHIK, Andrey, Olena LYGINA, Sergiy LYUBCHIK a Isabel FONSECA. Adsorptive removal of volatile organic compounds from gases streams Theoretical background. 1940.
- [44] MEMIM. Chemisorption [online]. 2020. Dostupné z: <https://memim.com/chemisorption.html>
- [45] ASKLLTIANS. *Adsorption of Gases on Solids* [online]. 2020. Dostupné z: <https://www.askiitians.com/iit-jee-chemistry/physical-chemistry/adsorption-of-gases-on-solid.aspx>
- [46] SIMS, Ruby A., Sarah L. HARMER a Jamie S. QUINTON. The role of physisorption and chemisorption in the oscillatory adsorption of organosilanes on aluminium oxide. *Polymers*

- [online]. 2019, **11**(3). ISSN 20734360. Dostupné z: doi:10.3390/polym11030410
- [47] KLEIN, Gerhard. *Principles of adsorption and adsorption processes* [online]. 1985. ISSN 01676989. Dostupné z: doi:10.1016/0167-6989(85)90037-6
- [48] TIMOTHY\_BOWEN. *LENNARD-JONES DYNAMICS* [online]. Dostupné z: <https://quizlet.com/182751604/lecture-3-lennard-jones-dynamics-flash-cards/>
- [49] HASSAN, H. Z. a A. A. MOHAMAD. A review on solar cold production through absorption technology. *Renewable and Sustainable Energy Reviews* [online]. 2012, **16**(7), 5331–5348. ISSN 13640321. Dostupné z: doi:10.1016/j.rser.2012.04.049
- [50] DU, S., R. Z. WANG, P. LIN, Z. Z. XU, Q. W. PAN a S. C. XU. Experimental studies on an air-cooled two-stage NH<sub>3</sub>-H<sub>2</sub>O solar absorption air-conditioning prototype. *Energy* [online]. 2012, **45**(1), 581–587. ISSN 03605442. Dostupné z: doi:10.1016/j.energy.2012.07.041
- [51] SARBU, Ioan a Calin SEBARCHIEVICI. Review of solar refrigeration and cooling systems. *Energy and Buildings* [online]. 2013, **67**, 286–297. ISSN 03787788. Dostupné z: doi:10.1016/j.enbuild.2013.08.022
- [52] SARBU, Ioan a Calin SEBARCHIEVICI. General review of solar-powered closed sorption refrigeration systems. *Energy Conversion and Management* [online]. 2015, **105**, 403–422. ISSN 01968904. Dostupné z: doi:10.1016/j.enconman.2015.07.084
- [53] TATSIDJODOUNG, Parfait, Nolwenn LE PIERRÈS a Lingai LUO. A review of potential materials for thermal energy storage in building applications. *Renewable and Sustainable Energy Reviews* [online]. 2013, **18**, 327–349. ISSN 13640321. Dostupné z: doi:10.1016/j.rser.2012.10.025
- [54] YU, N., R. Z. WANG a L. W. WANG. Sorption thermal storage for solar energy. *Progress in Energy and Combustion Science* [online]. 2013, **39**(5), 489–514. ISSN 03601285. Dostupné z: doi:10.1016/j.pecs.2013.05.004
- [55] WOLAK, Eliza. The cooling effect by adsorption-desorption cycles. *E3S Web of Conferences* [online]. 2017, **14**. ISSN 22671242. Dostupné z: doi:10.1051/e3sconf/20171401052



- [56] LI, S. L., J. Y. WU, Z. Z. XIA a R. Z. WANG. Study on the adsorption performance of composite adsorbent of CaCl<sub>2</sub> and expanded graphite with ammonia as adsorbate. *Energy Conversion and Management* [online]. 2009, **50**(4), 1011–1017. ISSN 01968904. Dostupné z: doi:10.1016/j.enconman.2008.12.014
- [57] LI, T. X., R. Z. WANG, R. G. OLIVEIRA, J. K. KIPLAGAT a L. W. WANG. A combined double-way chemisorption refrigeration cycle based on adsorption and desorption processes. *International Journal of Refrigeration* [online]. 2009, **32**(1), 47–57. ISSN 01407007. Dostupné z: doi:10.1016/j.ijrefrig.2008.07.007
- [58] DONKERS, P. A.J., L. C. SÖGÜTOĞLU, H. P. HUININK, H. R. FISCHER a O. C.G. ADAN. A review of salt hydrates for seasonal heat storage in domestic applications. *Applied Energy* [online]. 2017, **199**, 45–68. ISSN 03062619. Dostupné z: doi:10.1016/j.apenergy.2017.04.080
- [59] CASEY, Sean P., Jon ELVINS, Saffa RIFFAT a Andrew ROBINSON. Salt impregnated desiccant matrices for „open“ thermochemical energy storage - Selection, synthesis and characterisation of candidate materials. *Energy and Buildings* [online]. 2014, **84**, 412–425. ISSN 03787788. Dostupné z: doi:10.1016/j.enbuild.2014.08.028
- [60] RUZHU WANG, Liwei Wang and Jingyi Wu. *ADSORPTION REFRIGERATION TECHNOLOGY*. B.m.: John Wiley & Sons Singapore Pte. Ltd., 2014. ISBN 9781118197462.
- [61] GARCIA-OLALLA, C., L. C. ROBLES a A. J. ALLER. The Effect of Metal Chlorides, Sulfates and Nitrates on Atomization of Selenium in Graphite Furnace Atomic Absorption Spectrometry. *Analytical Sciences* [online]. 1991, **7**(4), 611–615. ISSN 13482246. Dostupné z: doi:10.2116/analsci.7.611
- [62] SILBERBERG, Martin S. Principles of General Chemistry - V1.0M [online]. 2009, 915. ISSN 1098-6596. Dostupné z: doi:10.1016/B978-1-85617-803-7.50022-5
- [63] QUACH, Nguyen Khanh Nguyen, Wein Duo YANG, Zen Ja CHUNG a Hoai Lam TRAN. The Influence of the Activation Temperature on the Structural Properties of the Activated Carbon Xerogels and Their Electrochemical Performance. *Advances in Materials Science*

- and Engineering* [online]. 2017, **2017**. ISSN 16878442. Dostupné z: doi:10.1155/2017/8308612
- [64] JRIBI, Skander, Takahiko MIYAZAKI, Bidyut Baran SAHA, Animesh PAL, Mohamed M. YOUNES, Shigeru KOYAMA a Aref MAALEJ. Equilibrium and kinetics of CO<sub>2</sub> adsorption onto activated carbon. *International Journal of Heat and Mass Transfer* [online]. 2017, **108**(July 2018), 1941–1946. ISSN 00179310. Dostupné z: doi:10.1016/j.ijheatmasstransfer.2016.12.114
- [65] MALEK, A. a S. FAROOQ. Kinetics of hydrocarbon adsorption on activated carbon and silica gel. *AIChE Journal* [online]. 1997, **43**(3), 761–776. ISSN 0001-1541. Dostupné z: doi:10.1002/aic.690430321
- [66] LI, Xin, Xiao CHEN a Zhong LI. Adsorption equilibrium and desorption activation energy of water vapor on activated carbon modified by an oxidation and reduction treatment. *Journal of Chemical and Engineering Data* [online]. 2010, **55**(9), 3164–3169. ISSN 00219568. Dostupné z: doi:10.1021/je100024r
- [67] CARDOSO, Beatriz, Ana S. MESTRE, Ana P. CARVALHO a João PIRES. Activated carbon derived from cork powder waste by KOH activation: Preparation, characterization, and VOCs adsorption. *Industrial and Engineering Chemistry Research* [online]. 2008, **47**(16), 5841–5846. ISSN 08885885. Dostupné z: doi:10.1021/ie800338s
- [68] ZHANG, Tengyan, Walter P. WALAWENDER a L. T. FAN. Preparation of carbon molecular sieves by carbon deposition from methane. *Bioresource Technology* [online]. 2005, **96**(17), 1929–1935. ISSN 09608524. Dostupné z: doi:10.1016/j.biortech.2005.01.026
- [69] SETHUPATHI, Sumathi, Mohammed Jk BASHIR, Zinatizadeh Ali AKBAR a Abdul Rahman MOHAMED. Biomass-based palm shell activated carbon and palm shell carbon molecular sieve as gas separation adsorbents. *Waste Management and Research* [online]. 2015, **33**(4), 303–312. ISSN 10963669. Dostupné z: doi:10.1177/0734242X15576026
- [70] RUTHERFORD, S. W. a D. D. DO. Characterization of carbon molecular sieve 3A. *Langmuir* [online]. 2000, **16**(18), 7245–7254. ISSN 07437463. Dostupné

z: doi:10.1021/la991634q

- [71] YANG, Xiong, Ziyi LI, Chuanzhao ZHANG, Haoyu WANG, Erlin ZHANG, Yi XING, Penny XIAO, Ralph T. YANG, Yingshu LIU a Paul A. WEBLEY. Practical separation performance evaluation of coal mine methane upgrading with carbon molecular sieves. *Chemical Engineering Journal* [online]. 2019, **367**(December 2018), 295–303. ISSN 13858947. Dostupné z: doi:10.1016/j.cej.2019.02.134
- [72] QIAO, Zhihua, Zhi WANG, Chenxin ZHANG, Shuangjie YUAN, Yaqun ZHU a Jixiao WANG. PVAm–PIP/PS composite membrane with high performance for CO<sub>2</sub>/N<sub>2</sub> separation. *AIChE Journal* [online]. 2012, **59**(4), 215–228. ISSN 12350621. Dostupné z: doi:10.1002/aic
- [73] D. L. BISH, D. W. Ming. NATURAL ZEOLITES: occurrence, properties, applications. 1955, **45**, 654.
- [74] SELS, Bert F. a Leonid M. KUSTOV. *Zeolites and Zeolite-like Materials* [online]. 2016. ISBN 9780444635068. Dostupné z: doi:10.1016/C2014-0-00257-2
- [75] DANTAS DE OLIVEIRA, Amanda a Cesar AUGUSTO GONÇALVES BEATRICE. Polymer Nanocomposites with Different Types of Nanofiller. *Nanocomposites - Recent Evolutions* [online]. 2019, (January). Dostupné z: doi:10.5772/intechopen.81329
- [76] ZETTL, Bernhard, Gerald ENGLMAIR a Gerald STEINMAURER. Development of a revolving drum reactor for open-sorption heat storage processes. *Applied Thermal Engineering* [online]. 2014, **70**(1), 42–49. ISSN 13594311. Dostupné z: doi:10.1016/j.applthermaleng.2014.04.069
- [77] JOHANNES, Kévyne, Frédéric KUZNIK, Jean Luc HUBERT, Francois DURIER a Christian OBRECHT. Design and characterisation of a high powered energy dense zeolite thermal energy storage system for buildings. *Applied Energy* [online]. 2015, **159**, 80–86. ISSN 03062619. Dostupné z: doi:10.1016/j.apenergy.2015.08.109
- [78] RIDHA, Firas N. a Paul A. WEBLEY. Entropic effects and isosteric heats of nitrogen and carbon dioxide adsorption on chabazite zeolites. *Microporous and Mesoporous Materials* [online]. 2010, **132**(1–2), 22–30. ISSN 13871811. Dostupné

z: doi:10.1016/j.micromeso.2009.07.025

- [79] TAKAHASHI, Ryoji, Satoshi SATO, Toshiaki SODESAWA, Machiko KAWAKITA a Katsuyuki OGURA. High surface-area silica with controlled pore size prepared from nanocomposite of silica and citric acid. *Journal of Physical Chemistry B* [online]. 2000, **104**(51), 12184–12191. ISSN 15206106. Dostupné z: doi:10.1021/jp002662g
- [80] CHEMICALBOOK. Silica gel. *ChemicalBook Inc.* [online]. 2016. Dostupné z: [https://m.chemicalbook.com/ProductCatalog\\_EN/1217.htm](https://m.chemicalbook.com/ProductCatalog_EN/1217.htm)
- [81] PATHAK, P. N. a G. R. CHOPPIN. Sorption studies of europium(III) on hydrous silica. *Journal of Radioanalytical and Nuclear Chemistry* [online]. 2006, **270**(2), 277–283. ISSN 02365731. Dostupné z: doi:10.1007/s10967-006-0345-9
- [82] SPEIGHT, James G. *The Chemistry and Technology of Petroleum* [online]. 2014. ISBN 9781439873908. Dostupné z: doi:10.1201/b16559
- [83] SORBENTSYSTEMS. *Desiccant Chart Comparisons* [online]. 2006. Dostupné z: [https://www.sorbentsystems.com/desiccants\\_charts.html](https://www.sorbentsystems.com/desiccants_charts.html)
- [84] SUZUKI, Motoyuki. *Adsorption Engineering, Suzuki (1990).pdf*. ISBN 0444988025
- [85] ARISTOV, Yuri I., Mikhail M. TOKAREV, Angelo FRENI, Ivan S. GLAZNEV a Giovanni RESTUCCIA. Kinetics of water adsorption on silica Fuji Davison RD. *Microporous and Mesoporous Materials* [online]. 2006, **96**(1–3), 65–71. ISSN 13871811. Dostupné z: doi:10.1016/j.micromeso.2006.06.008
- [86] CHAKRABORTY, Anutosh, Bidyut Baran SAHA a Yuri I. ARISTOV. Dynamic behaviors of adsorption chiller: Effects of the silica gel grain size and layers. *Energy* [online]. 2014. ISSN 03605442. Dostupné z: doi:10.1016/j.energy.2014.10.015
- [87] XIA, Zai Z., Chuan J. CHEN, Jeremiah K. KIPLAGAT, Ru Z. WANG a Jin Q. HU. Adsorption equilibrium of water on silica gel. *Journal of Chemical and Engineering Data* [online]. 2008, **53**(10), 2462–2465. ISSN 00219568. Dostupné z: doi:10.1021/je800019u
- [88] NG, K. C., H. T. CHUA, C. Y. CHUNG, C. H. LOKE, T. KASHIWAGI, A. AKISAWA a B. B. SAHA. Experimental investigation of the silica gel-water adsorption isotherm

- characteristics. *Applied Thermal Engineering* [online]. 2001, **21**(16), 1631–1642. ISSN 13594311. Dostupné z: doi:10.1016/S1359-4311(01)00039-4
- [89] OLIVIER, J. P. *Comparison of the experimental isosteric heat of adsorption of argon on mesoporous silica with density functional theory calculations* [online]. B.m.: Elsevier Masson SAS, 2000. ISSN 01672991. Dostupné z: doi:10.1016/s0167-2991(00)80011-7
- [90] ARISTOV, Yuri I, Mikhail M TOKAREV, Angelo FRENI, Giovanni RESTUCCIA, Boris N OKUNEV, Mikhail S SAFONOV a Lyudvig I HEIFETS. ISOTHERMS OF WATER SORPTION ON COMPOSITE “ CaCl<sub>2</sub> IN SILICA GEL ”: EXPERIMENT AND APPROXIMATION. *nedatováno*, (2), 300–305.
- [91] *Front Matter* [online]. 2019. ISBN 9780128164464. Dostupné z: doi:10.1016/b978-0-12-816446-4.09991-7
- [92] MOKHATAB, Saeid, William A. POE a John Y. MAK. *Handbook of natural gas transmission and processing: Principles and practices* [online]. 2018. ISBN 9780128158173. Dostupné z: doi:10.1016/C2017-0-03889-2
- [93] DO, Duong D. *ADSORPTION ANALYSIS : EQUILIBRIA AND KINETICS*. B.m.: Imperial College Press, 1998. ISBN 1860941303.
- [94] LIGHTSTONE, James M., Timothy B. ONASCH, Dan IMRE a Susan OATIS. Deliquescence, efflorescence, and water activity in ammonium nitrate and mixed ammonium nitrate/succinic acid microparticles. *Journal of Physical Chemistry A* [online]. 2000, **104**(41), 9337–9346. ISSN 10895639. Dostupné z: doi:10.1021/jp002137h
- [95] GREENSPAN, Lewis. Humidity Fixed Points of Binary Saturated Aqueous Solutions. *JOURNAL OF RESEARCH of the National Bureau of Standards - A. Physics and Chemistry Vol. 81 A, No.1 , January- February 1977 Humidity*. 1976, **23**(1), 53–66. ISSN 03009904.
- [96] LAHMIDI, H., S. MAURAN a V. GOETZ. Definition, test and simulation of a thermochemical storage process adapted to solar thermal systems. *Solar Energy* [online]. 2006, **80**(7), 883–893. ISSN 0038092X. Dostupné z: doi:10.1016/j.solener.2005.01.014
- [97] STITOU, Driss, Nathalie MAZET a Sylvain MAURAN. Experimental investigation of a

- solid/gas thermochemical storage process for solar air-conditioning. *Energy* [online]. 2012, **41**(1), 261–270. ISSN 03605442. Dostupné z: doi:10.1016/j.energy.2011.07.029
- [98] BAO, H. S., R. Z. WANG, R. G. OLIVEIRA a T. X. LI. Resorption system for cold storage and long-distance refrigeration. *Applied Energy* [online]. 2012, **93**, 479–487. ISSN 03062619. Dostupné z: doi:10.1016/j.apenergy.2011.12.022
- [99] SUZUKI, Motoyuki. Activated carbon fiber: Fundamentals and applications. *Carbon* [online]. 1994, **32**(4), 577–586. ISSN 00086223. Dostupné z: doi:10.1016/0008-6223(94)90075-2
- [100] WANG, J. Y., R. Z. WANG a L. W. WANG. Water vapor sorption performance of ACF-CaCl<sub>2</sub> and silica gel-CaCl<sub>2</sub> composite adsorbents. *Applied Thermal Engineering* [online]. 2016, **100**(March), 893–901. ISSN 13594311. Dostupné z: doi:10.1016/j.applthermaleng.2016.02.100
- [101] WANG, J. Y., J. Y. LIU, R. Z. WANG a L. W. WANG. Experimental research of composite solid sorbents for fresh water production driven by solar energy. *Applied Thermal Engineering* [online]. 2017, **121**, 941–950. ISSN 13594311. Dostupné z: doi:10.1016/j.applthermaleng.2017.04.161
- [102] FARZAD, S., V. TAGHIKHANI, C. GHOTBI, B. AMINSHAHIDI a E. NEMATI LAY. Experimental and Theoretical Study of the Effect of Moisture on Methane Adsorption and Desorption by Activated Carbon at 273.5 K. *Journal of Natural Gas Chemistry* [online]. 2007, **16**(1), 22–30. ISSN 10039953. Dostupné z: doi:10.1016/S1003-9953(07)60021-8
- [103] SARKAR, Jahar a Souvik BHATTACHARYYA. Application of graphene and graphene-based materials in clean energy-related devices Minghui. *Archives of Thermodynamics* [online]. 2012, **33**(4), 23–40. ISSN 12310956. Dostupné z: doi:10.1002/er
- [104] JÄHNIG, Dagmar, Robert HAUSNER, Waldemar WAGNER a Charlotta ISAKSSON. Thermo-chemical storage for solar space heating in a single-family house. *AEE – INTEC (Austria), Ecostock Conference, New Jersey; 31 May - 02 June. 2006*, 1–7.
- [105] DICAIRE, Daniel a F. Handan TEZEL. Regeneration and efficiency characterization of hybrid adsorbent for thermal energy storage of excess and solar heat. *Renewable Energy*

- [online]. 2011, **36**(3), 986–992. ISSN 09601481. Dostupné z: doi:10.1016/j.renene.2010.08.031
- [106] AMORIM, Joselma A., H. M. VIEIRA, Cicero H. T. ANDRADE, J. M. MEDEIROS, J. C. SANTOS a Jose Mauricio GURGEL. Experimental Sorption Dynamic in Packed Bed of Silica Gel. *Journal of Porous Media* [online]. 2013, **16**(6), 515–525. ISSN 1091-028X. Dostupné z: doi:10.1615/jpormedia.v16.i6.30
- [107] WANG, D. C., J. Y. WU, Z. Z. XIA, H. ZHAI, R. Z. WANG a W. D. DOU. Study of a novel silica gel-water adsorption chiller. Part II. Experimental study. *International Journal of Refrigeration* [online]. 2005, **28**(7), 1084–1091. ISSN 01407007. Dostupné z: doi:10.1016/j.ijrefrig.2005.03.002
- [108] GANTENBEIN, Paul, Dagmar JAENIG, Henner KERSKES a Martijn VAN ESSEN. Final report of Subtask B &quot; Chemical and Sorption Storage &quot; The overview A Report of IEA Solar Heating and Cooling programme -Task 32 Advanced storage concepts for solar and low energy buildings Report B7 of Subtask B. 2008, (January).
- [109] LU, Zisheng, Ruzhu WANG a Zaizhong XIA. Experimental analysis of an adsorption air conditioning with micro-porous silica gel-water. *Applied Thermal Engineering* [online]. 2013, **50**(1), 1015–1020. ISSN 13594311. Dostupné z: doi:10.1016/j.applthermaleng.2012.07.041
- [110] PAN, Huanhua, James a RITTER a Perla B BALBUENA. *from the Clausius - Clapeyron Equation*. 1998
- [111] SVOBODA, J., F. D. FISCHER, P. FRATZL a Ernst KOZESCHNIK. Modelling of kinetics in multi-component multi-phase systems with spherical precipitates I: Theory. *Materials Science and Engineering A* [online]. 2004, **385**(1–2), 166–174. ISSN 09215093. Dostupné z: doi:10.1016/j.msea.2004.06.018
- [112] AZAHAR, Fatin Hazwani M., Sourav MITRA, Akihiro YABUSHITA, Akira HARATA, Bidyut Baran SAHA a Kyaw THU. Improved model for the isosteric heat of adsorption and impacts on the performance of heat pump cycles. *Applied Thermal Engineering* [online]. 2018, **143**, 688–700. ISSN 13594311. Dostupné

z: doi:10.1016/j.applthermaleng.2018.07.131

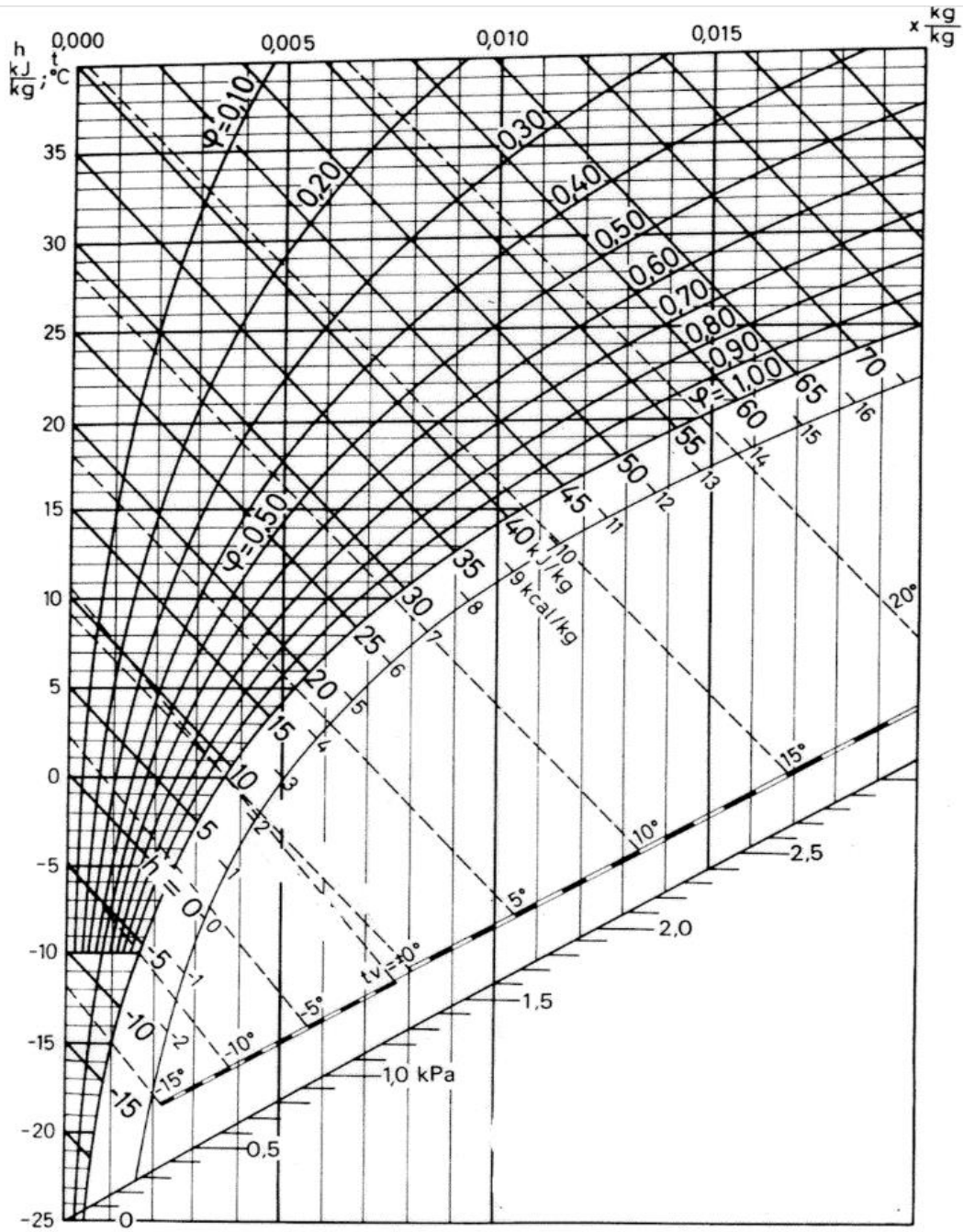
- [113] AYAWEI, Nimibofa, Augustus Newton EBELEGI a Donbebe WANKASI. Modelling and Interpretation of Adsorption Isotherms. *Journal of Chemistry* [online]. 2017, **2017**. ISSN 20909071. Dostupné z: doi:10.1155/2017/3039817
- [114] ÇELEBI, O., Ç ÜZÜM, T. SHAHWAN a H. N. ERTEN. A radiotracer study of the adsorption behavior of aqueous Ba<sup>2+</sup> ions on nanoparticles of zero-valent iron. *Journal of Hazardous Materials* [online]. 2007, **148**(3), 761–767. ISSN 03043894. Dostupné z: doi:10.1016/j.jhazmat.2007.06.122
- [115] GÜNAY, Ahmet, Ertan ARSLANKAYA a Ismail TOSUN. Lead removal from aqueous solution by natural and pretreated clinoptilolite: Adsorption equilibrium and kinetics. *Journal of Hazardous Materials* [online]. 2007, **146**(1–2), 362–371. ISSN 03043894. Dostupné z: doi:10.1016/j.jhazmat.2006.12.034
- [116] MOHAMMED, Ramy H., Osama MESALHY, Mohamed L. ELSAYED, Ming SU a Louis C. CHOW. Revisiting the adsorption equilibrium equations of silica-gel/water for adsorption cooling applications. *International Journal of Refrigeration* [online]. 2018, **86**, 40–47. ISSN 01407007. Dostupné z: doi:10.1016/j.ijrefrig.2017.10.038
- [117] CEVALLOS, Oscar Rodrigo Fonseca. Adsorption Characteristics of Water and Silica Gel System for Desalination Cycle [online]. 2012, 72. Dostupné z: [http://repository.kaust.edu.sa/kaust/bitstream/10754/273097/1/OscarFonseca113292\\_Thesis\\_final.pdf](http://repository.kaust.edu.sa/kaust/bitstream/10754/273097/1/OscarFonseca113292_Thesis_final.pdf)
- [118] CORRIGA, Thomas E. Adsorption Isotherms for Pure Hydrocarbons. nedatováno, 383–387.
- [119] BENZAOUI, Thouria, Ammar SELATNIA a Djaafar DJABALI. Adsorption of copper (II) ions from aqueous solution using bottom ash of expired drugs incineration. *Adsorption Science and Technology* [online]. 2018, **36**(1–2), 114–129. ISSN 20484038. Dostupné z: doi:10.1177/0263617416685099
- [120] FOO, K. Y. a B. H. HAMEED. Insights into the modeling of adsorption isotherm systems. *Chemical Engineering Journal* [online]. 2010, **156**(1), 2–10. ISSN 13858947. Dostupné



z: doi:10.1016/j.cej.2009.09.013

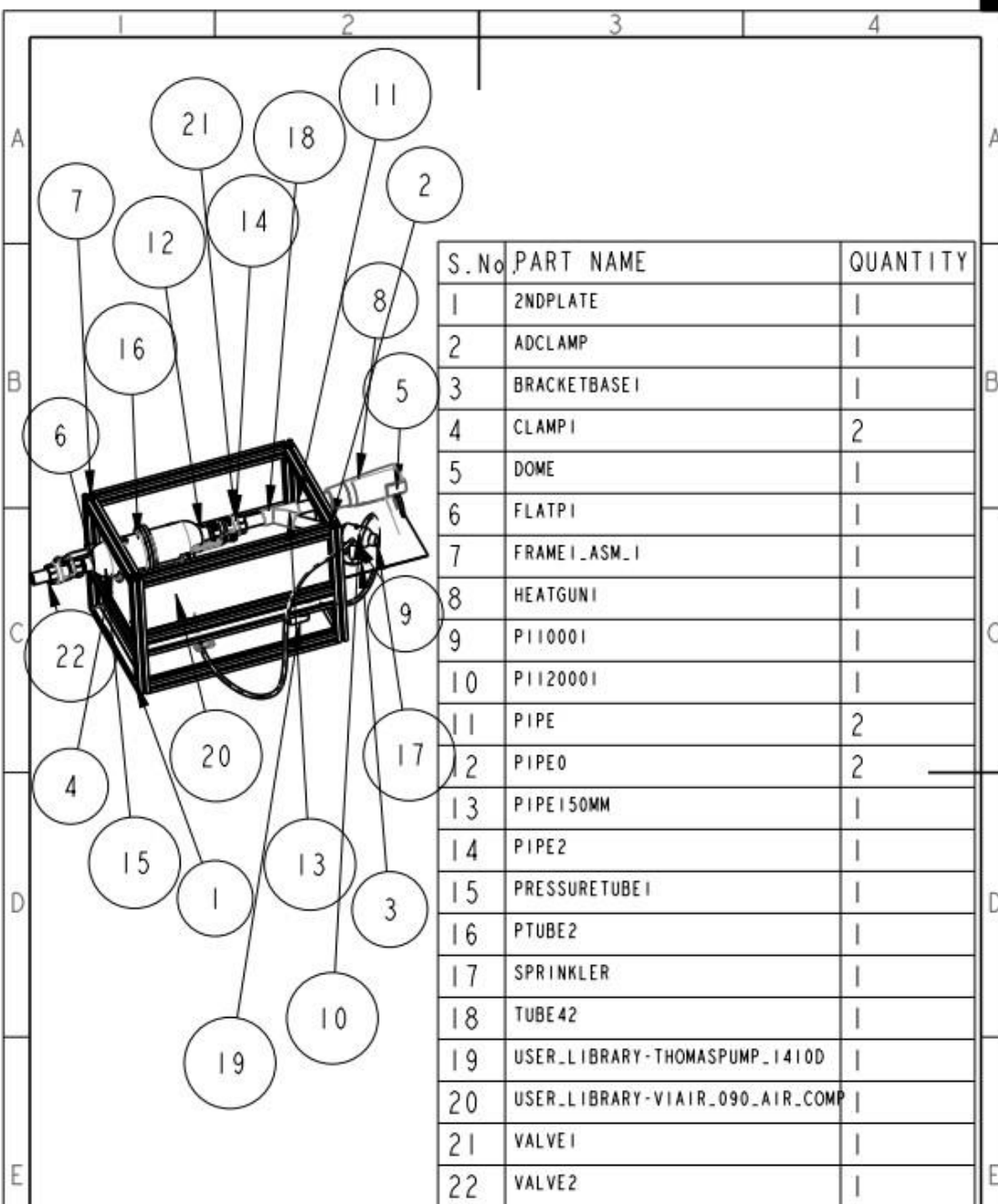
- [121] TRAIVA. *TECHNICKÝ - PRODUKTOVÝ LIST TECHNICKÝ - PRODUKTOVÝ LIST*. 2017.
- [122] MOHAMMED, Ramy H., Osama MESALHY, Mohamed L. ELSAYED, Sichao HOU, Ming SU a Louis C. CHOW. Physical properties and adsorption kinetics of silica-gel/water for adsorption chillers. *Applied Thermal Engineering* [online]. 2018, **137**(October 2017), 368–376. ISSN 13594311. Dostupné z: doi:10.1016/j.applthermaleng.2018.03.088
- [123] GAEINI, Mohammadreza. *Thermochemical seasonal heat storage for the built environment* [online]. 2017. ISBN 9789038643137. Dostupné z: [www.tue.nl/taverne%0Ahttps://pure.tue.nl/ws/files/70475072/20170704\\_Gaeini.pdf](http://www.tue.nl/taverne%0Ahttps://pure.tue.nl/ws/files/70475072/20170704_Gaeini.pdf)

APPENDIX



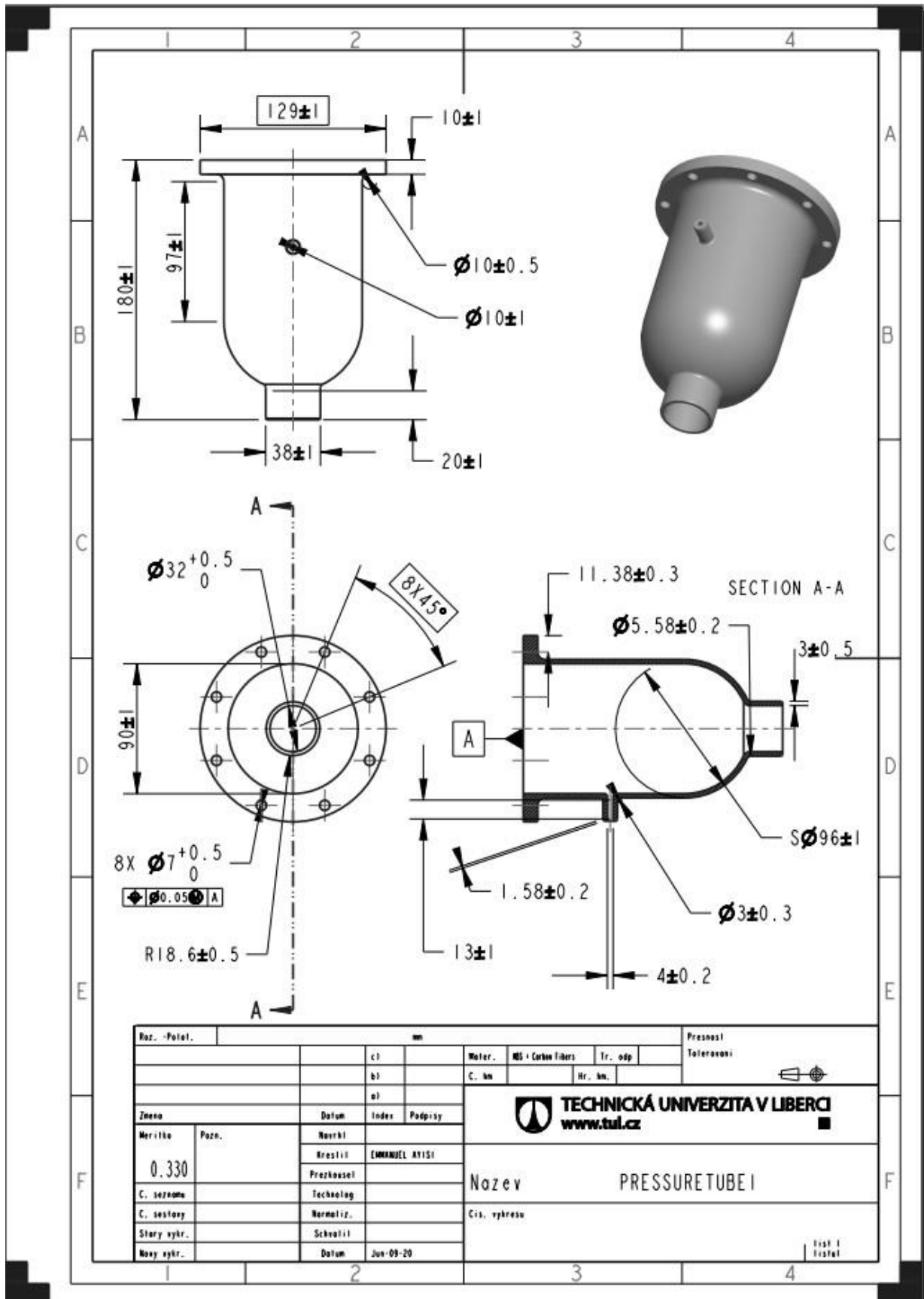
**APPENDIX A**

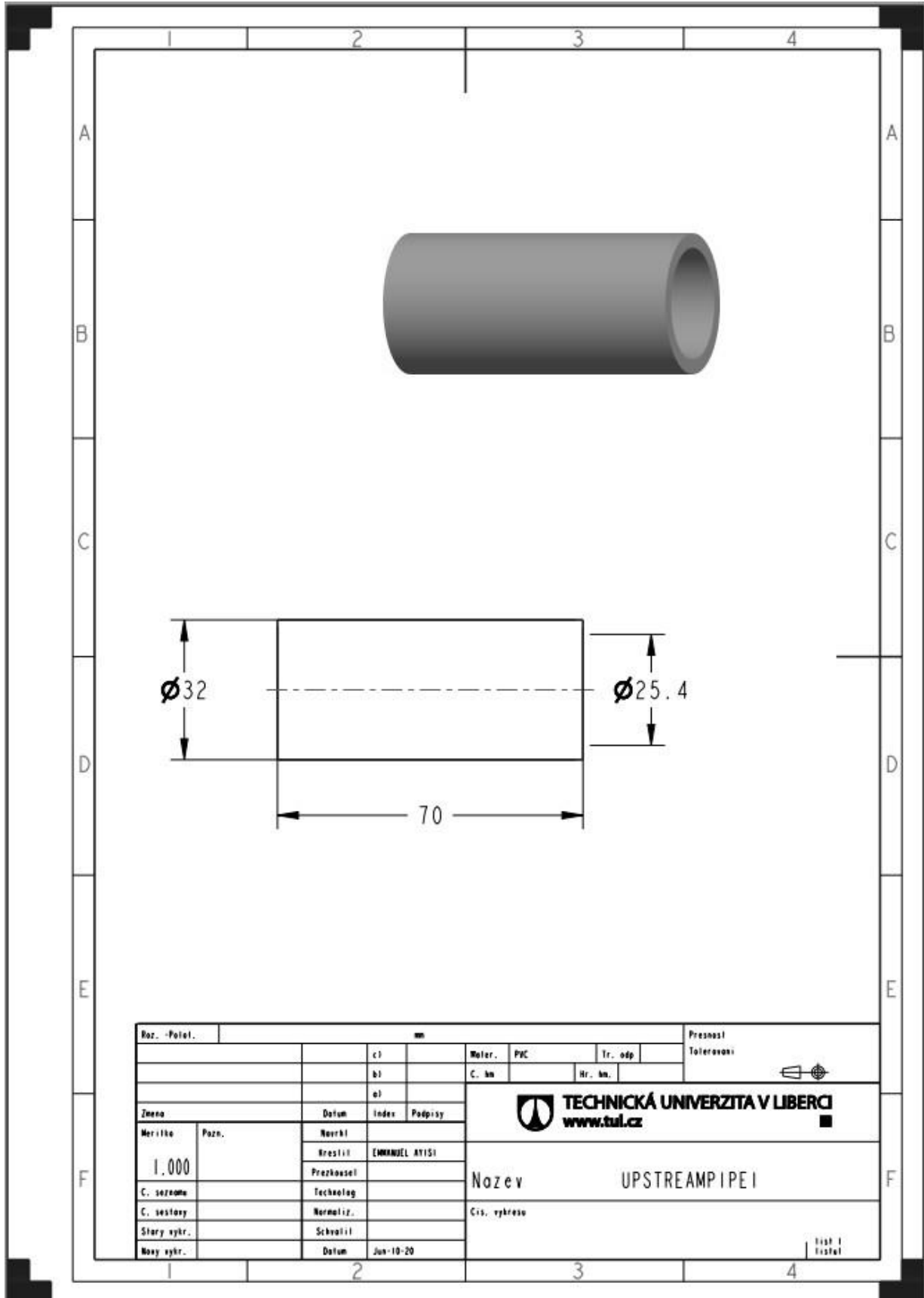
**Assembly and Part drawings**



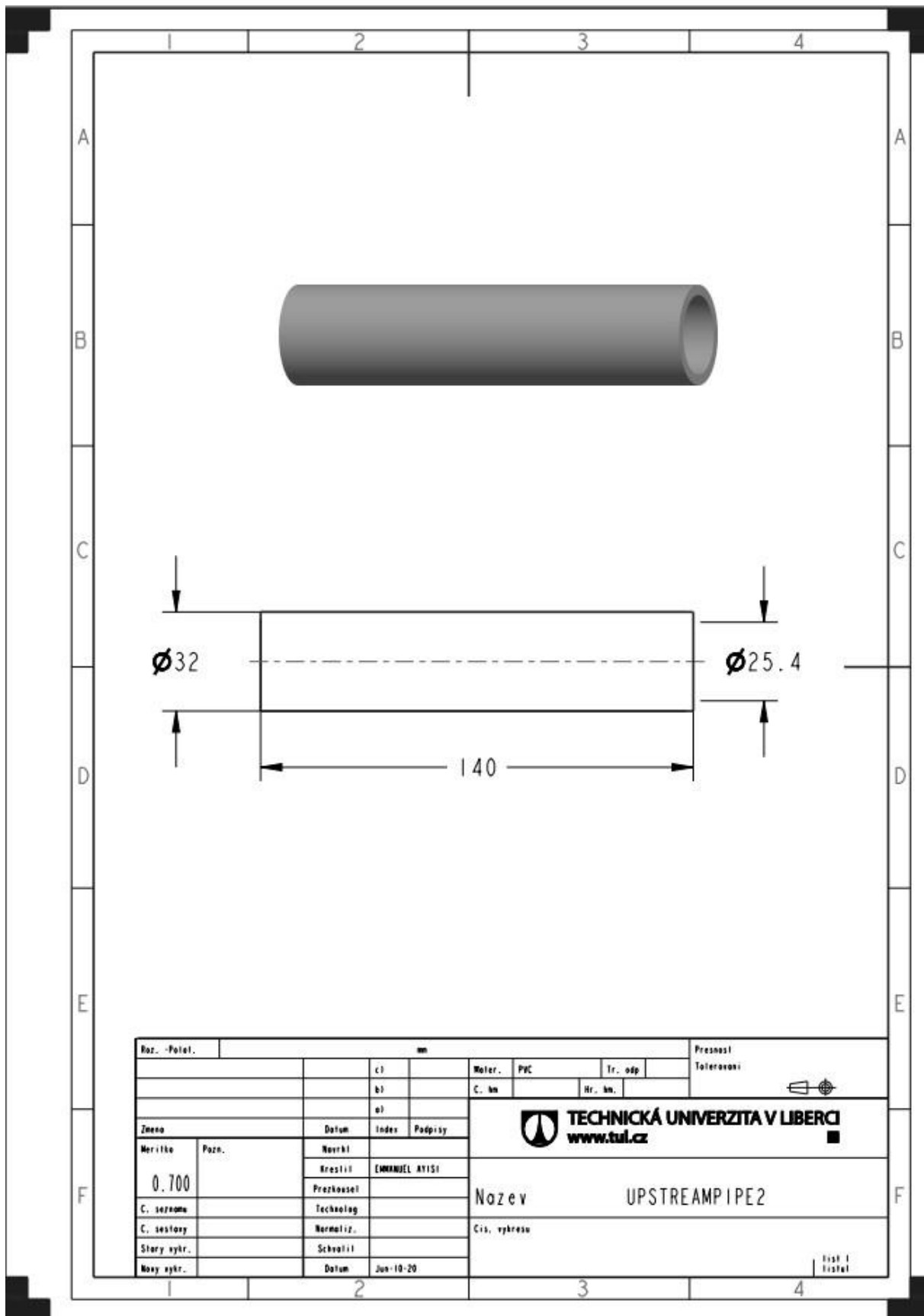
S.No	PART NAME	QUANTITY
1	2NDPLATE	1
2	ADCLAMP	1
3	BRACKETBASE I	1
4	CLAMP I	2
5	DOME	1
6	FLATPI	1
7	FRAME1.ASM.1	1
8	HEATGUN I	1
9	PI10001	1
10	PI120001	1
11	PIPE	2
12	PIPE0	2
13	PIPE150MM	1
14	PIPE2	1
15	PRESSURETUBE I	1
16	PTUBE2	1
17	SPRINKLER	1
18	TUBE42	1
19	USER_LIBRARY-THOMASPUMP_1410D	1
20	USER_LIBRARY-VIAIR_090_AIR_COMP	1
21	VALVE I	1
22	VALVE2	1

Koz. -Polat.		mm		Mater. -		Tr. odp.		Presnost Toleranci	
		c1		C. kn		Hr. kn.			
		b1							
		e1							
Zmena		Datum		Index		Podpisy		 <b>TECHNICKÁ UNIVERZITA V LIBERCI</b> <a href="http://www.tul.cz">www.tul.cz</a>	
Meritba		Navrh		Kreslil		EMMANUEL AYISI			
0.070								<b>Nozev</b> <b>SYSTEM</b>	
C. seznám		Technolog							
C. sestavy		Normaliz.						<b>Cis. vykresu</b>	
Stary vykr.		Schválil							
Novy vykr.		Datum		Jun-10-20				list 1 listal	

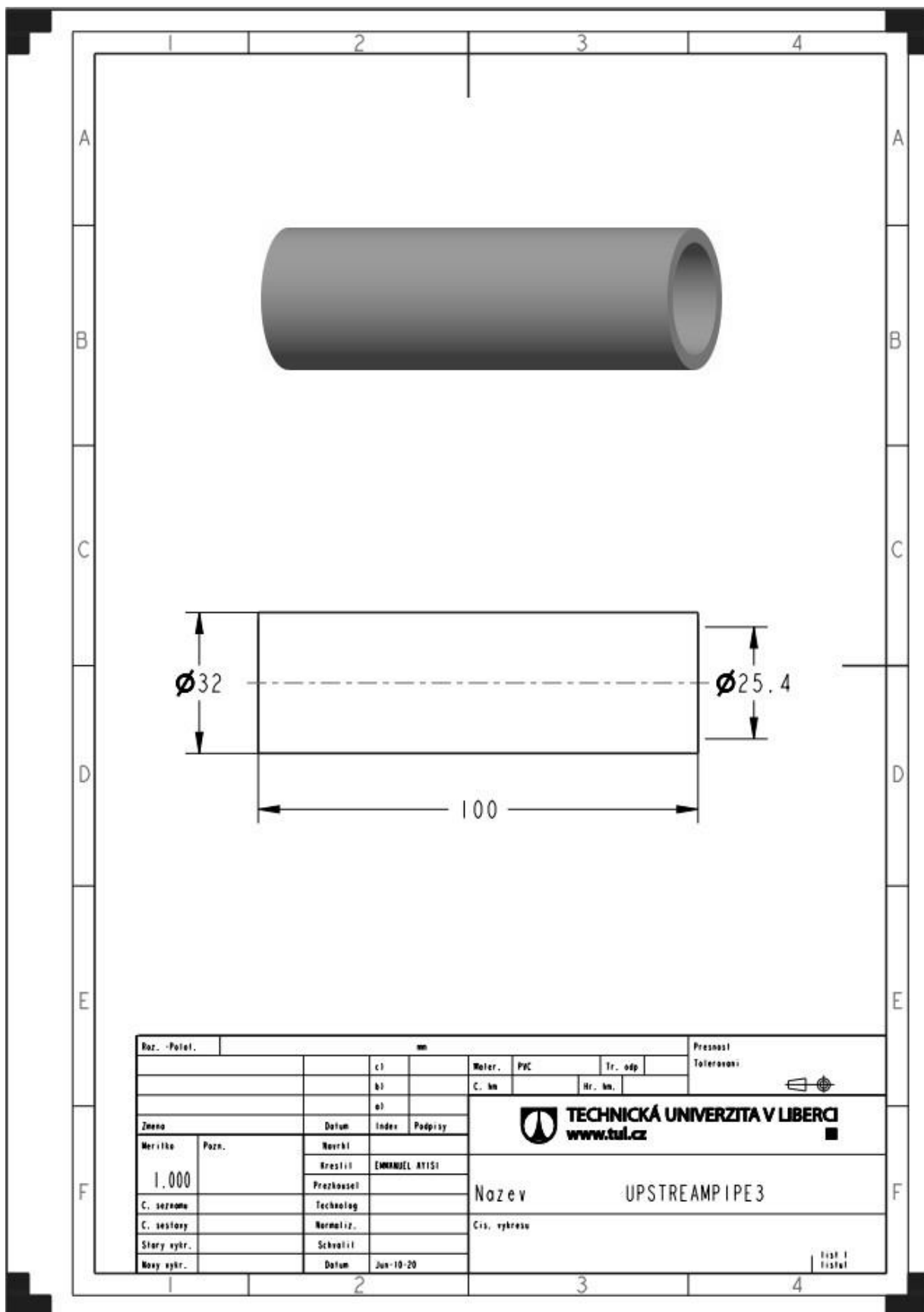




Roz. -Počet.		mm				Přesnost Tolerovaní	
		c1		Mater.	PVC	Tr. odp.	
		b1		C. kn.		Hr. kn.	
		a1					
Zmena		Datum	Index	<b>TECHNICKÁ UNIVERZITA V LIBERCI</b> <a href="http://www.tul.cz">www.tul.cz</a>			
Merilka	Pozn.	Navehl	Podpisy	<b>Nozev</b> UPSTREAMPIPE I			
1.000		Kreslil	EMMANUEL AYISI				
C. seznam		Průzkoušel		<b>Cis. vybrso</b>			
C. sestavy		Technolog					
Stary vykr.		Normaliz.		list 1 listal			
Novy vykr.		Schválil					
		Datum	Jun-10-20				

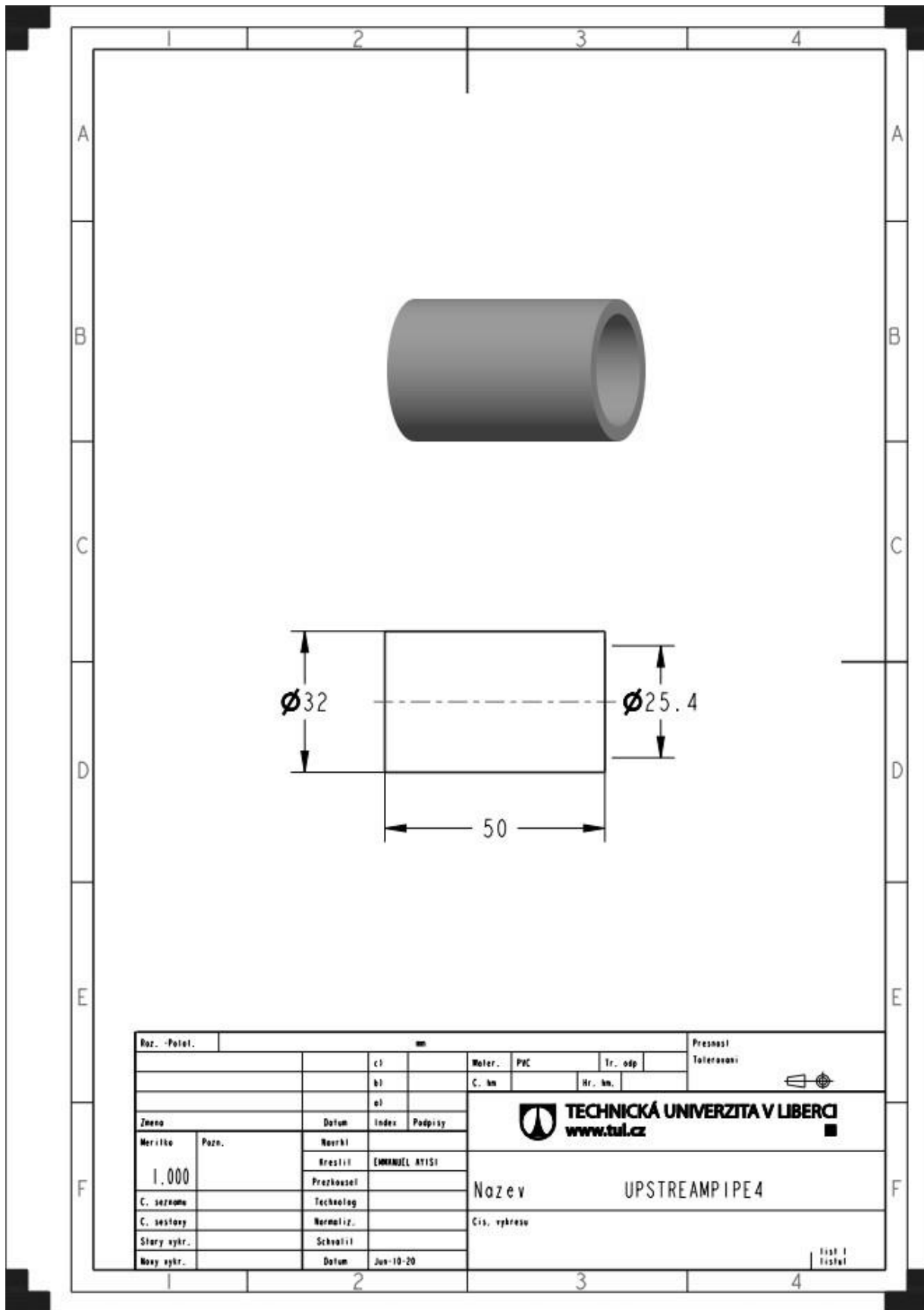


Roz. - Polot.		mm				Mater.		PVC		Tr. odp.		Přesnost Tolerovaní	
		c1				C. km				Hr. km			
		b1											
		e1											
Zmena		Datum		Index		Podpis		<b>TECHNICKÁ UNIVERZITA V LIBERCI</b> <a href="http://www.tul.cz">www.tul.cz</a>					
Meritka		Pozn.		Naukl		Kreslil							
0.700				Przkoušel						Navez <b>UPSTREAMPIPE2</b>			
C. seznam				Technologie						Cis. vykresu			
C. sestavy				Normaliz.									
Stary vykr.				Schválil									
Novy vykr.				Datum		Jun-10-20						List 1 z 1celk	

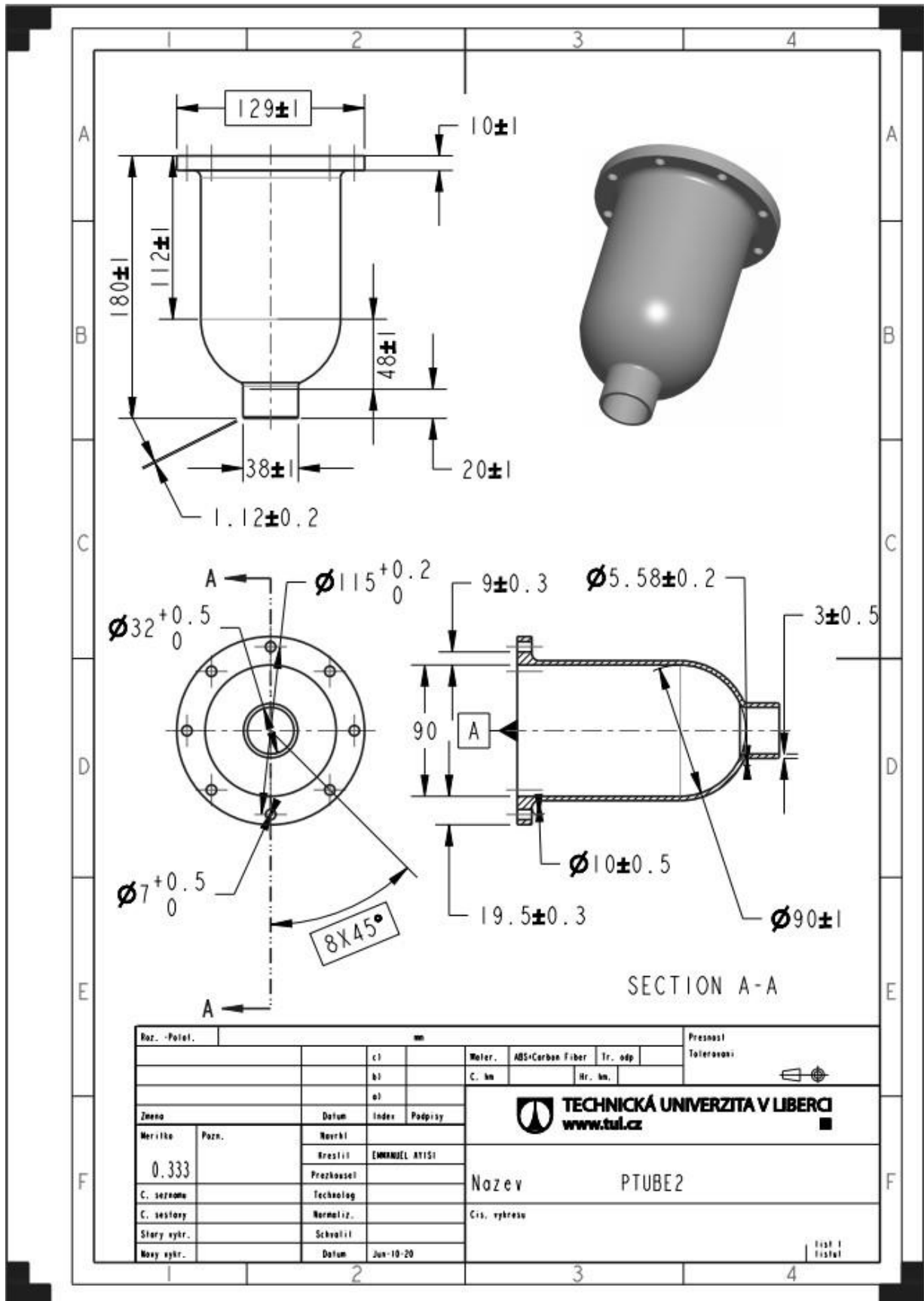



Roz. - Počet.		mm				Přesnost Toleranční	
		c1		Mater.	PVC	Tr. odp.	
		b1		C. km		Hr. km	
		a1		<b>TECHNICKÁ UNIVERZITA V LIBERCI</b> <a href="http://www.tul.cz">www.tul.cz</a>			
Zmena		Datum	Index				
Meritka	Pozn.	Navrhl	<b>Název</b> UPSTREAMPIPE3				
1.000		Kreslil					
C. seznam		Projekoval		<b>Cis. vykresu</b>			
C. sestavy		Normaliz.					
Starý vykr.		Schválil		<b>list 1</b> <b>listů 1</b>			
Nový vykr.		Datum	Jun-10-20				

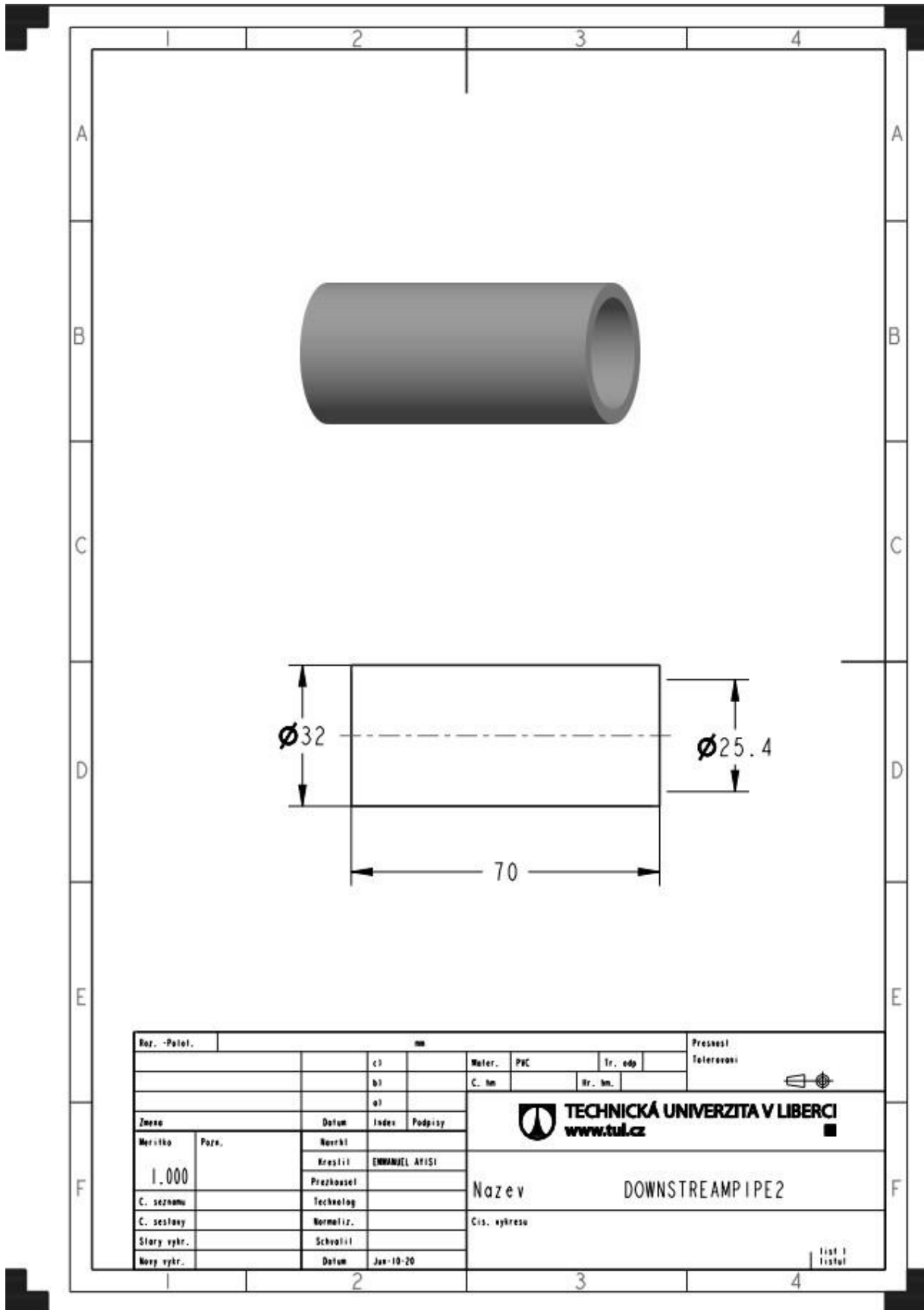




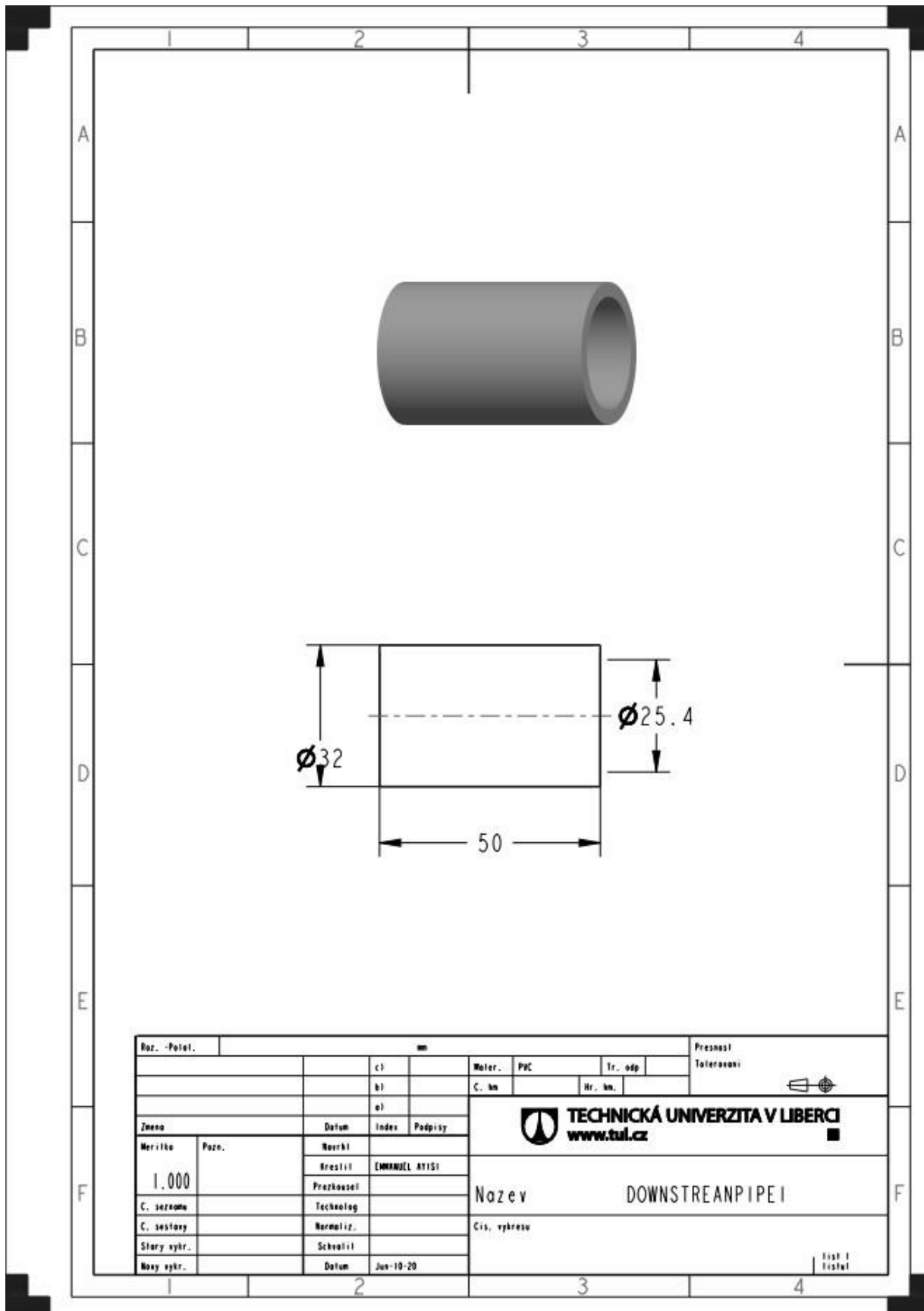
Roz. - Polat.		mm				Přesnost Toleranční	
		ci		Mater.	PVC	Tr. odp	
		bi		C. An		Hr. An	
		ei					
Zmena		Datum	Index	<b>TECHNICKÁ UNIVERZITA V LIBERCI</b> <a href="http://www.tul.cz">www.tul.cz</a>			
Meritko	Paže.	Naukl	Podpisy				
1.000		Kreslil	EMMANUEL ATISI	<b>Nazev</b> UPSTREAMPIPE4			
C. seznam		Przkoušel					
C. sestavy		Normaliz.					
Starý vykr.		Schválil					
Nový vykr.		Datum	Jun-10-20	list 1 listel			



Roz. -Počet.		mm			Mater.		Přesnost Toleranci	
		c)			ABS+Carbon Fiber	Tr. odp		
		b)			C. km	Nr. km.		
		a)						
Zmena		Datum	Index	Podpis	 <b>TECHNICKÁ UNIVERZITA V LIBERCI</b> <a href="http://www.tul.cz">www.tul.cz</a>			
Verz. číslo	Pozn.	Naučil						
0.333		Vytvořil	EMMANUEL AYISI					
C. seznam		Preklausel						
C. sestavy		Technologie						
C. sestavy		Normaliz.			Název PTUBE2			
Starý vykr.		Schválil			Cis. vykresu			
Nový vykr.		Datum	Jun-10-20		list 1 z 1			



Por. -Patol.		mm				Prácesť		Tolerovani	
		c3		Mater.		PAC		Tr. edg	
		b1		C. km				Tr. km	
		a1							
Zmena		Datum		Index		Podpisy		<b>TECHNICKÁ UNIVERZITA V LIBERCI</b> <a href="http://www.tul.cz">www.tul.cz</a>	
Meritko	Porz.	Naukl		Kreslil		EMMANUEL ATISI		Nazev	
1.000		Prezkouset		Technolog				DOWNSTREAMPIPE2	
C. seznamu		Normaliz.		Cis. vykresu					
C. sestavy		Schvalil							
Stary vykr.		Datum		Jan-10-20					
Novy vykr.								list 1 listul	



Roz. -Počet.		mm				Přesnost Toleranční	
		c)		Mater.	PVC	Tr. odp.	
		b)		C. km		Nr. km.	
		a)					
Zmena		Datum	Index	Podpis	<b>TECHNICKÁ UNIVERZITA V LIBERCI</b> <a href="http://www.tul.cz">www.tul.cz</a>		
Meritka	Pozn.	Naučil					
1.000		Kreslil	EMMANUEL AYISI		<b>Název</b> DOWNSTREAMPIPE I		
C. seznam		Technolog					
C. sestavy		Normaliz.			list 1 listal		
Stary vykr.		Schválil					
Novy vykr.		Datum	Jun-10-20				